

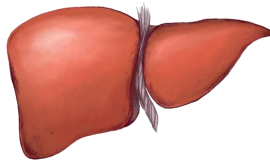


Universidad
de Navarra

School of Medicine

**Dosimetric and Clinical Parameters
Associated with Contralateral Liver
Hypertrophy after Lobar Selective
Internal Radiation Therapy**

Fabiana Grisanti Vollbracht



*Thesis dissertation submitted to the School of Medicine
of the University of Navarra in the fulfilment of the
requirements of the degree of Doctor of Philosophy
(PhD)*

Pamplona, 2021

Declaration

The present work entitled “Dosimetric and Clinical Parameters Associated with Contralateral Liver Hypertrophy after Lobar Selective Internal Radiation Therapy” has been conducted at Clínica Universidad de Navarra under the supervision of Dr. Bruno Sangro and Dr. Macarena Rodríguez-Fraile.

Heads gathered, we state that Ms. Fabiana Grisanti Vollbracht meets the requirements to obtain the PhD mention by the University of Navarra and declare that the work can be presented to the examining panel for judgment. And for the record, we hereby sign the present document:

A handwritten signature in black ink, appearing to read 'Bruno Sangro', with a horizontal line underneath.

Dr. Bruno Sangro

A handwritten signature in blue ink, appearing to read 'Macarena Rodríguez-Fraile', with a long horizontal line extending to the right.

Dr. Macarena Rodríguez-Fraile

This PhD thesis has been conducted at Clínica Universidad de Navarra. During the development of this PhD thesis, Fabiana Grisanti Vollbracht, part of the research work that forms the present doctoral thesis project has given rise to the manuscripts whose titles and authors are the following:

1. 3D voxel-based dosimetry to predict contralateral hypertrophy and an adequate future liver remnant after lobar radioembolization

Authors: Grisanti F, Prieto E, Bastidas JF, Sancho L, Rodrigo P, Beorlegui C, Iñarrairaegui M, Bilbao JI, Sangro B, Rodríguez-Fraile M

Journal: **EUROPEAN JOURNAL OF NUCLEAR MEDICINE AND MOLECULAR IMAGING**

DOI: <https://doi.org/10.1007/s00259-021-05272-9>

2. The joint use of ^{99m}Tc-MAA-SPECT/CT and cone-beam CT optimizes radioembolization planning

Authors: Rodríguez-Fraile M, Ezponda A, Grisanti F, Morán V, Calvo M, Berión P, Martínez de la Cuesta A, Sancho L, Iñarrairaegui M, Sangro B, Bilbao JI

Journal: **EUROPEAN JOURNAL OF NUCLEAR MEDICINE AND MOLECULAR IMAGING RESEARCH**

DOI: <https://doi.org/10.1186/s13550-021-00764-z>

These manuscripts are attached in the Annex.

It has also given rise to the following oral communications:

- 1. Clinical and Dosimetric Parameters Associated with Contralateral Liver Hypertrophy after Lobar Selective Internal Radiation Therapy**

Authors: [Grisanti, F \(Top Rated Oral Presentation\)](#), Prieto E, Bastidas JF, Sancho L, Rodrigo P, Beorlegui C, Iñarrairaegui M, Bilbao JI, Rodríguez-Fraile M

Name of the event: EANM 2020. Annual Congress of the European Association of Nuclear Medicine City: Virtual, Vienna. Country: Austria. Start date: 22/10/2020. End date: 30/10/2020.

- 2. Dose-response for yttrium-90 resin microsphere radioembolization in Hepatocellular carcinoma**

Authors: M. Rodríguez-Fraile, A. Cabrera, J. Rosales, J. Bastidas, [E. Grisanti](#), M. Sanchez, A. Martínez de la Cuesta, M. Iñarrairaegui, J. Bilbao, B. Sangro

Name of the event: EANM 2021. Annual Congress of the European Association of Nuclear Medicine. Virtual. Start date: 20/10/2021. End date: 23/10/2021.

Ms. Fabiana Grisanti Vollbracht is also co-author of the following EANM abstract:

- 1. The joint use of MAA SPECT/CT and CBCT enables better dosimetry planning for SIRT procedures.**

Name of the event: EANM 2019. Annual Congress of the European Association of Nuclear Medicine. City: Barcelona. Country: Spain. Start date: 12/10/2019. End date: 16/10/2019.

Authors: Rodríguez-Fraile, Macarena; Morales, María Isabel; Ezponda, Ana; Calvo, Marta; [Grisanti, FL](#); Berián, P; Sancho, Lidia; Erhard, Alvaro; Morán, Verónica; Iñarrairaegui, Mercedes; [Sangro, Bruno](#).

Ms. Fabiana Grisanti Vollbracht received no funding for this research project.

*“Caminante son tus huellas
el camino y nada más;
Caminante, no hay camino,
se hace camino al andar.
Al andar se hace el camino,
y al volver la vista atrás
se ve la senda que nunca
se ha de volver a pisar.
Caminante no hay camino
sino estelas en la mar.”*

- Antonio Machado

Acknowledgements

I am very grateful to have had this opportunity to work on a project from the beginning until the end. It was challenging, from the weekends collecting data, segmenting livers, to writing the publication and dissertation, but also very rewarding. I believe therapy with radionuclides is one of the growing fields within Nuclear Medicine and getting to participate in a treatment where you not only see the images before treatment, but actively plan the activity to be administered, and then get confirmation of where the activity was deposited through PET/CT is also rewarding.

It was also particularly special to be able to carry this out in my second alma mater, Clínica Universidad de Navarra (CUN). Macarena, thank you for your vision, expertise, and countless support. I have learned a lot about the type of doctor I want to be, and I couldn't have done it without you. Dr. Sangro, thanks for taking the time to give me feedback in every step of the way, and for reminding me to put things into clinical perspective. Lidia, thanks for your help; your encouragement was always appreciated. Carmen, thanks for your contribution, I enjoyed our collaboration with statistics. Maria José, thanks for teaching me your attention to detail, teamwork skills and encouraging me every step of the way. Javier, thanks for including me in other research projects which helped prepare me for this one. Dr. Richter, thanks for being a fine example of leadership and for your guidance. Thank you all for showing me that with commitment comes success.

As part of the team at CUN, I want to thank the Department of Medical Physics, particularly Verónica, Elena and Josep, and the Department of Radiopharmacy, particularly Ivan, Gemma and Rocío, the nurses and technicians at the Nuclear Medicine Department, for making all this possible. Thanks to all of you

and to my former resident colleagues, both before and after me, for all your encouragement.

I would also like to thank the people at Sahlgrenska University Hospital for welcoming me to their staff and for all your support.

Thanks to all my friends for your best wishes, and to Patri de Blas for her illustrations.

Thanks to my family, particularly my parents, my sister and my husband for your unconditional support. I'm very happy to share this success with you.

Finally, I want to thank our patients, who give us purpose and make our work and our research have meaning.

To my parents, my sister and my husband

Abbreviations

3D: Three-dimensional

^{99m}Tc-MAA: ^{99m}Tc-MacroAggregated Albumin

A(GBq): Activity in GBq

BSA: Body Surface Area

CBCT: Flat panel cone-beam CT

D20: The minimum dose to 20% of the volume of interest (VOI) in Gy

D50: The minimum dose to 50% of the VOI in Gy

D70: The minimum dose to 70% of the VOI in Gy

D90: The minimum dose to 90% of the VOI in Gy

D95: The minimum dose to 95% of the VOI in Gy

D98: The minimum dose to 98% of the VOI in Gy

Dmean: Mean dose in Gy

DNA: Deoxyribonucleic acid

DVH: Dose-volume histogram

FLR: Future liver remnant (the non-treated liver, expressed as a ratio to the total liver volume in percent)

GBq: Giga Becquerel

Gy: Grey

HBS: Hepatobiliary scintigraphy

HCC: Hepatocellular carcinoma

Holmium-166: ¹⁶⁶Ho

IQR: Interquartile range

LSF: Lung shunt fraction

MIRD: Medical internal radiation dose

MRI: Magnetic resonance imaging

NTL: Non-tumoral liver

PET/CT: Positron Emission Computed Tomography /Computed Tomography

PVE: Portal vein embolization

REILD: Radioembolization-induced liver disease

ROI: Region of interest

SIRT: Selective Internal Radiation Therapy

SPECT/CT: Single photon emission computed tomography/computed tomography

T/N index: Tumor/non-tumor index

T: Tumor

T0: baseline

T1: 0-2 months after SIRT

T2: 2-6 months after SIRT

T3: 6-12 months after SIRT

TOF: Time-of-flight

VOI: Volume of interest

V100: The percentage of the VOI that receives at least 100 Gy

V120: The percentage of the VOI that receives at least 120 Gy

V30: The percentage of the VOI that receives at least 30 Gy

V40: The percentage of the VOI that receives at least 40 Gy

V50: The percentage of the VOI that receives at least 50 Gy

V70: The percentage of the VOI that receives at least 70 Gy

Yttrium-90: ^{90}Y

Table of Contents

Table of Contents

I. Introduction	- 3 -
1. Selective Internal Radiation Therapy (SIRT)	- 3 -
1.1 Concept of SIRT	- 3 -
1.2 Radionuclides and radioactive compounds	- 9 -
2. Steps in the procedure	- 13 -
2.1 Selection of patients	- 14 -
2.2 Angiography + treatment simulation	- 15 -
2.3 Methods to determine the activity to be administered	- 22 -
Activity calculation: Treatment protocol at Clínica Universidad de Navarra	- 33 -
2.4 Administration of treatment	- 34 -
2.5 Verification of treatment and dosimetry with ⁹⁰ Y PET	- 35 -
3. Atrophy- Hypertrophy Complex	- 37 -
II. Hypothesis	- 41 -
III. Objectives	- 43 -
1. Main objective	- 45 -
2. Secondary objectives	- 45 -
IV. Materials and methods	- 46 -
1. Patient cohort. inclusion criteria and clinical outcomes	- 49 -

Table of Contents

2. Ethics.....	- 51 -
3. Pre-treatment and treatment	- 51 -
4. PET ⁹⁰ Y Imaging.....	- 52 -
5. Dosimetric analysis	- 53 -
6. Volumetric analysis	- 58 -
7. Statistical analysis	- 58 -
V. Results.....	- 61 -
Results. Patient, Treatment Characteristics and Outcomes	63 -
Results of Objective 1	- 68 -
Results of Objective 2.....	- 71 -
Univariable regression	- 72 -
Multivariable regression	- 74 -
Results of Objective 3.....	- 75 -
To predict an increase in FLR to reach at least 30%	- 76 -
To predict an increase in FLR to at least 40%	- 77 -
Results of Objective 4.....	- 78 -
Univariable regression	- 78 -
Multivariable regression	- 79 -
Results of Objective 5	- 81 -
Changes in liver function	- 81 -

Table of Contents

Univariable regression	- 82 -
Multivariable regression	- 83 -
VI. Discussion	- 85 -
VII. Conclusions	- 97 -
VIII. Figures and Tables	- 101 -
1. Figures.....	- 103 -
2. Tables.....	- 104 -
IX. References	- 107 -
X. Annex	- 129 -

I. Introduction

1. SELECTIVE INTERNAL RADIATION THERAPY (SIRT)

1.1 Concept of SIRT

Selective internal radiation therapy (SIRT), also termed radioembolization, is an established treatment for primary and secondary unresectable hepatic malignancies [1], in which radioactive microspheres are injected in the arterial vasculature of the liver. ^{90}Y , a nearly pure (99.9 %) β -emitter, is the most commonly used radionuclide, although Holmium-166 (^{166}Ho) is also available. Since tumors have a preferentially arterial blood flow from the hepatic artery, most radioactive microspheres get embedded in the tumor microvasculature and selectively irradiate tumors rather than the surrounding liver tissue that receives the majority of its blood supply from the portal vein [1,2].

The aim of SIRT is to selectively target radiation to liver tumors while limiting the dose to normal liver parenchyma[3]. For the effectiveness of this intra-arterial treatment, optimal tumoral perfusion and blood flow is necessary for cell damage. Cell damage is performed by free radicals, which are generated by ionization of water molecules near to the tumor cells deoxyribonucleic acid (DNA). Therefore, for maximal cytoreduction by radiation, along with oxygen supply, sufficient microsphere coverage of tumors is needed to induce cell death with the high-energy β -radiation emitted [4].

SIRT does not produce occlusion of the large and medium arteries, thus maintaining perfusion of the hepatic parenchyma [5]. For that reason, SIRT results are largely due to the effects



Introduction. Selective Internal Radiation Therapy (SIRT)

of radiation and microembolization, and not to ischemia produced by macroembolization, as in chemoembolization [6,7].

SIRT provides a different treatment approach with respect to traditional treatments (Sorafenib, systemic chemotherapy) and largely spares the non-tumoral liver from the effect of radiation[8], although the off-target delivery beta radiation from ^{90}Y microspheres can occur. It is a good locoregional treatment option compared with external radiotherapy, which has the disadvantage of high radiosensitivity of the hepatic parenchyma[5] that makes it a challenge to safely deliver radiation to large liver tumors [9].

In patients with primary and metastatic liver cancer, hepatic tumor involvement plays a critical role for survival and quality of life as the liver is an essential organ of metabolism and regulation. In fact, the presence of hepatic disease is directly related to mortality and morbidity [2]. Surgical resection is the most effective method for enhancing survival in selected cases of primary or metastatic liver cancer with no evidence of extrahepatic disease (with or without adjuvant chemotherapy)[2]. However, in the majority of patients, hepatic malignancies are unresectable.

Only 30% of patients are eligible for curative intervention upon initial diagnosis with hepatocellular carcinoma (HCC) [10]. SIRT should be indicated after thorough discussion of alternative treatment options in a multidisciplinary team involving all relevant therapeutic disciplines [8]. SIRT is recommended in guidelines such as the National Comprehensive Cancer Network (NCCN) guidelines for HCC [11] and in the European Society for Medical Oncology (ESMO) guidelines [12,13], mostly in intermediate or



Introduction. Selective Internal Radiation Therapy (SIRT)

advanced stages of HCC based on the Barcelona Clinic of Liver Cancer (BCLC) classification. SIRT is currently used in several situations instead of chemoembolization, such as when transarterial chemoembolization has failed to produce a tumor response, when chemoembolization is not indicated, because the tumors are too large, too numerous or because they have invaded the portal vein branches [8]. For advanced HCC, sorafenib was considered the standard of care for more than a decade. Recently, the combination of atezolizumab and bevacizumab has become standard of care for these patients without contraindications to either immune checkpoint inhibitors or antiangiogenic therapy[11,14,15]. SIRT is recommended for advanced HCC when the disease liver confined, good liver function and no systemic therapy feasible; patients with extrahepatic disease including those with regional lymph nodes are likely better served by systemic therapies rather than loco-regional therapies[8].

Depending on the circumstances, SIRT is not only used as a palliative treatment in bilobar or multifocal unilobar HCC, but also:

- To control tumor burden while awaiting a transplant organ, referred to as “bridging” a patient to transplantation.
- For “downstaging”, in order to reduce tumor burden such that patients will subsequently meet criteria for curative therapies, such as surgical resection or transplantation [16,17] (see Fig. 1).



Introduction. Selective Internal Radiation Therapy (SIRT)

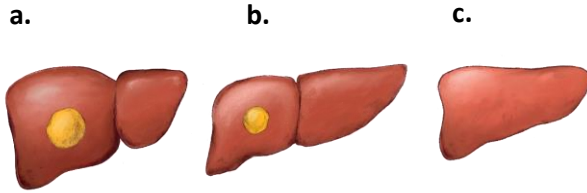


Fig. 1. Surgical resection after SIRT with hypertrophy of the contralateral liver lobe. Illustration by Patri de Blas. (a) Patient with solitary tumor in the right lobe. (b) Solitary tumor in the right lobe treated with SIRT. The right lobe has atrophied while the contralateral liver has increased in size and the patient is now candidate for liver resection. (c) Left lobe post right lobe hepatectomy.

- For “radiation lobectomy”, an additional avenue to curative therapy for HCC patients which consists of ablation of an entire hepatic lobe [18]. The intent is to develop marked ipsilateral lobar atrophy, resulting in the management of potential microvascular and macrovascular spread of disease with the potential benefit of producing contralateral lobe hypertrophy after unilobar SIRT[18].
- As a potential curative therapy, in the form of a “radiation segmentectomy” with the aim to eradicate solitary liver tumors[19] non-amenable for surgical resection due to concomitant disease or comorbidities, such as cholangiocarcinoma [20]. In this case, a high dose is usually delivered to no more than two hepatic segments [21].

Similarly, according to the intended treated liver territory, the treatment approach can be whole-liver/ bi-lobar, usually performed in sequentially, lobar (lobar right or lobar left), lobar with intention to hypertrophy the contralateral lobe or

Introduction. Selective Internal Radiation Therapy (SIRT)

segmental. Extended right lobar can also be performed (lobar right + segment IV).

The first recommendations for activity calculation were based either on an activity of ^{90}Y in GBq to administer related to the body surface area with resin microspheres, also called SIR-Sphere® [22] or on an absorbed dose delivered to the liver (80 to 150 Gy) with glass microspheres, also called TheraSphere® (see section 1.2: Radionuclides and radioactive compounds) [23]. Although these were some of the first recommendations, activity calculation has become increasingly more personalized, as has treatment planning. As a principle, as Garin et al. highlight[24], SIRT planning should be based on a tumoricidal tumor dose (TD) necessary to induce a tumor response and on a normal liver dose (NLD) not to exceed to avoid liver decompensation. Congruent with this is our published protocol used at Clínica Universidad de Navarra for resin microspheres in order to prevent Radiation Induced Liver Disease (REILD) [25], which will be described in section 3.

Efforts to refine personalized activity prescription are ongoing, and knowing the true absorbed dose to different tissue compartments is the key way to safely individualize therapy for maximal response while respecting normal tissue tolerances[26]. In an international and multidisciplinary expert panel convened to formulate state-of-the-art recommendations for optimization of SIRT with ^{90}Y resin microspheres [26], one of the areas evaluated was dosimetry. To start with, it stated that the calculation of the ^{90}Y -resin microspheres activity is needed. More specifically, a personalized approach was recommended using dosimetry for activity prescription, particularly according to the partition model and/or 3D voxel-based (see section 2.3).



Introduction. Selective Internal Radiation Therapy (SIRT)

The phase 3 trials comparing SIRT with sorafenib (SIRveNIB trial by Chow et al. [27] and SARA trial by Vilgrain et al. [28]) or the combination of SIRT + sorafenib versus sorafenib alone (SORAMIC trial by Ricke et al. [29]) in patients with advanced hepatocarcinoma failed to demonstrate any overall survival (OS) improvement. The absence of dosimetry endpoints was questionable, which could explain in part the negativity of those studies, particularly despite the fact that SIRT is a radiation oncology approach, where radiobiological rules apply [30].

In fact, on a secondary analysis of prospectively acquired data from participants who received SIRT in the Sorafenib versus Radioembolization in Advanced Hepatocellular Carcinoma (SARA) trial, predicted that tumor radiation-absorbed dose computed at ^{99m}Tc -MAA SPECT/CT was associated with better overall survival and disease control in hepatocellular carcinoma [31]. The patients were studied in two groups: 121 in the dose-survival group, and 109 were evaluated in the dose-tumor response group. In the dose-survival group, participants who received at least 100 Gy ($n = 67$) had longer survival than those who received less than 100 Gy (median, 14.1 months vs 6.1 months, respectively; $p < 0.001$). In the dose-tumor response group, tumor radiation-absorbed dose was higher in participants with disease control versus those with progressive disease (median, 121 Gy [IQR: 86–190 Gy] vs 85 Gy [IQR: 58–164 Gy]; $P = .02$). The highest disease control rate was observed in 78% of patients with a tumor radiation-absorbed dose greater than or equal to 100 Gy and optimal agreement among CT, ^{99m}Tc -MAA SPECT/CT, and ^{90}Y SPECT/CT or PET/CT [31].

A personalized versus standard dosimetry approach impacts response rate. In a recent randomized phase 3 trial of SIRT for



Introduction. Selective Internal Radiation Therapy (SIRT)

hepatocellular carcinoma, a personalized versus standard dosimetry approach was compared, with ^{90}Y glass microspheres [32]. This study was named the DOSISPHERE-01 trial. Before the DOSISPHERE-01 trial, there had not been a controlled prospective trial comparing personalized dosimetry and standard dosimetry in patients with hepatocellular carcinoma. The primary endpoint was the investigator-assessed objective response rate in the index lesion, according to European Association for the Study of the Liver criteria [33], at 3 months after selective internal radiation therapy. Compared with standard dosimetry, personalized dosimetry significantly improved the objective response rate in patients with locally advanced hepatocellular carcinoma. It suggests that personalized dosimetry could become the definitive standard-of-care method of administering SIRT. To improve patient outcomes in patients with locally advanced hepatocellular carcinoma, this study provides a strong rationale for new randomized studies to compare SIRT using personalized dosimetry (alone or in combination with standard of care) with standard of care alone.

1.2 Radionuclides and radioactive compounds

Currently, there are three types of microspheres, two with Yttrium-90 (resin, SIR-Spheres or glass, TheraSpheres) and one with Holmium-166 (Quiremspheres) and each of them has different properties (Table 1) [34]. In patients treated with SIR-Spheres, the number of particles typically injected is higher than patients treated with TheraSphere (20-40 million vs. 5 million) producing a more relative embolic effect, with lower specific activity per microsphere (20-70 vs. 4354 Bq per microsphere). Quiremspheres have an intermediate position in



Introduction. Selective Internal Radiation Therapy (SIRT)

terms of number of particles (20 million), specific activity (240-375 Bq/microsphere) and embolic effect [25].

Table 1. Types of microspheres for SIRT [34]

	SIR-Spheres®	TheraSphere®	QuiremSpheres®
Radioisotope	Yttrium-90	Yttrium-90	Holmium-166
Half-life (h)	64.1	64.1	26.8 h
Main emitted radiation	Beta	Beta	Beta and gamma
Mean (maximum) tissue penetration (mm)	2.5 (11)	2.5 (11)	2.5 (8.4)
Visualization method	Bremsstrahlung-SPECT	Bremsstrahlung-SPECT	MRI
	Yttrium-90 PET	Yttrium-90 PET	SPECT
Material	Resin	Glass	Poly-l-lactic acid
Microsphere size (µm; range)	32.5 (20–60)	25 (20–30)	30 (25–35)
Specific activity per sphere (Bq)	40–70	4354*, 1539†, 544‡	200–400
Millions of spheres in a typical administration	20–40	1.7† 4.8‡	12–24
Embolic effect	Moderate	Low	Moderate



Introduction. Selective Internal Radiation Therapy (SIRT)

Treatment planning method indicated in product leaflet.	BSA (two compartment)	Mono-compartment	Mono-compartment
---	-----------------------	------------------	------------------

BSA, body surface area; MRI, magnetic resonance imaging; PET, positron emission tomography; SPECT, single photon emission computed tomography.

** Measured, at the reference date [6].*

† Four days after the reference time.

‡ Eight days after the reference time

According to quantitative data describing the deposition patterns of radioembolic microspheres in tumor tissue, it has been found that microspheres are not deposited randomly in the tumor, but that they are deposited in clusters[35–37], and one of those studies found that increasing the number of microspheres increases not the number of clusters but the number of spheres in each cluster[37]. Due to interest in this phenomenon, Pasciak et al. has been studying what effect the number of microspheres may have, if any, on tumor control in ⁹⁰Y SIRT. In one study, they used Monte Carlo sampling techniques to model the distribution of microspheres on both a microscopic and a macroscopic level, combining ⁹⁰Y PET data with microscopic probability-density functions describing microsphere clustering [38]. They found that decreasing the microsphere density per unit volume (ml) in tumor resulted in a decrease in D70, the minimum dose to 70% of the tumor. They concluded that a lower microsphere-number density may cause a greater portion of tumor to receive a lower absorbed dose. This would particularly affect glass microspheres. One can compensate for the effect of number density on clinical dose metrics such as D70 by increasing the treatment dose, which is built into the glass treatment-planning model [23] in comparison to resin microspheres.



Introduction. Selective Internal Radiation Therapy (SIRT)

They stated that clinicians should be aware of the potential effect of microsphere-number density on absorbed-dose inhomogeneity as it relates to different microsphere devices [38]. On the other hand, since number density will change with the amount of time that glass microspheres are allowed to decay before use, this factor may also be considered in the treatment-planning process [38]. The differences observed begin to explain differences in treatment planning strategies between glass and resin microsphere devices [38].

In another study by the same group, healthy pigs received lobar SIRT with glass ^{90}Y microspheres at 4, 8, and 12 days post-calibration (Fig. 2), as well as at 16 days post-calibration (not represented in the figure) [39]. Dose distributions were normalized as a function of average absorbed dose either to the tumor as a whole or to the entire volume in the case of the uniform approach. A consistent number of microspheres per sphere cluster was found at 4, 8, and 12 days postcalibration, despite an 8-fold increase in total microspheres infused from days 4 to 12. It was observed that the additional microspheres resulted in more clusters formed and, therefore, a more homogeneous microscopic absorbed dose. According to their radiobiologic model, the increased absorbed dose homogeneity resulted in a greater volume fraction of the liver receiving a potentially toxic absorbed dose.

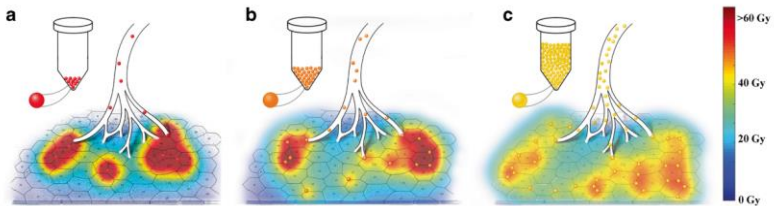


Fig. 2. Artistic rendering of microscopic microsphere deposition at days 4–12 post-calibration. Microscopic microsphere deposition at days (a) 4, (b) 8 and (c) 12 post-calibration. Increased homogeneity of absorbed dose is apparent in the day 12 post-calibration treatment which may result in toxicity to a greater fraction of hepatic lobules. Color bar indicates differences in absorbed dose as exemplified by the number of lobules receiving 30–40 Gy in each scenario. Day 16 was not included since dose-volume histogram was similar to day 12. From Pasciak et al. [39]

2. STEPS IN THE PROCEDURE

The treatment consists of several stages (see Fig. 3).

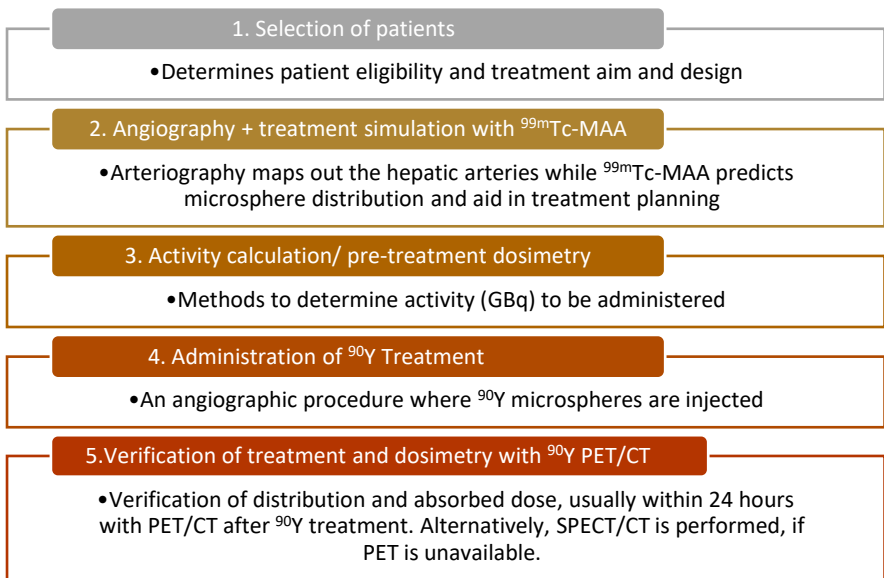


Fig. 3. Steps in ^{90}Y SIRT.

Some steps must be followed in order to guarantee the safety of the procedure for patients: the clinical evaluation, the pre-



treatment angiogram, the simulation of treatment, usually with technetium-99m macroaggregated albumin ($^{99m}\text{Tc-MAA}$), the SIRT treatment per se, and the clinical follow-up [2]. After SIRT, PET is performed (or SPECT/CT, if PET is unavailable).

2.1 Selection of patients

For patients to be candidates for SIRT, they must have unresectable primary or secondary liver carcinoma, a predominantly hepatic tumor burden, and a life expectancy of at least 3 months [40]. According to Sangro et al. [41], patients with poor liver functional reserve as those that present with a total bilirubin >2 mg/dL or have non-tumoral ascites should not be considered candidates to SIRT. They described that individual, yet conservative decisions should be made in patients with bilirubin values slightly below this threshold in which a rapid increase is observed within the weeks previous to SIRT evaluation.

The incidence of complications after SIRT for appropriately selected patients and if the treatment is properly targeted to the target is low [42]. Post-radioembolization syndrome (PRS) may occur [124], defined as the occurrence of self-limited fever, fatigue, abdominal pain, nausea, vomiting, or anorexia. More serious complications may be non-target delivery of radiation to lung or gastrointestinal tract (pneumonitis, gastrointestinal ulceration, cholecystitis), or radioembolization-induced liver disease (REILD) [2]. REILD is characterized by jaundice and ascites developing 4 to 8 weeks after treatment in the absence of tumor progression or bile duct occlusion, with pathologic changes consistent with veno-occlusive disease in the most severe cases [25].



In a recent systematic review and meta-analysis, ^{90}Y SIRT was associated with significantly lower rates of grade ≥ 3 adverse events compared to standard of care [43]. However, the authors found in subgroup analyses that it may be related to the use of sorafenib as a comparator, the absence of an active co-intervention and a balanced proportion of the different BCLC stages. It stated that the small number of trials and limited sample size may explain this later finding [43].

2.2 Angiography + treatment simulation

Treatment simulation with $^{99\text{m}}\text{Tc}$ MAA

$^{99\text{m}}\text{Tc}$ MAA simulates SIRT treatment due to similarities in size (10-100 μm in diameter) and density, in order to predict the distribution of activity in the liver [44,45]. Treatment simulation is part of the workup before SIRT and most commonly performed with $^{99\text{m}}\text{Tc}$ -MAA. A calibrated amount of $^{99\text{m}}\text{Tc}$ -MAA is administered at selected sites within the hepatic arterial tree during pre-treatment angiography. There are a few objectives to $^{99\text{m}}\text{Tc}$ -MAA imaging. 1) To identify intrahepatic distribution and extrahepatic distribution, 2) for assessment of lung-shunt fraction and 3) for calculation of the activity to be injected [20]. According to international recommendations, intrahepatic $^{99\text{m}}\text{Tc}$ -MAA distribution should be evaluated using SPECT/CT, instead of planar scintigraphy or SPECT alone [26]. It should preferably demonstrate focal uptake within all tumor sites in the treatment field with limited uptake in the non-tumoral liver parenchyma. With the simulation, the vascular anatomy of the liver can be studied, including possible anatomic variants, and a possible arterial-venous shunt to the lung or communication to gastroduodenal vessels can be detected. The detection of these communications is important for performing modifications to



the initial treatment plan. For identifying extrahepatic uptake sites, SPECT/CT has also been revealed to be more effective than planar imaging [46]. Therefore, the angiography and SPECT/CT should be performed prior to treatment to identify the vasculature of the tumor and to avoid complications. It is recommended to identify and, if possible, correct the vascular source of extrahepatic uptake before proceeding with treatments [26]. Vascular redistribution is an endovascular technique routinely performed during work-up angiography to proximally occlude extrahepatic or intrahepatic vessels that supply the target volume with microcoils [47].

The estimation of the lung shunt fraction (LSF) is important, as a high LSF value is indicative of an increased risk of radiation pneumonitis [48] and can be a contraindication of treatment. The LSF corresponds to fraction of MAA particles that arrived into the lungs due to arteriovenous shunts [49], which are common in liver tumors[50]. The LSF can be estimated on images from the ^{99m}Tc -MAA simulation, either planar or SPECT/CT [26]. SPECT/CT can reduce errors in estimation with attenuation and scatter correction [51] and aid in the correct evaluation of lung volume. The highest tolerable pulmonary-absorbed dose has been set at 30 Gy following a single treatment and up to 50 Gy after repeat treatments [43], while if percentages are used, a cut-off of 20% is recommended [26]. Both SIR-sphere and TheraSphere threshold values are based on a maximum dose of 30 Gy for a lung mass of 1.0 kg[52]).

The risk of pneumonitis increases when the LSF is $>20\%$ or when the estimated absorbed dose by the lungs is >30 Gy[41], however rarely, it can occur even with a lower predicted pulmonary absorbed dose of less than 30 Gy (see example in Fig. 4).



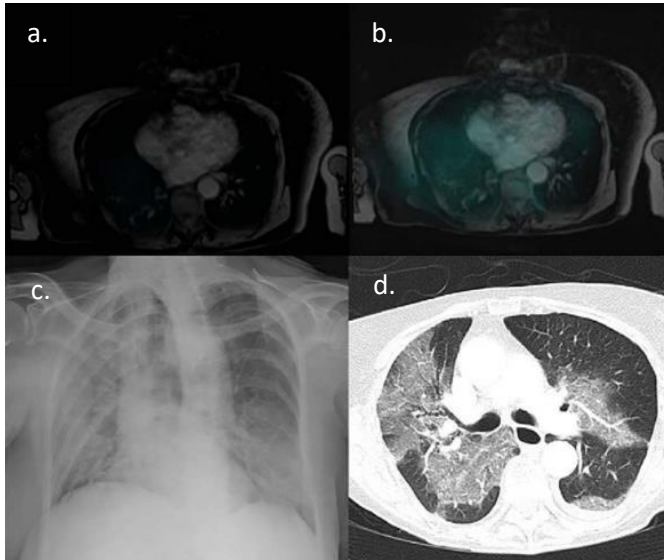


Fig. 4. Radiation pneumonitis. Superselective SIRT was indicated in a patient with HCC who had a 27% LS fraction based on pretreatment ^{99m}Tc -MAA scan (a). A dose of 0.5 GBq of resin microspheres was prescribed, which should have resulted in an estimated dose of radiation to the lungs of 7 Gy. A higher exposure was suspected based on the post-SIRT Brehmsstrahlung-SPECT images (b). Cough, dyspnea, and hypoxemia developed 22 days after SIRT. Chest X-ray (c) and CT scan (d) showed the typical pattern of radiation pneumonitis, which was fatal in this case. From Sangro *et al.* [41]

Even though ^{99m}Tc MAA is still the gold standard for simulation of treatment, it is not a perfect surrogate for ^{90}Y -microspheres [53], and some studies show differences between the distribution of microspheres in MAA compared to ^{90}Y [54–57]. These differences can be due to changes in the position of the micro-catheter point, changes in the regional blood flow between the simulation and SIRT, and differences in the shape and size of MAA compared to microspheres[57].

For the calculation of activity as part of the individualized planning of the treatment with pre-treatment simulation, the goal is one that would provide an optimal tumor response while sparing healthy tissues [58]. It is useful to analyze the tumor/non-tumoral ratio (T/N ratio) which is used in the partition model for calculation of activity to be administered [59]. The T/N ratio is obtained by contouring regions of interest (ROI) over tumoral and healthy liver and dividing average counts per ml in tumor by average counts per ml in non-tumoral liver. There is no standardized method to obtain the T/N ratio, however the EANM recommends using the SPECT image corrected by attenuation [60]. A simple method is to draw the same number of ROIs of the same size in the tumoral and non-tumoral parenchyma [61], that way, the masses can be omitted.

In the absence of significant extrahepatic activity, the main dosimetric limitation is the total absorbed radiation dose in healthy liver parenchyma, also called the non-tumoral dose [1]. It varies between patients depending on multiple variables, including the type of microsphere and the treatment approach. For resin microspheres, safety cut-offs have been recommended [26] (see Table 2) depending on a whole liver/bi-lobar approach, lobar and segmental treatment, lobectomy or segmentectomy. In unilobar treatment, if the function of the treated lobe is to be preserved, a mean absorbed dose cut-off of 40 Gy has been proposed. In cases where some loss of function is acceptable, a higher cut-off could be used [26]. On the other hand, when the volume and function of the contralateral liver lobe is sufficient (FLR cut-off of the contralateral liver lobe of 30–40%), a more aggressive treatment (than for whole liver treatment) may be useful (depending on several factors such as the intent of treatment, liver function and tumor type) [26].



Table 2. Safety cut-off for individual activity prescription recommendations for the use of SIRT with ⁹⁰Y-resin microspheres (adapted from Levillain et al. [26] with the inclusion of recommendations no. 29-36).

	Recommendation	Strength of agreement
Whole liver/bi-lobar treatment	When patients have a ‘non-compromised’ liver, the recommended mean absorbed dose limit for safety to non-tumoral liver is 40 Gy, when doing whole liver treatment. When the liver is heavily pretreated or when there is suspicion of compromised liver function, this cut-off should be reduced to 30 Gy but should be estimated on an individualized basis	Strong
Lobar and segmental treatment	There was no clear agreement on whether to use the same absorbed dose safety limits for unilobar treatment as used for whole liver treatment, most experts would not	None
	For unilobar or segmental treatment, when the volume and function of the contralateral liver lobe is sufficient (FLR cut-off of the contralateral liver lobe of 30–40%), a more aggressive treatment (than for whole liver treatment) may be useful (depending on several factors	Strong



Introduction. Steps in the procedure

	such as the intent of treatment, liver function and tumor type)	
	In unilobar or segmental treatment, if the function of the treated lobe is to be preserved, a mean absorbed dose cut-off of 40 Gy is proposed. In cases where some loss of function is acceptable, a higher cut-off could be used	Moderate
	There was no clear agreement on whether to perform a more aggressive unilobar treatment in cirrhotic patients	None
Lobectomy and segmentectomy	In lobectomy a mean absorbed dose to the non-tumoral liver of > 70 Gy for ablative therapy is proposed	Strong
	A higher mean absorbed dose should be used for segmentectomy—possibly > 150 Gy	Strong

In the treatment of resin microspheres, in a previous study performed by our group, imaging with ^{99m}Tc MAA revealed to be essential in SIRT workup because baseline characteristics may not adequately predict ^{99m}Tc -MAA results [62]. Furthermore, abdominal SPECT images are sufficiently predictive of tumor response in more than 80% of patients [63], and SPECT ^{99m}Tc -based dosimetry predicts overall survival (OS) in patients with HCC, according to Garin et al. [64].



Treatment simulation with ^{166}Ho microspheres

Ideally, ^{90}Y microspheres would also be used for the pretreatment procedure, but their imaging is challenging at the low activity required to avoid unintended radiation damage. Some groups use ^{166}Ho microspheres instead of ^{90}Y microspheres for hepatic SIRT, using the same type of microsphere for treatment simulation [65], and this has been proven to be a safe alternative to $^{99\text{m}}\text{Tc}$ -MAA [66]. The variation in intrahepatic distribution between the scout dose in treatment simulation and treatment dose is expected to be minimal, due to the identical morphology of the microspheres, which can aid accuracy of intrahepatic dosimetry. In a study by Elschot et al. [67], pretreatment diagnostic ^{166}Ho -microsphere SPECT/CT imaging accurately predicted lung absorbed doses after ^{166}Ho SIRT, while lung absorbed doses were significantly overestimated by $^{99\text{m}}\text{Tc}$ -MAA planar and SPECT/CT imaging. Since a high lung shunt fraction (LSF) may impose lower prescribed treatment activity or even impede treatment, studying these patients with ^{166}Ho microspheres can be considered. Another benefit of holmium is its large magnetic susceptibility, which may permit MRI-based dosimetry [67] and MR-guided treatments in the future[68].

Chiesa et al. [69] highlight how ^{166}Ho scout dose in comparison to $^{99\text{m}}\text{Tc}$ -MAA obtained a higher accuracy in predicting intra-hepatic distribution of SIRT treatment with ^{166}Ho -microspheres in a study limited to colorectal metastases. Better prediction of lesion absorbed dose was observed, with narrower 95%-limits of agreements; they were reduced from (-164 Gy, 197 Gy) with $^{99\text{m}}\text{Tc}$ -MAA, to (- 90 Gy, 105 Gy) with ^{166}Ho [70]. Chiesa et al. [69] also recalled the results of Jadoul et al. in which better $^{99\text{m}}\text{Tc}$ -MAA prediction of hepatic distribution after SIRT was observed for HCC rather than for



metastases[71], and argued that the use of the same particle for simulation and therapy is promising in all applications[69].

2.3 Methods to determine the activity to be administered

Before delving into the activity determination methods, a simple review of the definition of terms may be helpful.

- **Absorbed dose** refers to the amount of exposure to radiation deposited in a tissue. The basic unit of absorbed dose is the gray, abbreviated Gy, where $1\text{ Gy} = 1\text{ joule of radiation energy per kilogram of matter}$ [72].
- On the other hand, **activity** refers to disintegrations per unit of time, and is a measure of “how radioactive” a sample is. In the International System (SI), the unit of activity is the becquerel (Bq), where a sample has an activity of 1 Bq if it is decaying at an average rate of 1 sec^{-1} (1 disintegration per second). In SIRT, activity is commonly measured in gigabecquerel (GBq) [72].
- **Dosimetry** is defined as the amount of absorbed dose delivered by ionizing radiation [60].

In other words, when it comes to SIRT’s current clinical dosimetry, the ^{90}Y microspheres are calibrated, measured, and administered in activity (GBq). However, radiation therapy doses are normally planned in Gy (J/kg) to quantify absorbed dose from a radiation source in tissue. Similarly, SIRT plans the prescribed doses to the patient in Gy, but converts it into prescribed activity before treatment [49]. In general, 1 Gbq of ^{90}Y per kg of tissue provides an absorbed dose of 49.38 ± 0.5 Gy, typically rounded up to 50 Gy [49] but this is affected by



non-uniform distribution of the dose between the tumor and normal liver tissue.

Accurate prediction of absorbed dose to the tumor and to the healthy liver can help to optimize patient selection and individualize treatment planning [73]. Currently, the success of the treatment depends largely on the knowledge and experience of the treatment team, who can tailor the amount of injected microspheres or activity and predict the absorbed dose [73]. Over the past several years, dosimetry refinements have led to marked improvements in this therapy from both a safety and efficacy standpoint [74]. There is a strong correlation between the radiation dose absorbed by the tumor and improvement in progression-free and overall survival [64,75,76], as mentioned previously. On the other hand, excessive radiation to healthy hepatic parenchyma or other organs (i.e., nontarget dose) may result in toxicity.

The activity to be administered must be established taking into account factors that may influence the result of the treatment, such as how much healthy liver is involved, tumor uptake, possible side effects due to healthy liver radiation, baseline condition of the patient and the prediction of absorbed doses. The activity should be reduced if there is compromised liver function. The calculation of activity is different for resin and glass ^{90}Y microspheres. For resin microspheres, a commonly used method is the body surface area (BSA)-based method for resin microspheres. For glass microspheres and holmium-loaded micro-spheres, a commonly used method is the MIRD mono-compartment method [23,77].

BSA method for resin microspheres



Introduction. Steps in the procedure

In the BSA method, the activity is calculated according to the size of the tumor in the liver and the size of the patient. The BSA-based method is based on the observation that BSA correlates with liver volume in the healthy population [78] and the planned activity is adjusted to an individual patient's liver volume. The activity is calculated according to the following formula:

$$A[\text{GBq}] = (\text{BSA} [\text{m}^2 - 0.2]) + \frac{V_{\text{tumor}}}{V_{\text{tumor}} + V_{\text{normal liver}}}$$

Where V_{tumor} and $V_{\text{normal liver}}$ indicate the volumes of the tumor in the liver and the non-tumor liver tissue, respectively. For lobar or superselective treatment, the activity is reduced in proportion to the size of the liver volume being treated [79]. The prescribed activity is reduced if the LSF is between 10 and 15% (reduction of 20%) or between 15 and 20% (reduction of 40%), while an LSF higher than 20% is a contraindication for the treatment [64] and lung radiation dose must be limited to < 30 Gy.

A modified BSA method was employed for the SIRFLOX, FOXFIRE, and FOXFIRE-global studies combining first-line chemotherapy with SIRT using resin microspheres in patients with metastatic colorectal cancer with liver metastases, where activity was reduced relative to the BSA method, based on LSF and tumor involvement [80]. The safe use of modified BSA when a more selective treatment, such as lobar treatment is performed has been confirmed [26]. In the case of the SIRFLOX study, both liver lobes were treated in 92.3% of patients[81]. The addition of SIRT to first-line FOLFOX chemotherapy for patients with liver-only and liver-dominant metastatic colorectal cancer did not improve overall survival compared with that for FOLFOX alone, but did significantly



delayed progression in the liver [82]. The adverse events profile in the SIRFLOX study was anticipated and manageable[82].

Medical Internal Radiation Dose (MIRD) mono-compartment dosimetry for glass and holmium microspheres

For glass microspheres, the activity calculation is based on the desired mean absorbed dose to the target liver mass and is independent of tumor burden.

$$A[\text{GBq}] = \frac{\text{Desired dose [Gy]} \times M_{\text{target}}[\text{kg}]}{50 [\text{J/GBq}]}$$

The desired absorbed dose is set assuming a completely homogeneous distribution of the microspheres over the target volume [79]. The recommended absorbed dose ranges from 80 to 150 Gy, and this relies on the judgment of the treating physician [65].

For the administration of holmium microspheres, a methodology akin to the MIRD mono-compartment method for glass microspheres is used [65].

$$A[\text{GBq}] = \frac{\text{Liver dose[Gy]} \times M_{\text{liver}}[\text{kg}]}{15.9 [\text{J/GBq}]}$$

Based on the findings of the phase 1 dose escalation study, an aimed whole-liver absorbed dose of 60 Gy is recommended [83].

Multi-compartment dosimetry

It was initially developed for dosimetry of ^{90}Y resin microspheres and subsequently adopted for dosimetry of ^{90}Y



glass microspheres. Also called the partition model, it further expanded on the MIRD method by considering the lungs, the tumor, and the healthy liver tissue as separate compartments.

The absorbed dose “D” in a volume of interest (VOI) of mass “M” (in kg) and containing an activity “A” of ^{90}Y (in GBq) is calculated using the following simplified MIRD equation:

$$D(\text{Gy}) = A (\text{GBq}) \times 50/M.$$

Doses can be calculated for different compartments; in the multicompartment approach, rather than total liver dose, both tumoral and non-tumoral dose are evaluated.

Taking into account the fact that there is no microsphere redistribution after embolization in the microvasculature and no biodegradation, it is assumed that microsphere deposition is limited to the liver (including tumors) and eventually lungs (if arterio-venous shunt is present). In this case, the activity of ^{90}Y within a VOI depends on the activity of ^{90}Y injected to the patient and the fraction of ^{90}Y uptake in this VOI [24].

The partition model provides a way to determine activity with more precision, although it requires the correct identification of absorbed dose to ensure the hepatic tolerability and depends on the possibility to simulate the treatment. By using the $^{99\text{m}}\text{Tc}$ -MAA distribution as a predictor for the subsequent ^{90}Y distribution, it may be used for multi-compartment dosimetry. The expected activities in each compartment are usually based on the distribution of $^{99\text{m}}\text{Tc}$ -MAA.

The compartment volumes (the injected liver, tumor, healthy injected liver, and non-injected liver) can be measured using CT, cone-beam CT or MR. Recently, however, it has been shown that volumes can be accurately measured using



SPECT/CT (corrected by attenuation). Although SPECT alone cannot achieve accurate volume measurement while depending only on the threshold used for the volume of interest (VOI) delineation, a phantom study demonstrated that SPECT/CT volume measurement can be accurate if the thresholding is guided by an anatomical visualization of the VOI on the fusion images, producing a mean error rate $<7\%$ [84]. Both Garin et al. [64] and Rodriguez-Fraile et al. [85] have used software allowing for semiautomatic generation of the VOI in the injected liver and tumor using an isocontour method. The threshold value was adjusted so that the isocontours of the volume of distribution of the ^{99m}Tc -MAA match on the fusion images with the boundaries of the liver and tumor [64].

Rodriguez-Fraile et al.'s study aimed to determine which imaging method used during SIRT work-up more accurately predicts the final target volume, either contrast-enhanced CT, ^{99m}Tc -MAA-SPECT/CT or cone beam-CT (CBCT) (see Fig. 5) [85]. The target volume in ^{99m}Tc -MAA-SPECT/CT was defined using the multimodality reading software Syngo.via for MI (Siemens Healthineers), where the “molecular tumor volume” or MTV in milliliters (ml) obtained was used as the ^{99m}Tc - MAA -SPECT/CT target volume. The isocontour threshold was set at 3% and visually adjusted to include the ^{99m}Tc -MAA uptake volume into the VOI (range = 1–9%). This value was used for the definition of the target value in 67% of the patients for ^{99m}Tc -MAA-SPECT/CT and in 71% of the patients for ^{90}Y PET/CT. In the CBCT, the target volume was obtained by adding the volumes of each slice, independent of anatomical landmarks. ROI were manually drawn in each slice involving the target/tumor volume [85].

The information obtained from ^{99m}Tc -MAA-SPECT/CT was determinant in 71% of the patients. It was able to define and



confirm the target volume in segmental and subsegmental treatments or after flow redistribution, and also helped to detect tumoral areas not receiving ^{99m}Tc -MAA with the selected arterial access. On the other hand, the use of ^{99m}Tc -MAA-SPECT/CT volumes reduces the risk of underdosing, while ^{99m}Tc -MAA-SPECT/CT tends to overestimate posttherapy dosimetry in tumor, being more accurate for the non-tumor liver dosimetric assessment.

The results showed that ^{99m}Tc -MAA-SPECT/CT predicted ^{90}Y PET/CT target volume better than CBCT or CECT, even for selective or superselective administrations. ^{99m}Tc -MAA SPECT/CT also showed dosimetric values more similar to those obtained with ^{90}Y PET/CT [85]. On the other hand, CBCT provided essential information for SIRT planning, such as ensuring the total coverage of the tumor and, in cases with more than one feeding artery, splitting the activity according to the volume of tumor perfused by each artery. Therefore, it was concluded that the joint use of ^{99m}Tc -MAA-SPECT/CT and CBCT optimizes dosimetric planning for SIRT procedures, enabling a more accurate personalized approach [85].

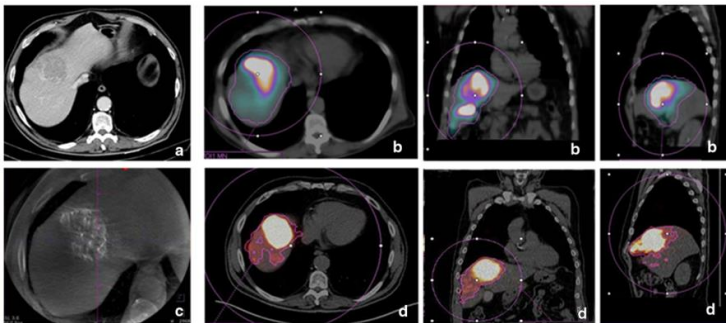


Fig. 5. ^{99m}Tc -MAA SPECT/CT and CBCT to optimize dosimetric planning for SIRT. (a) Contrast-enhanced computed

tomography (CECT) image in a patient with HCC located between segments IV and VIII. (b) Volumetric assessment of the target volume in SPECT/CT fusion images after the injection of ^{99m}Tc -MAA through IV and VIII segments arteries. The volume was obtained using a “volume of interest and isocontour” tool, drawn in purple. (c) C-arm cone-beam CT (CBCT) showing contrast uptake in the tumoral lesion with no perfusion in non-tumoral parenchyma. (d) Volumetric assessment of the final target volume in the ^{90}Y PET/CT fusion images. From Rodriguez-Fraile et al. [85]

The use of ^{99m}Tc -MAA SPECT/CT for volume measurement offers the advantage of providing a more functional evaluation of the volume. Garin et al. described two available methods for tumor segmentation. The first is morphological, with the tumor VOI delineated by means of CT, and then copied onto the SPECT imaging (or SPECT/CT) for count evaluation. The second method, based only on SPECT (or SPECT/CT), is more functional, where only the hypervascularized part of the tumor is taken into account, with its dosimetry providing the basis of the tumor dosimetry, excluding tumor necrosis. Finally, the nontumoral liver (NTL) volume can be defined by subtracting the tumor volume from the total liver volume.

Several dosimetry algorithms providing the physically absorbed dose D in SIRT are described including the medical internal radiation dose (MIRD) approach, Monte Carlo simulation, and kernel point evaluation [44].

Limitations of these methods

The main limitation of the mono-compartment methods is that the actual spatial dose distribution of an individual patient is neglected. They assume a homogeneous distribution between the tumor and the normal liver. The treated ‘mono-compartment’ encompasses both tumor and non-tumorous



tissue and does not differentiate between the two, even though these two recommended absorbed dose limits are markedly different [34]. Since these methods seek to prevent overdosing liver and lung parenchyma, these can result in under-dosing in some patients [86–88]. Furthermore, BSA was later shown to be a poor surrogate for liver volume, leading to underdosing in patients with large livers relative to their BSA and overdosing in relatively small livers [89].

The partition model is considered more accurate and personalized, and accounts for tumor avidity but assumes a uniform dose distribution within each compartment [56]. In fact, both the BSA and partition assume a homogeneous ^{90}Y -microsphere distribution [90,91], despite the fact that many studies have shown ^{90}Y -microsphere deposition heterogeneity at microscopic and macroscopic levels [37,90–93].

The compartment volumes (the injected liver, tumor, healthy injected liver, and non-injected liver) can be measured using CT, cone-beam CT or MR. Recently, however, it has been shown that volumes can be accurately measured using SPECT/CT (corrected by attenuation). Although SPECT alone cannot achieve accurate volume measurement while depending only on the threshold used for the volume of interest (VOI) delineation, a phantom study demonstrated that SPECT/CT volume measurement can be accurate if the thresholding is guided by an anatomical visualization of the VOI on the fusion images, producing a mean error rate $<7\%$ [71]. Garin et al. [59] used a software allowing for semiautomatic generation of the VOI in the injected liver and tumor using an isocontour method. The threshold value was adjusted so that the isocontours of the volume of distribution of the $^{99\text{m}}\text{Tc}$ -MAA match on the fusion images with the boundaries of the liver and tumor [59].



Voxel-based dosimetry

Doses can be calculated as a mean dose of a VOI, which is the simplest approach. However, doses can also be calculated at the voxel level. The shift towards personalized SIRT is essential and includes using voxel-based dosimetry methods. As Alsultan et al. mention, the next step in improving SIRT treatment planning may lie in voxel-based dosimetry [34]. In simple terms, a voxel is a three-dimensional pixel, and the reconstructed voxel is taken as the smallest independent spatial unit for activity [56]. Using voxel-based dosimetry one can extract information on the heterogeneity of the distribution of microspheres within each compartment. This is advantage with respect to the partition model, in which the absorbed dose is averaged over each compartment [79]. In addition to greater accuracy, dose map calculation provides analysis tools (dose profiles, isodose displays, dose-volume histograms or DVH) similar to those used in external- beam radiation therapy to help the medical team optimize treatment planning [56].

With voxel dosimetry, DVH can be obtained, and then a mixed parameter based on the dose and the volume can be generated. For example, the D70 is the minimum dose applied to 70% of a VOI and currently used with external beam radiotherapy [94].

According to the convolution method, it is considered that each voxel of the image is a specific radiation source, so that the dose absorbed in each voxel is the sum of the contributions from each source, assuming that the activity in each voxel is uniform. That is how a three-dimensional map is acquired, providing an image of the dose absorbed with ^{90}Y PET. The dosimetry process for SIRT is acquired through segmentation of the tumoral and non-tumoral liver, first with SPECT/CT for



Introduction. Steps in the procedure

the treatment simulation, and then with ^{90}Y PET/CT for treatment verification (Fig. 6).

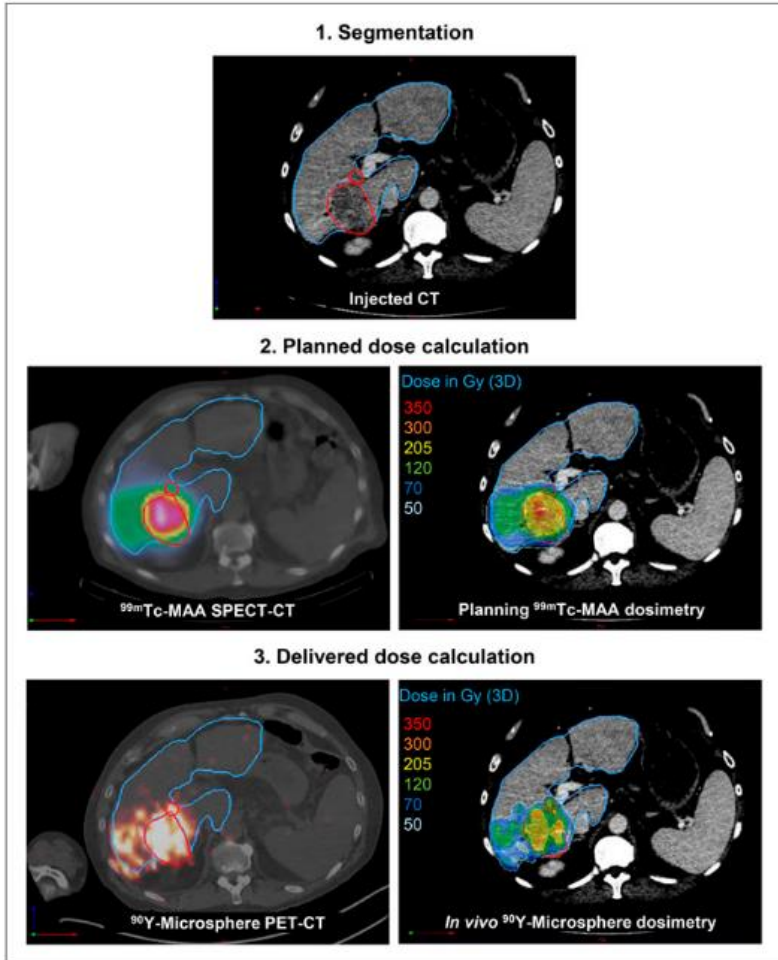


Fig. 6. Process of retrospective pre- and post-treatment dosimetry. Tumor and NTL are delineated in red and blue, respectively [56].

Activity calculation: Treatment protocol at Clínica Universidad de Navarra

The following comprehensive treatment protocol (Fig. 7) performed in our center for activity calculation is used with the aim of increasing safety and more accuracy in activity calculation [25]. When the BSA method is used, the activity must be reduced towards 0.8 GBq/L if the patient presents any of the following factors: small liver (less than 1.5 L) or tumor volume (less than 5 % of the liver tissue), concomitant cirrhosis or prior chemotherapy. Even in those situations in which none of these factors are present, for whole liver treatments it is advisable to reduce the activity calculated by the BSA method between 10 and 20%. If a selective treatment is planned, the partition method is used and the size and quality of the remnant liver segments must be taken into account. If both parameters are adequate, the activity that implies an absorbed dose by the tumor greater than or equal to 100 Gy may be prescribed. However, if the maximum dose is conditioned by the number and quality of the remnant liver, the non-tumoral liver tissue should not receive a dose greater than 40 Gy [25]

Therefore, taking into account toxicity a failure in global liver function (bilirubin, albumin, prothrombin time), the maximum tolerated absorbed dose by the healthy parenchyma varies according to the kind of treatment and the organ functional reserve, in which a lobar or segment treatment supports higher absorbed dose with respect to whole liver treatment, since the remainder of the tissue can supply the liver function [60]. With



the modified protocol at Clínica Universidad de Navarra, the incidence of REILD was reduced from 22.7% to 5.4% with respect to the standard protocol group. REILD appeared only in patients with cirrhosis or in non-cirrhotic patients exposed to systemic chemotherapy prior to RE.

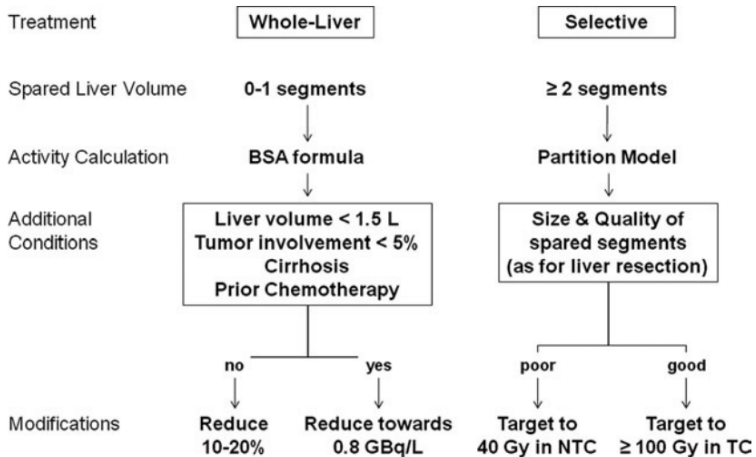


Fig. 7. Work-up of activity calculation in our modified protocol [30]. NTC: nontumor compartment, TC: tumor compartment.

2.4 Administration of treatment

The interval between pre-treatment evaluation and treatment should be as short as possible to avoid the revascularization of the arteries embolized during pre-treatment angiography. Once the activity to be administered is calculated, the treatment is administered after checking by means of angiography that no new collaterals have been formed. It is important to verify that the position/location of the catheter during the ^{99m}Tc -MAA simulation is consistent with the position during the



administration of ^{90}Y -microspheres [60]. Although factors such as flow, perfusion and nonlaminar hydrodynamics limit the ability to optimally reproduce position and flow dynamics, at least fluoroscopic reproduction of the catheter position should be performed during all administrations [26].

When using ^{90}Y -resin microspheres, contrast can be administered during the procedure to confirm vascular flow to the liver and the absence of retrograde arterial reflux.

Post-SIRT residual activity of microspheres in the vial, tubing system and syringe should be measured [26]. See Fig. 8.

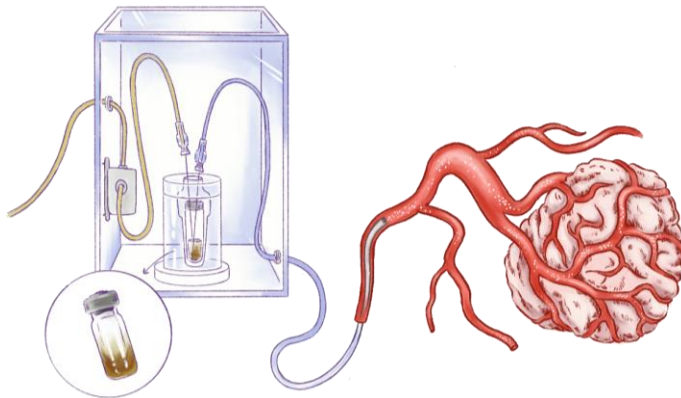


Fig. 8. Administration of treatment with ^{90}Y - resin microspheres. Illustration by Patri de Blas.

2.5 Verification of treatment and dosimetry with ^{90}Y PET

After the treatment, a study is performed to confirm the adequate deposition of microspheres ^{90}Y and detect the non-target activity, with ^{90}Y SPECT/CT (Bremsstrahlung) [2,44,45] or PET/CT. However, the image quality of ^{90}Y scintigraphy is not the best compared to other conventional

radiopharmaceuticals [55,95]. PET has been used for post-evaluation, since a small fraction of ^{90}Y also emits a pair of 0.511-MeV annihilation photons that can be detected by PET. As this disintegration is very improbable (only 32 of each 1,000,000 disintegrations of ^{90}Y) [96], there are limitations to the quality of the image and require a longer acquisition time.

Even so, the image quality of ^{90}Y PET is better than that of the Bremsstrahlung SPECT and better than the indirect image with $^{99\text{m}}\text{Tc}$ -MAA[97–104]. However, simulation studies with $^{99\text{m}}\text{Tc}$ -MAA before SIRT only depict what the microsphere biodistribution will likely be after injection. The benefit of post-SIRT imaging is that it provides an accurate estimation of the actual microsphere biodistribution [70].

The ^{90}Y PET/CT provides accurate information that represents the heterogeneity of the distribution of the microspheres within the lesion and the absorbed dose in each part of the lesion. It is useful to predict the response to treatment or the need for alternative or adjuvant treatment. Identifying technical failure with lack of uptake in the target liver parenchyma and/or in certain lesions allows consideration of additional therapies without delay [105].

According to the international and multidisciplinary expert panel convened in 2020 for optimization of SIRT with resin microspheres, post-SIRT verification with ^{90}Y PET/CT was recommended, and similarly post-SIRT dosimetry was also recommended, both with strong agreement among experts ($\geq 80\%$) [26].

Dosimetric parameters in post-SIRT studies may predict tumor response [57,98,106–110] and are associated with hepatic toxicity or overall survival [109,110].



Although there are methods for generating absorbed dose maps through data from ^{90}Y PET, there is no standardization as to the dose variable used to predict response to SIRT treatment. Various authors have used the mean absorbed dose [57,108,111]. In contrast, Kao et al. [106] used the minimum dose to 70% of the tumor volume (D70) and the percent of volume that receives > 100 Gy (V100).

3. ATROPHY- HYPERTROPHY COMPLEX

In order to look for a curative surgical treatment in patients with tumor(s) in one lobe, an evaluation of the liver function and volume must be performed (Fig. 9). The contralateral liver should have a certain volume in order to be adequate to avoid postoperative hepatic insufficiency and carry the burden of preserving hepatic function after partial or lobar hepatectomy. The future liver remnant (FLR) refers to the non-treated liver and may be expressed as a ratio to the total liver volume, the latter definition being more appropriate for surgical practice [21].

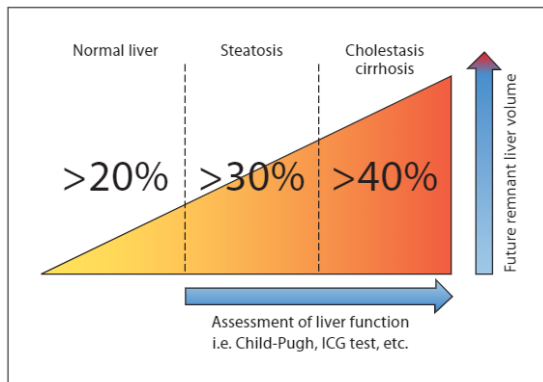


Fig. 9. Limit for safe hepatic resection [112].

Introduction. Atrophy- Hypertrophy Complex

In patients with a preserved hepatic function, a remnant of at least 25-30% is considered sufficient to prevent hepatic insufficiency [113]. However, in patients with cirrhosis, up to 40% should be preserved [114,115]. The importance of atrophy-hypertrophy complex is that it is a mechanism that can increase tumor resectability for curative surgical intervention in patients with insufficient FLR [116].

Therefore, patients with a lower FLR who don't qualify for surgery can benefit from SIRT as part of the oncologic treatment as an either primary or secondary objective to make a tumor resectable with enough FLR.

For patients with inadequate FLR, portal vein embolization (PVE) may be indicated to induce hypertrophy of the FLR. PVE has been shown to promote hypertrophy by 31% in the FLR at 4 to 6 weeks [114,117,118]. However, a major drawback of PVE is that tumors continue to grow during interval between PVE and liver resection [119]. Here is where interest in SIRT has grown, with the simultaneous goal of both achieving tumor control and inducing hypertrophy of FLR a bridge to resection for patients with small FLR [21,120,121].

Lobar SIRT treatment with ^{90}Y has been noted to induce ipsilateral atrophy of treated lobe, as well as simultaneous contralateral hypertrophy [122–125]. Following the systematic revision of Teo et al.[116], a hypertrophy of 26–47% was observed at an interval between 44 days to 9 months after unilobar SIRT, and slower than with other modalities such as portal vein embolization, where hypertrophy of 10-46% has been observed in 2-8 weeks after SIRT [117]. However, the patient cohorts were very heterogenous, so a meta-analysis was not attempted. In addition, dosage of ^{90}Y varied, which influence the magnitude of treatment effect, and this was not



studied in this article. The true degree of hypertrophy as well as the impact on dose were considered relatively unstudied and unknown [117].

The mechanism by which lobar SIRT induces contralateral hypertrophy is not completely known. Given that this hypertrophy is associated with ipsilateral atrophy, this suggests that it may be a compensatory mechanism. Total liver SIRT can cause atrophy [122,126,127], portal triaditis [47] and liver disease, including periportal fibrosis[128], fibrosis and regenerative activity in the periphery [129,130], where the maximum amount of radiation necrosis occurs. Similarly, portal vein embolization can produce contralateral hypertrophy and signaling pathways that provoke hepatic proliferation [131,132].

Vouche et al. [21] postulated that radiation induced parenchymal lesions and a decreased blood supply shrinks the irradiated lobe and induces the portal flow to redirect towards the contralateral lobe. According to this hypothesis, the portal flow redirection induces the contralateral lobe to increase in size and, correspondingly, increase its functionality[21,122]. This phenomenon of atrophy and compensatory hypertrophy has been a source of interest for Fernandez-Ros et al. [125], who demonstrated that the partial SIRT induces significant hypertrophy of the non-treated liver. In their study, subclinical liver damage was observed with an increase in bilirubin. In addition, it was also noted that the magnitude of the hypertrophy was lower in patients with cirrhosis and altered baseline bilirubin. A greater number of studies are required to determine the mechanism of this process and its relevance in the treatment of hepatic tumor with SIRT.



Introduction. Atrophy- Hypertrophy Complex

In a study by our group, the atrophy-hypertrophy complex and liver damage was studied in an animal model (this article has been sent for publication). SIRT with ^{90}Y - resin microspheres was performed in three groups of rabbits, with 0.3, 0.6 and 1.2 GBq. This corresponded to a predicted absorbed radiation of 200, 400 and 800 Gy, respectively. Contralateral lobe hypertrophy was detected after 0.6 GBq at 15 days (median increase 34%, non-significant) and after 0.3 GBq at 30 days (median increase 82%, $p=0.04$). Doses in the range of 200 Gy produced marked liver atrophy that was nonetheless tolerated and later compensated, and reproduced the atrophy-hypertrophy complex. It was described that this contralateral lobe hypertrophy could be secondary to both hepatocyte hyperplasia and hypertrophy, as the degree of hepatocyte hyperplasia was similar at days 15 and 30, thus suggesting that hepatocyte hypertrophy also contributes to progressive contralateral lobe enlargement. They emphasized that they observed a relationship of both atrophy and hypertrophy with the dose of radiation and referenced Palard et al.'s study [133], which found a dose-response effect in patients.

Another finding in that study was that marked atrophy in their model occurred with mild and transient elevation of transaminases, also similar to what happens in patients [125]. This negative, often subclinical effect on liver function in patients with hepatocellular carcinoma may impair prognosis after treatment[134]. While a degree of subclinical liver damage may be expected due to radiation, as an indirect consequence of the liver atrophy, careful patient selection for SIRT should be taken.



II. Hypothesis

The atrophy generated in a liver volume treated with SIRT, as well as the compensatory hypertrophy produced in the non-treated liver, depend at least in part on the dose of radiation absorbed and consequently can be predicted by dosimetric parameters obtained from the post-treatment ^{90}Y PET/CT.



III.Objectives

1. Main objective

To evaluate the relationship between the dose of radiation absorbed by the treated liver (measured in the ^{90}Y PET/ CT study) and the development of atrophy of the treated liver and compensatory hypertrophy.

2. Secondary objectives

Objective 1. To determine the magnitude and relationship between atrophy of the treated liver, hypertrophy of the non-treated liver and increase in FLR after lobar or extended lobar SIRT.

Objective 2. To define which parameters in the absorbed dose-volume histogram best predict atrophy of the treated liver, hypertrophy of the non-treated liver, and increase in future liver remnant (FLR).

Objective 3. To determine the best dosimetric cut-off to predict an increase in FLR.

Objective 4. To study which clinical and volumetric variables of the patient and the tumor influence the development of atrophy of the treated liver, hypertrophy of the non-treated liver, and increase in FLR.

Objective 5. To study the relationship between atrophy of the treated liver and clinical liver damage.



IV. Materials and methods

1. PATIENT COHORT. INCLUSION CRITERIA AND CLINICAL OUTCOMES

This retrospective study included all patients with primary or secondary hepatic tumors treated with ^{90}Y -loaded resin microspheres (SIR-Spheres, Sirtex Medical Europe GmbH) at our institution between December 2011 and December 2019 in whom:

- (i) lobar (right or left) or extended lobar (right lobe plus segment IV) SIRT was performed
- (ii) ^{90}Y PET/CT (^{90}Y PET) was obtained (post-treatment)
- (iii) one or more cross-sectional imaging studies were completed at least within two months after SIRT.

Imaging studies at follow-up were scheduled by clinicians at different points in time, depending on tumor type, treatment aim and other factors. For the purpose of this study, they were grouped in three time intervals, namely 0-2 months (T1), 2-6 months (T2), and at 6-12 months (T3) after SIRT. In patients that received a second SIRT treatment or were submitted to any hepatic intervention after SIRT, including hepatectomy or biliary drainage, their subsequent images were excluded from analysis.

The current general inclusion criteria for SIRT in our center are:

- (i) an unequivocal diagnosis of unresectable cancer with liver-only or liver-dominant tumor burden
- (ii) a life expectancy of >3 months



Materials and methods. Patient cohort. Inclusion criteria and Clinical Outcomes

- (iii) an Eastern Cooperative Oncology Group (ECOG) performance status of 0–1
- (iv) a lung shunt fraction (LSF) $\leq 20\%$
- (v) adequate pulmonary, hematological, hepatic and renal function[60].

As in many patients SIRT was not applied to induce hypertrophy of the FLR as a primary aim (i.e. palliative or curative intent, as salvage therapy), FLR was not necessarily insufficient. However, for analytical purposes, the patients were divided into two groups according to baseline FLR: $<30\%$ (would require hypertrophy to prevent postoperative liver failure [113]) and $\geq 30\%$ (would not require hypertrophy to prevent postoperative liver failure unless cirrhotic [114,115].). An FLR $\geq 40\%$ was considered adequate for both patients with and without cirrhosis[114,115].).

Clinical and laboratory data were retrospectively collected from each time point. The ALBI score was calculated using the formula: ALBI score = $(\log_{10} \text{bilirubin} \times 0.66) + (\text{albumin} \times -0.085)$, and grades were attributed as follows: grade 1 if score ≤ -2.60 ; grade 2 if score > -2.60 but ≤ -1.39 ; grade 3 if score > -1.39 [135].

Specific SIRT complications that were searched in medical records included:

- a) post-radioembolization syndrome (PRS), defined as the occurrence of self-limited fever, fatigue, abdominal pain, nausea, vomiting, or anorexia [136];
- b) radioembolization-induced liver disease (REILD) [2];
- c) non-target delivery of radiation to lung or gastrointestinal tract (pneumonitis, gastrointestinal ulceration, cholecystitis).



The presence of decompensation events in cirrhotic patients was assessed (classically, the acute development of ascites, gastrointestinal hemorrhage or hepatic encephalopathy)[137] up to 9 months after SIRT. Tumor response was assessed using Response Evaluation Criteria in Solid Tumors version 1.0 [138]. It was evaluated until 9 months after SIRT or until a surgical, systemic or new local treatment in the same lobe was used. Patients who received hepatectomy post-SIRT were also recorded.

2. ETHICS

The institutional Ethics Committee at the University of Navarra approved the protocol (212/2019) for this retrospective study and waived the need for patient informed consent. The study was performed in accordance with the ethical standards laid down in the 1964 Declaration of Helsinki and all subsequent revisions.

3. PRE-TREATMENT AND TREATMENT

Pre-treatment investigations included CT or MRI scans, blood cell count and serum biochemistry. Our protocol for SIRT has already been published [25]. In summary, images were carefully assessed before angiographic mapping of the abdominal and hepatic arteries. Planar scans of the lung and liver area in anterior and posterior views were acquired after injection of ^{99m}Tc -MAA into selected arterial branches followed by SPECT/CT. They were used for a) calculation of LSF, b) calculation of tumor/non tumor (T/N) ratio, and c) detection of any non-target infused liver volume and the unintentional delivery of radioactive particles to organs outside the liver.



For lobar or lobar extended SIRT (all the patients in this study), the prescribed ^{90}Y activity was calculated using the partition model, taking into account LSF, T/N ratio, target tumor volume and target hepatic volume from the $^{99\text{m}}\text{Tc}$ -MAA study, considering optimal absorbed doses by tumoral and non-tumoral volumes [25]. In general terms, if the size and quality of spared segments was good, the absorbed dose to the tumor volume was targeted to ≥ 100 Gy. If not, the dose of the non-tumoral liver was targeted to no greater than 40 Gy.

SIR-Spheres were injected within 15 days of the $^{99\text{m}}\text{Tc}$ -MAA scan. In all cases a same-day calibration 3 GBq vial was used (44 ± 2.6 million spheres per vial)[25].

4. PET ^{90}Y IMAGING

The day after SIRT (14-17 hours after treatment), ^{90}Y PET imaging was performed to evaluate extrahepatic activity deposition and intrahepatic microsphere distribution, and to permit voxel dosimetry quantification.

^{90}Y PET images were acquired on a Siemens Biograph mCT TrueV scanner (Siemens Medical Solutions, USA). The ^{90}Y PET acquisition duration was 30 min (10 min per bed position) where complete chest and abdomen areas were included. ^{90}Y PET images were reconstructed on 200 x 200 matrix using an iterative method (OSEM) with 1 iteration and 21 subsets, including algorithms for PSF (point spread function) recovery and TOF (time of flight) calculation, as well as a Gaussian post-reconstruction filter (5 mm) with CT-based correction, as published elsewhere [139]. CT images were acquired in a spiral mode (pitch 1.2, 120 kVp, and care dose 4D).



5. DOSIMETRIC ANALYSIS

Retrospective ^{90}Y PET 3D-based voxel dosimetry was performed using a dedicated treatment-planning system (PLANET[®] Dose; DOSIsoft SA). PLANET Dose is an internal dosimetry software platform which can provide dosimetry based on ^{99}Tc -MAA-SPECT, liver-lung shunt based on SPECT, dosimetry based on ^{90}Y PET and comparison between treatment planning from $^{99\text{m}}\text{Tc}$ -MAA SPECT vs. in vivo control from ^{90}Y PET.

The image files for baseline and follow up studies were imported. Baseline and follow-up images were co-registered with the ^{90}Y PET/CT according to rigid registration (see Fig. 10), using the software tool-set for registration assessment: checkerboard, adjustable magnifying glass overlapping and image fusion transparency.

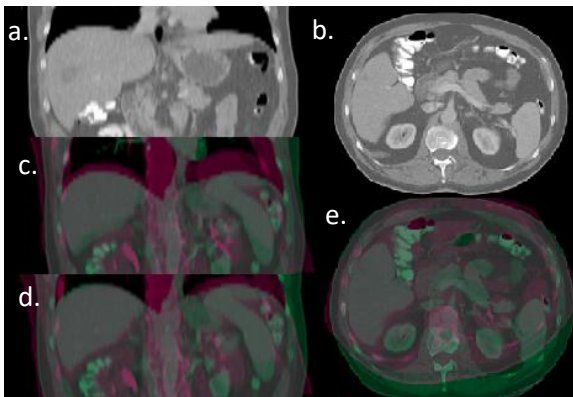


Fig. 10. Rapid registration with PLANET[®] Dose. (a, b) Contrast-enhanced CT, coronal (a) and axial (b). Proposal for registration of contrast-enhanced CT+ CT of the PET and (c) final registration between contrast-enhanced CT+ CT after manual millimetric adjustment of the liver contour (d, e)

The segmentation of the image was performed, where anatomic outlines were manually drawn on the axial plane of the corresponding volume from top to bottom (see Fig. 11).

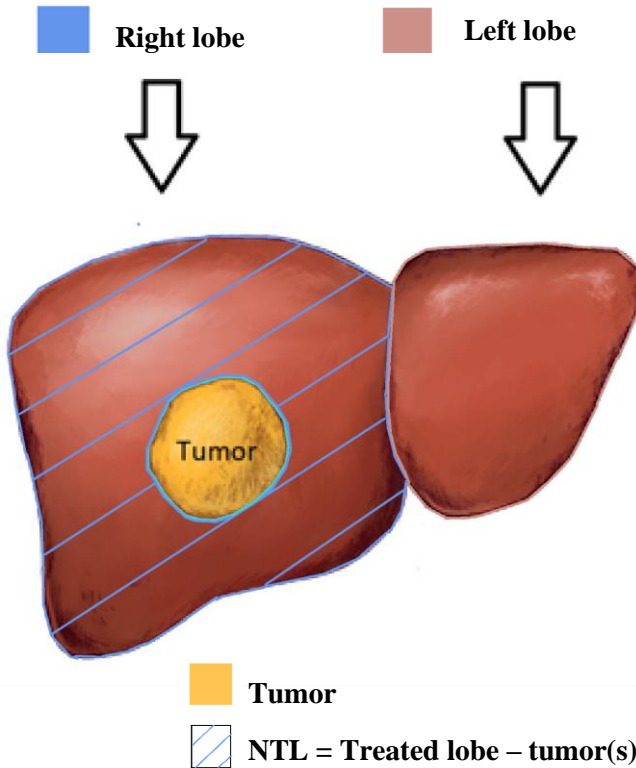


Fig. 11. Schematic representation of the segmentation process after right lobar SIRT. The treated side is segmented (right lobe, blue) as well as the contralateral lobe (left lobe, tan), that is formed by the non-treated segments. The treated target liver includes the tumor (yellow) and the non-tumoral liver (NTL, blue lines). The NTL was obtained by excluding the tumor volume from the target liver.

This was done on the portal phase contrast-enhanced CT if available, on MR images or on the CT of the PET/CT by a nuclear medicine resident (see Fig. 12).

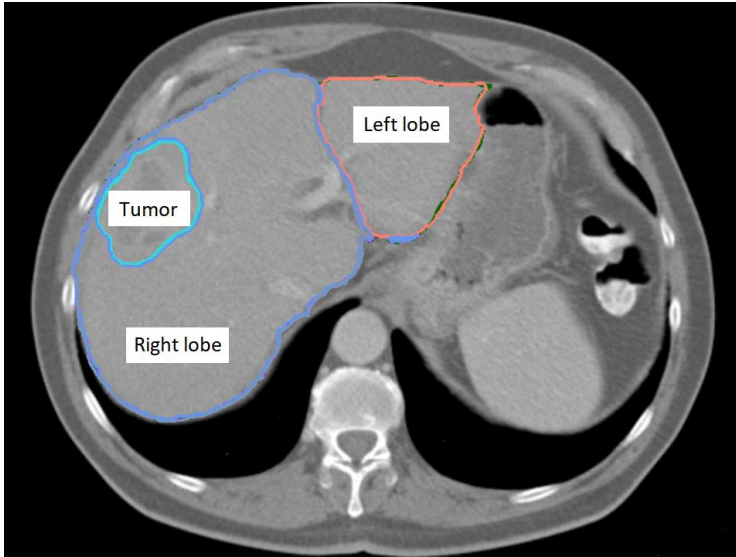


Fig. 12. Anatomical contours on contrast-enhanced CT of right lobe (blue), tumor (green) and left lobe (tan).

First, the treated lobe was segmented, either right lobe, right lobe plus segment IV or the left lobe according to the treatment approach. The software converted these outlines into 3D volumes in milliliters. Then the contralateral, non-treated volume was defined. These outlines were aided by ^{90}Y distribution on PET, particularly with the limit between the left and right liver lobes. When a discrepancy was observed between the anatomical limit of left and right lobe vs. the treated and non-treated liver according to PET distribution, the latter was chosen to establish the limit between treated and non-treated liver.

Contours were propagated to the ^{90}Y PET and adjusted manually as needed in order to correct millimetric errors in registration. The total liver volume was acquired through volumetric Boolean sum (addition of the two complementary parts “AND” as a new structure). Within the treated volume, the delineation of the tumor was also contoured on the axial planes. The non-tumoral target liver (NTL) volume was defined by excluding the tumor volume from the target liver (Fig. 13).

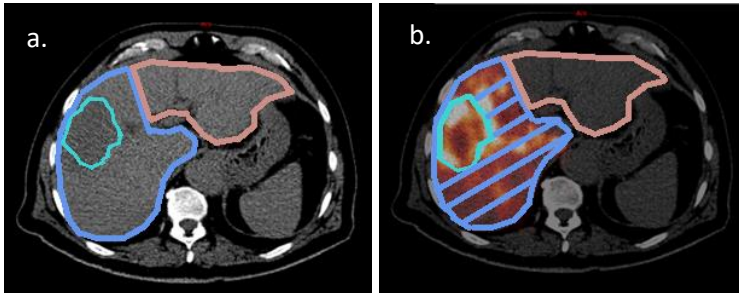


Fig. 13. Segmentation of non-tumoral liver (NTL) on ^{90}Y PET. (a) CT and (b) ^{90}Y PET/CT on the axial plane. After the right lobe (blue), left lobe (tan) and tumor(s) (green) are segmented on the CT (a) and propagated to the PET/CT (b), the NTL is obtained by excluding the tumor volume from the target liver (blue lines).

A 3-dimensional dose map was calculated using a kernel convolution algorithm at the voxel level and dose/volume histograms (DVH) were extracted (Fig. 14). The mean dose (Dmean) to the total target liver, NTL and tumor volumes were studied, as well as other metrics extracted from DVH (Fig. 14): the minimum dose to 20%, 50%, 70%, 90% 95% and 98% (D20, D50, D70, D90, D95 and D98, respectively) of the NTL or tumor volume. The percentage of the volume receiving at

least 30, 40, 50, 70, 100 and 120 Gy was also obtained (V30, V40, V50, V70, V100 and V120 respectively).

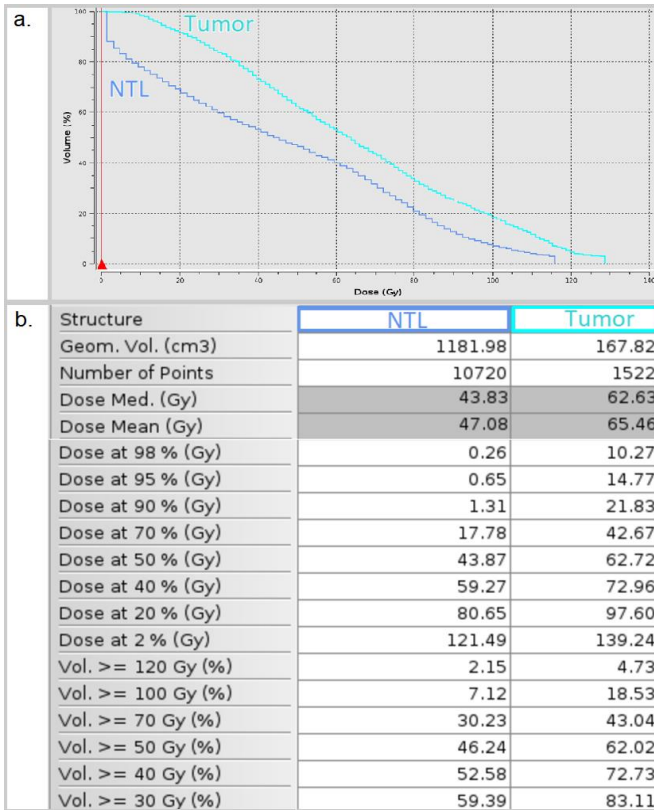


Fig. 14. Dose-volume histograms (DVH) and extracted dosimetric parameters. (a) DVH to the tumor (green) and non-tumoral liver or NTL (blue), and (b) the dosimetric variables extracted from them: dose mean, the minimum dose to 98%, 95%, 90%, 70%, 50% and 20% (D20, D50, D70, D90, D95 and D98, respectively) of the volume, and percentage of the volume receiving at least 120, 100, 70, 50, 40 and 30 Gy (V120, V100, V70, V50, V40, V30).



For ^{99m}Tc -MAA, the voxel dosimetry analysis was not performed. Mean doses estimated to the tumor and NTL were obtained by formula derived from the ^{99m}Tc -MAA study (bidimensional T/N ratio and LSF), and from CT/MRI (tumor volume and non-tumor volume) and used for activity calculation. Median (IQR) dose to the NTL and to the tumor were compared between ^{99m}Tc -MAA and ^{90}Y PET.

6. VOLUMETRIC ANALYSIS

Atrophy and hypertrophy were assessed as absolute (ml) and relative (%) changes between volumes at T0 (corresponding to the most recent CT or MR images prior to SIRT), and T1, T2 and T3.

The FLR was defined as the ratio between the volume of non-treated liver and total liver volume. The FLR was calculated at T0, T1, T2 and T3. Maximal hypertrophy and its time of occurrence were also calculated.

7. STATISTICAL ANALYSIS

Categorical variables were expressed in percentage, while quantitative variables were expressed in mean \pm standard deviation for normal distributions or median (interquartile range: IQR) for non-normal distributions.

Univariate regression analysis was performed in the entire cohort, and in patients with FLR $< 30\%$ and $\geq 30\%$. Dosimetric variables considered were injected activity, mean dose to tumor and NTL according to ^{99m}Tc -MAA dosimetry by formula, as well as parameters extracted from DVH to the tumor and NTL by 3D voxel-based dosimetry from ^{90}Y PET mentioned in IV Materials and Methods, 5. Dosimetric



analysis. Clinical variables considered were age, sex, presence of cirrhosis, baseline laboratory values (total bilirubin, aspartate aminotransferase or AST, alanine aminotransferase or ALT, gamma-glutamyl transferase or GGT, alkaline phosphatase and serum albumine), prior chemotherapy, prior TACE, treatment-naïve status, chemotherapy post-SIRT. Other variables considered were the presence of primary vs. secondary tumors, unifocal vs. multifocal tumors, and SIRT treatment approach: right lobar, extended right lobar or left lobar). Finally, volumetric variables were considered (target and non-target liver volume, tumor volume, tumors larger or smaller than 100 ml, and tumor to target liver volume ratio).

Variables associated with hypertrophy or increase in FLR in the total cohort with a p value < 0.2 were further considered; **multivariate analyses** were performed to identify the best predictors of atrophy, hypertrophy and increase in FLR in patients with FLR $< 30\%$ and $\geq 30\%$. Adjusted R^2 was obtained in order to quantitatively measure of how well the independent variables account for the outcome, ranging from 0 (the independent variables do not explain the outcome) to 1 (the independent variables completely account for the outcome).

The correlation between atrophy of the treated lobe and contralateral hypertrophy was also determined with Spearman's Rho. The concordance between these last two variables was measured by means of Lin's concordance coefficient.

Receiver operator characteristic (ROC) curves were used to identify optimal cut-off points for prediction of increase in FLR to $\geq 30\%$ and $\geq 40\%$ (the latter, an adequate FLR for surgery even in cirrhotic patients [112]). Sensitivity, specificity, positive predictive value (PPV), negative



predictive value (NPV), positive likelihood ratio (LR+), negative likelihood ratio (LR-) and accuracy of predictors were calculated. Different dosimetric and volumetric parameters were correlated with atrophy of the treated liver and contralateral hypertrophy through Spearman's Rho. Volume changes in the total target liver, in NTL as well as in the non-treated liver (in ml and percentage change) between different time periods were studied using the Wilcoxon test for related samples. Atrophy and hypertrophy in cirrhotic and non-cirrhotic patients, as well as in patients with other clinical variables were compared using the Mann-Whitney-U Test.

Univariate regression analysis was also performed in the entire cohort in order to study dosimetric variables associated with increase in bilirubin after SIRT (as a surrogate for liver damage), as well as basal bilirubin as a clinical variable. Dosimetric variables considered were injected activity, mean dose to tumor and NTL according to ^{99m}Tc -MAA dosimetry by formula; and 3D voxel based in ^{90}Y PET parameters (mean dose and DVH values to the tumor and NTL mentioned in IV Materials and Methods, 5. Dosimetric analysis). Variables associated with increase in bilirubin after SIRT with a p value < 0.2 were further considered for multivariate analyses. R^2 was obtained.

Stata version 12.0 (Stata Corporation, College Station, Texas, USA) was used for statistical analysis. Values of $p < 0.05$ was considered statistically significant.



V. Results

RESULTS. PATIENT, TREATMENT CHARACTERISTICS AND OUTCOMES

Fifty-six patients met patient selection criteria and their general characteristics are summarized in Table 3. Most patients had primary liver tumors (71.4%) and 40.4% had cirrhosis. In baseline imaging scans (T0), 39 patients (69.6%) had a CT and 17 patients (30.4%) had an MRI. Liver and hematological functions were basically preserved, with total bilirubin at baseline ≤ 2 mg/dl. During follow-up, 51 patients had imaging studies at T1, 45 at T2, and 23 at T3. Median time from SIRT was 1.79 months (IQR: 0.63) for T1, 4.12 months (IQR: 1.45) for T2, and 8.97 months (IQR: 2.53) for T3.

Dosimetric parameters are summarized in Table 4. The median (IQR) of Dmean to the NTL and to the tumor varied according to the presence of cirrhosis. In the 19 patients with cirrhosis, the median predicted dose to the NTL in ^{99m}Tc -MAA was 43 Gy (38-59 Gy), and true median with ^{90}Y PET was 37.5 Gy (28.3-48 Gy), of which 13/19 patients received a Dmean to NTL ≤ 40 Gy and 6/19 received > 40 Gy.

Clinically, post-radioembolization syndrome occurred in ten patients (17.8%). Two patients with gastric or duodenal uptake detected on ^{90}Y PET developed a gastric and a duodenal ulcer respectively, diagnosed two to three months after SIRT, both treated symptomatically and one requiring endoscopic treatment. No patients developed gastrointestinal hemorrhage. Four cirrhotic patients and two non-cirrhotic patients with progressive disease developed ascites within 9 months after SIRT, of whom one required paracentesis. One cirrhotic patient with progressive disease developed hepatic encephalopathy.



Results. Patient, Treatment Characteristics and Outcomes

Six patients were lost to follow up, one patient died at two months after SIRT, and five were followed in another hospital (images were made available but not clinical data). Out of the remaining 50 patients, 10 showed stable disease, 15 obtained a partial response, and 4 obtained a complete response. After SIRT, 11 patients (19.6%) underwent hepatectomy. Progressive disease was observed in 21 patients (6 ipsilateral to the treated lobe, 11 contralateral and 4 bilateral). One patient with progressive disease died 5 months after SIRT.



Results. Patient, Treatment Characteristics and Outcomes

Table 3. General characteristics of patients in the present series

Characteristics	N	(%)
Type of Tumor		
• Primary liver tumors	40	71.4
Hepatocellular carcinoma (HCC)	29	51.8
Cholangiocarcinoma (CCA)	9	16.1
Mixed HCC/CCA	2	3.6
• Liver metastases		
Colorectal cancer	16	28.5
Neuroendocrine tumors	7	12.5
Other	4	7.1
	5	8.9
Prior therapies		
Hepatic resection	10	17.8
Radiofrequency ablation	11	19.6
Transarterial chemoembolization	12	21.4
Prior chemotherapy	22	39.3
Antiangiogenic drugs	6	10.7
Number of nodules		
Single	16	28.6
Multiple	40	71.4
Tumor burden <100 ml	28	50
Median: 31.6, IQR 50.5 ml		
Tumor burden ≥ 100 ml	28	50
Median: 332.2, IQR 400.7		
Largest tumor volume: 1495 ml		
Cirrhosis	19	40.4
SIRT approach		
Right lobar	38	67.9
Extended right lobar (right lobe + segment IV)	6	10.7
Left lobar	12	21.4



Results. Patient, Treatment Characteristics and Outcomes

Laboratory data	Median	IQR
AST, UI/l	31	22
ALT, U/l	27	24
Alkaline phosphatase, UI/l	109	73
γ -GTP, UI/l	115.5	183
Total bilirubin, mg/dl	0.55	0.43
Albumin, g/dl	3.78	0.665
ALBI score	-2.62	0.35
Platelets, 10 ⁹ /l	177	125
International Normalized Ratio (INR)	1.1	1

HCC: Hepatocellular carcinoma, CCA: Cholangiocarcinoma, ALBI score: albumin-bilirubin score



Results. Patient, Treatment Characteristics and Outcomes

Table 4. Dosimetric Parameters

Variables	Median (IQR)
• Injected Activity	1.4 (1.05) GBq
• Total target liver	
- Dmean in ⁹⁰ Y PET	52.84 (27.38) Gy
• NTL	
- Dmean in ^{99m} Tc-MAA	47 (36) Gy
- Dmean in ⁹⁰ Y PET	42.7 (30.7) Gy
- D20 in ⁹⁰ Y PET	63.6 (41.9) Gy
- D40 in ⁹⁰ Y PET	42.2 (35.4) Gy
- D50 in ⁹⁰ Y PET	35.3 (30.2) Gy
- D70 in ⁹⁰ Y PET	22.2 (21.5) Gy
- D90 in ⁹⁰ Y PET	9.6 (11.4) Gy
- D95 in ⁹⁰ Y PET	5.7 (7.6) Gy
- D98 in ⁹⁰ Y PET	2.6 (3.7) Gy
- V30 in ⁹⁰ Y PET	59.6 (31.7)%
- V40 in ⁹⁰ Y PET	43.4 (36.1)%
- V50 in ⁹⁰ Y PET	30 (35)%
- V70 in ⁹⁰ Y PET	17.7 (27.1)%
- V100 in ⁹⁰ Y PET	6.7 (13.9)%
- V120 in ⁹⁰ Y PET	3.8 (7.5)%
• Tumor	
- Dmean predicted from ^{99m} Tc-MAA	117 (86) Gy
- Dmean in ⁹⁰ Y PET	96.1 (64.5) Gy
- D20 in ⁹⁰ Y PET	139.4 (81.5) Gy
- D40 in ⁹⁰ Y PET	102.4 (82.7) Gy
- D50 in ⁹⁰ Y PET	88.3 (75.8) Gy
- D70 in ⁹⁰ Y PET	65 (56.2) Gy
- D90 in ⁹⁰ Y PET	38 (50.4) Gy



Results of Objective 1

-	D95 in ⁹⁰ Y PET	24.4 (46.6) Gy
-	D98 in ⁹⁰ Y PET	16 (41.8) Gy
-	V30 in ⁹⁰ Y PET	91.8 (21.1)%
-	V40 in ⁹⁰ Y PET	88.9 (28.6)%
-	V50 in ⁹⁰ Y PET	82 (37.1)%
-	V70 in ⁹⁰ Y PET	66.7 (45.4)%
-	V100 in ⁹⁰ Y PET	41.7 (43.9)%
-	V120 in ⁹⁰ Y PET	29 (47.8)%

IQR: interquartile range, Dmean: mean dose (Gy), NTL: non-tumoral target liver D20, D40, D50, D70, D95, D98: The minimum dose to 20%, 40%, 50%, 70%, 95%, 98% respectively of the volume in Gy, V30, V40, V50, V70, V100, V120: percent of treated volume that receives at least 30, 40, 50, 70, 100, and 120 Gy respectively

RESULTS OF OBJECTIVE 1

To determine the magnitude and relationship between atrophy of the treated liver, hypertrophy of the non-treated liver and increase in FLR after lobar or extended lobar SIRT.

Atrophy and hypertrophy

There was a progressive decrease in the volume of the treated segments (Fig. 15, Table 5) that was statistically significant in each time period compared to the previous one. These results remained consistent in patients in whom the right hemi-liver or right + segment IV were treated. A progressive increase in the volume of the non-treated liver was observed (Fig. 15, Table 5). This was statistically significant between T0 and T1 ($p < 0.001$), and between T1 and T2 ($p=0.002$), but not between T2 and T3 ($p=0.178$).



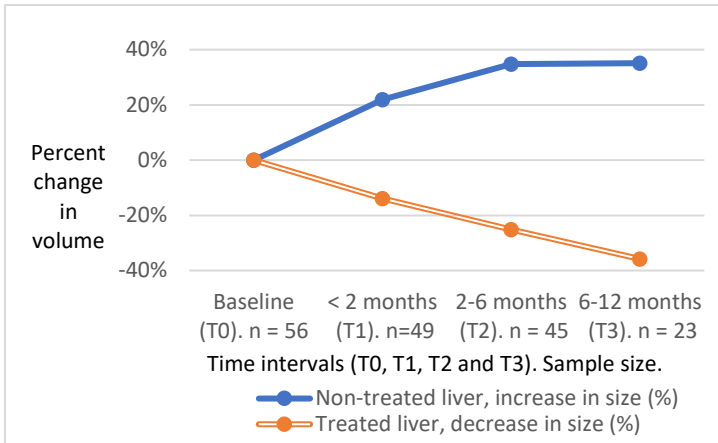


Fig. 15. Changes in volume (%) of the treated (blue) and non-treated liver (orange) after SIRT at baseline (T0), ≤ 2 months (T1), 2-6 months (T2) and 6-12 months (T3)

Total liver volume progressively decreased, although differences were not statistically significant in any time period. Compared to T0 (1919.7 ± 671.8 ml), total liver volume decreased at T1 (1891.2 ± 725.5 ml; $p=0.290$), to T2 (1791 ± 639.8 ml; $p=0.052$), and T3 (1567.7 ± 522.9 ml; $p=0.059$), because hypertrophy of the non-treated liver partially compensated for the atrophy of the treated segments. Maximal hypertrophy was 36.40 ± 40.64 % and mostly at T2 (time to maximal hypertrophy: 4.47 ± 2.82 months).

Increase in FLR

FLR progressively increased in all patients, including patients with FLR < 30% and ≥ 30% at T0 (see Table 5).



Table 5. Atrophy of the treated liver, hypertrophy of the non-treated liver and future liver remnant at baseline and during follow-up

	T0	T1	T2	T3
Atrophy of the treated liver				
Change in %*		-13.9 ± 13.4	-25.1 ± 18.7	-35.8 ± 17.9
Volume in ml	1183.1 ±	1037.9 ±	904.9 ±	679.9 ±
<i>p</i> value**	571.3	519.7	522.1	391.7
		< 0.001	< 0.001	0.007
Hypertrophy of the non-treated liver				
Change in %*		+21.9 ± 29.8	+34.8 ± 54.4	+35.1 ± 35.2
Volume in ml	762 ± 379	882.5 ± 514	906.2 ±	959.1 ± 356
			399.8	
<i>p</i> value**		< 0.001	0.002	0.178
Future liver remnant (FLR; %)				
All patients	40.4 ± 17	46.1 ± 17	51.9 ± 17.3	64.5 ± 16.5
<i>p</i> value**		< 0.001	< 0.001	0.002
FLR < 30% at baseline	25.2 ± 4.4	32.7 ± 9.4	38.1 ± 11.6	44.7 ± 12.1
<i>p</i> value**		< 0.001	< 0.001	0.225
FLR ≥ 30% at baseline	50.3 ± 14.6	55.4 ± 14.8	62 ± 13.3	70 ± 13.1
<i>p</i> value**		< 0.001	< 0.001	0.004

FLR future liver remnant, T0 baseline, T1 0–2 months after SIRT, T2 2–6 months after SIRT, T3 6–12 months after SIRT

Mean ± standard deviation. Positive and negative changes are indicated with (+) and (-) respectively.

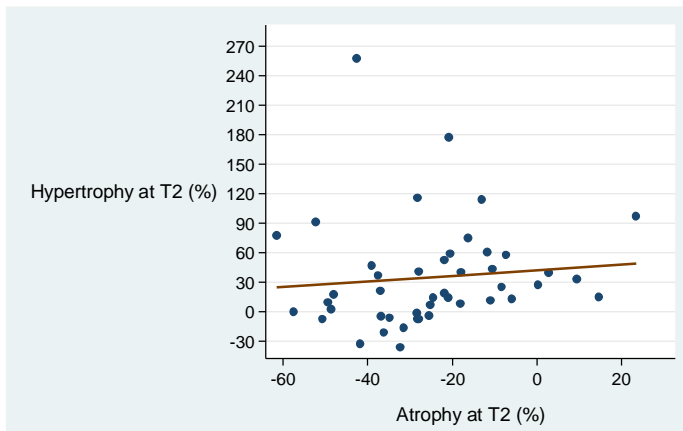
** Compared to baseline*

*** Compared to the previous time period*



Moreover, a weak correlation was observed between atrophy of the treated volume and hypertrophy of the non-treated liver (see Fig. 16). Spearman's Rho correlation of these variables was -0.213 in T1, 0.362 in T2 and 0.351 in T3). Concordance between both variables showed a Lin coefficient of 0.308.

Fig. 16. Scatter plot between atrophy of the treated volume and hypertrophy of the non-treated volume at T2



Blue dots represent cases, with their respective percent of atrophy of the treated volume and percent of hypertrophy of the non-treated volume at T2

RESULTS OF OBJECTIVE 2

To define which parameters in the absorbed dose-volume histogram best predict atrophy, hypertrophy, and increase in FLR.

Analyses focused on atrophy and hypertrophy between T0 and T2, given that the number of patients with available imaging

studies was larger in T2 than in T3, and T2 is when maximal hypertrophy was mostly found.

Univariable regression

Atrophy

No dosimetric parameter related to the dose to the NTL was significantly associated with atrophy of the treated volume at T2. Injected activity approached but did not reach significance ($p=0.06$). Atrophy of the treated volume was also not significantly associated with any dosimetric variable related to tumor dose or tumor size.

Hypertrophy and increase in FLR

Regression results of dosimetric variables associated with hypertrophy and increase in FLR are shown in Table 6, for all patients and subgroups according to baseline FLR. For every variable, the three rows express the slope, 95% confidence intervals and p value. The slope represents how much you can expect Y (hypertrophy or increase in FLR) to change as X (below, dosimetric variables) changes. For example, in patients with baseline FLR < 30%, hypertrophy is expected to increase by 2% for every 1% increase in the percent of the NTL that receives at least 30 Gy or NTL-V30 (95% CI: 0.61-3.36%).



Table 6. Univariate regression analysis results. Dosimetric variables associated with hypertrophy and increase in FLR.

		All patients		Patients with baseline FLR < 30 %		Patients with baseline FLR ≥ 30 %	
		Hypertrophy	FLR increase	Hypertrophy	FLR increase	Hypertrophy	FLR increase
Dosimetric Variables							
Injected activity	Slope	14.324	15.36	-3.67	7.50	11.72	11.84
	95% CI	10.03 - 38.68	(-1.92) - 32.64	(-62.34) - 55.00	(-32.86) - 47.87	(-6.26) - 29.70	(-3.66) - 27.34
	<i>p</i>	0.242	0.08	0.897	0.7	0.191	0.128
V30 of NTL	Slope	0.53	0.55	1.98	1.44	0.12	0.15
	95% CI	(-0.04) - 1.10	0.05 - 1.06	0.61 - 3.36	0.52 - 2.36	-0.41 - 0.64	-0.31 - 0.61
	<i>p</i>	0.066	0.033*	0.007*	0.004*	0.653	0.509
D95 of NTL	Slope	1.62	1.60	1.98	1.48	0.15	1.49
	95% CI	(-0.37) - 3.61	0.20 - 3.00	(-1.27) - 5.23	(-0.75) - 3.71	(-1.99) - 2.29	(-0.27) - 3.25
	<i>p</i>	0.107	0.026*	0.215	0.179	0.888	0.093
D98 of NTL	Slope	2.53	2.38	2.61	1.96	0.43	2.64
	95% CI	(-0.16) - 5.23	0.48 - 4.27	(-1.6) - 6.87	(-0.96) - 4.87	(-2.95) - 3.81	(-0.09) - 5.38
	<i>p</i>	0.065	0.015*	0.214	0.176	0.794	0.058
Dmean to NTL (MAA)	Slope	.06	0.03	1.22	.76	-.20	-.12
	95% CI	(-.39) - .49	(-0.31) - 0.37	.18 - .72	(-.05) - 1.58	(-.52) - .10	(-.40) - .15
	<i>p</i>	0.801	0.860	0.024*	0.06	0.18	0.367
Dmean to NTL (PET)	Slope	.26	0.17	2.5	2.03	-.03	-.10
	95% CI	.39 - .92	(-0.31) - 0.65	.72 - 4.29	.92 - 3.13	(-.03) - .20	(-.40) - .15
	<i>p</i>	0.422	0.475	0.009*	0.001*	0.86	0.545

V30: percent of volume that receives at least 30 Gy, NTL: non-tumoral target liver, D95: dose that 95% of the volume receives, D98: dose that 98% of the volume receives, Dmean: mean dose, MAA: in ^{99m}Tc-MAA SPECT, PET: ⁹⁰Y PET.

* Statistically significant *p* values (<0.05) of predicted are highlighted with an asterisk.

NTL-Dmean, obtained from ^{99m}Tc-MAA and ⁹⁰Y PET, was significantly associated with contralateral hypertrophy among patients with T0 FLR < 30 %. Similarly, NTL-Dmean obtained from ⁹⁰Y PET was a significant predictor of the increase in FLR



among patients with T0 FLR < 30%. NTL-V30 was a significant predictor of the increase in FLR in the total cohort and in patients with T0 FLR < 30%. Likewise, it was a predictor of contralateral hypertrophy in patients with T0 FLR < 30%.

NTL-D95 and NTL-D98 were also significantly associated with increase in FLR in the total cohort of patients, but not in subgroups with T0 FLR < 30% or $\geq 30\%$.

Injected activity was not a predictor of hypertrophy. Hypertrophy and increase in FLR were not associated with any dosimetric variable related to tumor dose or tumor size.

Multivariable regression

Atrophy

Dosimetric variables were not independent predictors of atrophy.

Hypertrophy and increase in FLR

In patients with the smaller FLR, NTL-V30 was the most significant independent predictor of an increase in FLR ($p < 0.01$; adjusted R^2 : 0.609; see Fig. 17). It also predicted the degree of hypertrophy (adjusted R^2 : 0.336) at T2. In these patients, the correlation between NTL-V30 and increase in FLR at T2 was 0.608 with Spearman's Rho.



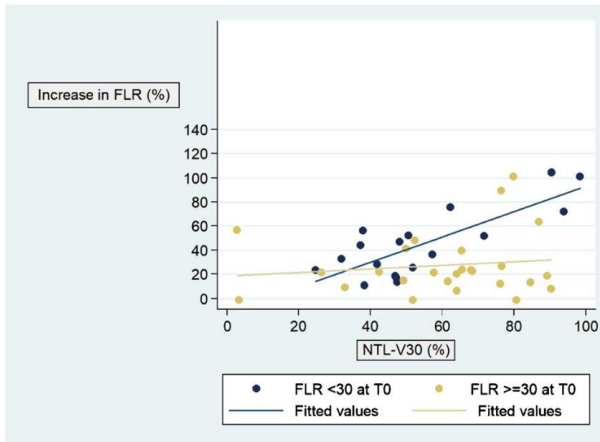


Fig. 17. Scatter plot of percent increase in FLR in T2 according to patients with FLR < 30% and \geq 30% at T0. FLR: the ratio between the volume of non-treated liver and total liver volume in percent, NTL-V30: percent of the non-treated volume that receives at least 30 Gy, T0: baseline, T2: 2-6 months after SIRT.

In contrast, in patients with the larger FLR \geq 30% at T0, NTL-V30 was not significantly associated with hypertrophy or increase in FLR (R^2 : 0.02, $p=0.508$, see Fig. 17). Other variables were significantly associated with hypertrophy or increase in FLR (see Results of Objective 4).

RESULTS OF OBJECTIVE 3

To determine the best dosimetric cut-off to predict an increase in FLR.

ROC analysis was performed with dosimetric parameters to identify cut-off points to predict increase in FLR (see Table 7).

Table 7. Dosimetric cut-offs to predict an increase in FLR at T2 in the total cohort of patients.

Endpoint	Source of Dosimetry	Dosimetric Parameter	Cut-off	Sensitivity	Specificity	Accuracy	LR +	LR -	AUC
FLR \geq 30%	^{99m} Tc-MAA	NTL-Dmean	≥ 43 Gy ¹	64.6%	80%	66%	3.229	0.442	0.772
	⁹⁰ Y PET	NTL-Dmean	≥ 40.1 Gy ¹	60.8%	80%	62.5%	3.039	0.490	0.765
		NTL-V30	$\geq 48\%$ ¹	74.5%	80%	75%	3.726	0.319	0.796
		NTL-D95	6 Gy ¹	51%	80%	53.6%	2.549	0.618	0.608
		NTL-D98	3.2 Gy ¹	47.1%	80%	50%	2.353	0.662	0.577
FLR \geq 40%	^{99m} Tc-MAA	NTL-Dmean	≥ 55 Gy ¹	53.7%	91.7%	62.3%	6.439	0.505	0.749
	⁹⁰ Y PET	NTL-Dmean	≥ 56.5 Gy ¹	48.8%	92.3%	58.9%	6.349	0.554	0.680
		NTL-V30	$\geq 49.1\%$ ²	79.1%	69.2%	76.8%	2.570	0.302	0.734
		NTL-D95	≥ 7.4 Gy ¹	51.2%	92.3%	60.7%	6.651	0.529	0.667
		NTL-D98	≥ 4 Gy ¹	41.9%	92.3%	53.6%	5.442	0.630	0.629

NTL: non-tumoral target liver, Dmean: mean dose (Gy), V30: percent of treated volume that receives at least 30 Gy, D95: dose that 95% of the treated volume receives, D98: dose that 98% of the treated volume receives, LR+: positive likelihood ratio, LR-: negative likelihood ratio, AUC: area under the curve.

¹With the highest LR+

²With the highest accuracy

To predict an increase in FLR to at least 30%

A cut-off of $\geq 48\%$ in the percentage of the non-tumor volume that receives 30 Gy (NTL-V30) obtained the highest accuracy, 75% (see Table 7). A cut-off of mean dose ≥ 43 Gy to the NTL



(NTL-Dmean) was the best from ^{99m}Tc -MAA, with lower accuracy (66%). Similar results were observed from NTL-Dmean obtained from ^{90}Y PET.

To predict an increase in FLR to at least 40%

In the total cohort of patients, a NTL-V30 cut-off of $\geq 49\%$ obtained the highest accuracy, 76.8% (see Table 7 and Fig. 18). In the group of patients with T0 FLR $< 30\%$, a NTL-V30 cut-off of $\geq 49\%$ obtained a sensitivity, specificity, PPV, NPV, and accuracy of 80.00%, 81.82%, 80.00%, 81.82% and 80.95% (AUC: 0.809) respectively.

A cut-off of NTL-Dmean of 55 Gy obtained from ^{99m}Tc -MAA was less accurate but had high specificity (91.7%). Similar results were observed from NTL-Dmean obtained from ^{90}Y PET (see Table 7).

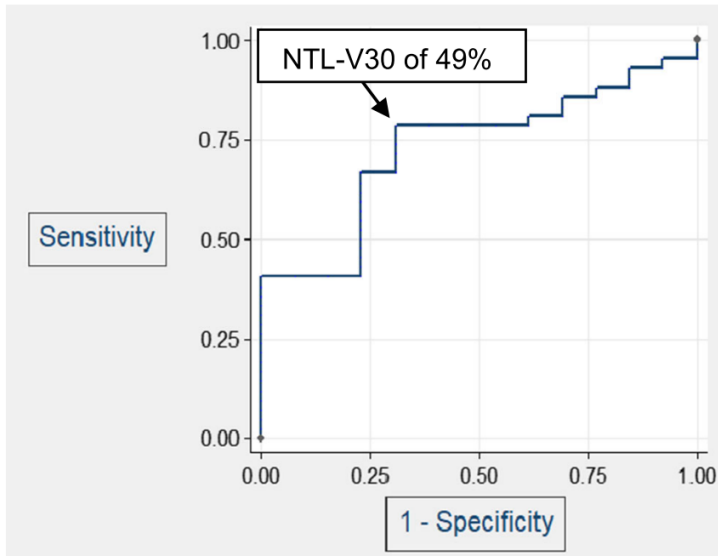


Fig. 18. ROC curve with the highest accuracy to predict an

increase in FLR to $\geq 40\%$ with a cut-off of 49% of NTL-V30.
Figure obtained from Stata 12.0. ROC, receiver operator characteristic; NTL-V30, percent of the non-treated volume that receives at least 30 Gy

Higher NTL-Dmean were needed to increase FLR to at least 40% (≥ 55 Gy in ^{99m}Tc -MAA) than to increase FLR to 30% (≥ 43 Gy in ^{99m}Tc -MAA), with similar results observed from NTL-Dmean obtained from ^{90}Y PET (see Table 7).

RESULTS OF OBJECTIVE 4

To study which clinical and volumetric variables of the patient and the tumor influence the development of atrophy of the treated liver, hypertrophy of the non-treated liver, and increase in FLR.

Univariable regression

Atrophy

A higher baseline bilirubin and smaller non-treated liver volumes showed a trend to lower degree of atrophy at T2, without reaching significance ($p=0.192$ and 0.140 respectively). The presence of cirrhosis was not significantly associated with a higher degree of atrophy.

Hypertrophy and increase in FLR

The presence of a secondary tumor and prior chemotherapy were significantly associated with hypertrophy and increase in FLR (see Table 8). The volume of the non-target liver was also inversely associated with hypertrophy and increase in FLR in the total cohort of patients, where a larger volume was associated with lower degree of hypertrophy and increase in FLR (see Table 8).



Table 8. Univariate regression analysis results. Clinical and baseline volumetric variables.

		All patients		Patients with baseline FLR < 30 %		Patients with baseline FLR ≥ 30 %	
		Hypertrophy	FLR increase	Hypertrophy	FLR increase	Hypertrophy	FLR increase
Clinical Variables							
Prior chemotherapy	Slope	37.66	32.64	53.01	42.29	7.03	13.53
	95% CI	5.57 - 69.75	10.08 - 55.20	(-12.55) - 118.56	(-1.69) - 86.26	(-20.46) - 34.53	(-9.94) - 36.99
	<i>p</i>	0.023*	0.006*	0.106	0.058	0.603	0.246
Primary vs. secondary tumor	Slope	40.09	35.66	61.45	51.44	1.19	8.53
	95% CI	4.77 - 75.40	10.91 - 60.41	(-4.91) - 127.82	8.08 - 94.81	(-29.93) - 32.31	(-18.41) - 35.47
	<i>p</i>	0.027*	0.006*	0.067	0.023*	0.938	0.52
Volumetric variables							
Volume of the non-target liver	Slope	-0.06	-0.04	-0.08	-0.05	-0.02	-0.03
	95% CI	(-0.10) - 0.02	(-0.08) - 0.01	(-0.21) - 0.05	(-0.14) - 0.04	(-0.06) - 0.01	(-0.06) - 0.00
	<i>p</i>	0.008*	0.006*	0.19	0.245	0.180	0.09

* Statistically significant *p* values (<0.05) of predicted are highlighted with an asterisk.

Sex, abnormal platelet count, serum transaminases, prior TACE or chemotherapy post-SIRT were not significantly associated with atrophy, hypertrophy or increase in FLR. A tendency was observed towards lower degree of increase in FLR after SIRT in cirrhotic patients. Patients with a higher total bilirubin at baseline also tended to have a lower degree of hypertrophy (*p* < 0.2), without reaching statistical significance.

Multivariable regression

Atrophy

The best model to predict atrophy of the treated lobe in T2 was total bilirubin at T0, baseline volume of the non-treated lobe and previous anti-cancer treatments, though this association was not robust (Adjusted R²: 0.220, see Table 9).



Table 9. Regression analysis of atrophy of the treated lobe in T2

Independent Variable	Slope	Standard error	t-ratio	Prob > t	95% Confidence interval	
Total bilirubin at T0	14.455	7.490	1.93	0.061	-0.703	29.618
Baseline volume of non-treated lobe	-.022	.007	-3.07	0.004	-0.036	-0.007
Previous anti-cancer treatments	-12.408	5.112	-2.43	0.020	-22.758	-2.059
Constant	-12.898					
R ²	0.277					
Adjusted R ²	0.220					
F	4.87					
Prob > F	0.0058					

Hypertrophy and increase in FLR

Dosimetric variables predicted hypertrophy and increase in FLR better than clinical and volumetric variables in patients with T0 FLR<30% (see Results of Objective 2). In patients with T0 FLR > 30%, the volume of the non-treated liver at T0 and total injected activity were independent predictors of an increase in FLR (R²: 0.34, adjusted R²: 0.28; Table 10). The slope of the regression with volume of the non-treated liver was negative, which meant that smaller contralateral livers were more significantly associated with hypertrophy or increase in FLR. On the other hand, the slope of regression with injected activity was positive. In other words, higher injected activities were more significantly associated with increase in FLR.



Table 10. Regression analysis of FLR change in T2: Patients with FLR \geq 30% at baseline

Independent Variable	Slope	Standard error	t-ratio	Prob > t	95% Confidence interval	
Activity injected	19.671	7.094	2.77	0.011	4.995	34.347
Baseline volume of non-treated lobe	-.041	.014	-2.9	0.008	-0.070	-0.012
Constant	36.436					
R ²	0.337					
Adjusted R ²	0.279					
F	5.84					
Prob > F	0.0089					

RESULTS OF OBJECTIVE 5

To study the relationship between atrophy of the NTL and clinical liver damage.

Changes in liver function

Laboratory data are presented in Table 11. A statistically significant increase in total bilirubin was observed from T0 to T1 ($p < 0.001$), T2 ($p < 0.001$) and T3 ($p = 0.006$). Albumin was available only in fewer than 15 patients at any time point. A non-significant decrease in albumin was observed. Median ALBI grade increased from grade 1 at baseline to grade 2 at T1, T2 and T3. Platelet count significantly decreased from T0 to T1 ($p = 0.02$). No significant changes in INR were seen.



Table 11. Laboratory data of patients at baseline and at each follow up

	T0*	T1*	T2*	T3*
AST, UI/l	31 (22)	37 (32.4)	31 (34)	36.5 (29)
ALT, U/l	27 (24)	28.5 (33.5)	27.5 (32.5)	27 (27.5)
Alkaline phosphatase, UI/l	109 (73)	157.5 (134.5)	149.5 (137.5)	123.5 (154)
γ -GTP, UI/l	115.5 (183)	127.5 (179)	160.5 (158)	117.5 (270)
Total bilirubin, mg/dl	0.55 (0.43)	0.75 (0.60)	0.9 (0.80)	1 (0.93)
Albumin, g/dl	3.78 (0.66)	3.80 (0.815)	3.59 (0.75)	3.6 (0.55)
ALBI score	-2.66 (-0.63)	-2.54 (-0.63)	-2.36 (-1)	-2.25 (-0.30)
ALBI grade	1	2	2	2
Platelets, 109/l	177 (125)	157 (151)	146 (77)	136 (83)
International Normalized Ratio (INR)	1.1 (0.1)	1.1 (0.01)	1.18 (0.1)	1.18 (0.1)

T0: baseline; T1: 0-2 months; T2: 2-6 months; T3: 6-12 months

*Median (IQR)

Univariable regression

Several dosimetric parameters were predictors of increase in bilirubin from T0 to T2: NTL-Dmean (Adjusted R^2 : 0.277; $p=0.002$), the minimum dose to a certain percentage of the NTL volume (NTL-D20, NTL-D50 and NTL-D70), of which the most significant was NTL-D20 (Adjusted $R^2=0.33$; $p=0.001$), and the percentage of the NTL that receives at least a certain amount of Gy (NTL-V50, NTL-V70, NTL-V100 and NTL-V120) of which the most significant was NTL-V120 (Adjusted $R^2= 0.35$; $p<0.001$).

Injected activity was not a predictor of increase in bilirubin. Increase in bilirubin was not associated with any dosimetric



variable related to tumor dose or tumor size, nor with baseline bilirubin.

Multivariable regression

The independent variables that best accounted for an increase in bilirubin from T0 to T2 were NTL-Dmean and NTL-V50 (Adjusted R²: 0.33).



VI. Discussion

In this investigation, dosimetric and clinical parameters were evaluated in ^{90}Y PET following lobar SIRT with ^{90}Y -loaded resin microspheres, in order to identify variables associated with atrophy of the treated lobe (as a surrogate for subclinical or clinical liver damage induced by radiation) and with contralateral hypertrophy in the non-treated liver after SIRT (as a potential primary or secondary treatment aim).

To our knowledge, this is the first study to investigate the relation between dosimetric findings on ^{90}Y PET/CT after SIRT with ^{90}Y -loaded resin microspheres and both ipsilateral atrophy and contralateral hypertrophy.

Currently, the use of SIRT has been challenged by phase 3 trials, where either SIRT vs. sorafenib [27,28] or the combination of SIRT + sorafenib versus sorafenib alone for patients with advanced hepatocellular carcinoma [29] failed to demonstrate any OS improvement. However, these studies did not have dosimetry endpoints, which could explain in part the negative results. A dosimetric approach to activity calculation could maximize the chances of tumor response and minimize the chances of subclinical or clinical liver damage. Moreover, in a subsequent retrospective analysis of the SARAH trial, tumor radiation-absorbed dose predicted at $^{99\text{m}}\text{Tc}$ -MAA SPECT/CT was in fact associated with better overall survival and disease control in hepatocellular carcinoma [31]. Such dosimetric approach may be even more important in clinical scenarios in which SIRT can be most beneficial, such as large tumors or those lobar tumors that have invaded the portal vein branches [8]. All of these provide a strong rationale for new randomised studies to compare SIRT using personalised dosimetry (alone or in combination with standard of care) with standard of care alone [31].



The shift towards personalized SIRT is crucial, and as Alsultan et al. mention, the next step in improving SIRT treatment planning may lie in voxel-based dosimetry [34]. Voxel-based dosimetry can take into account the dose to the smallest independent special unit for activity [56]. Using voxel-based dosimetry information can be extracted on the heterogeneity of the distribution of microspheres within each compartment. The main limitation of the mono-compartment methods is that the actual spatial dose distribution of an individual patient is neglected, and they assume a homogeneous distribution between the tumor and the normal liver. Though the partition model considers the distribution of activity among each compartment, the absorbed dose is still averaged over each compartment [79]. 3D-voxel-based dosimetry provides a dose map calculation dose profiles and DVH similar to those used in external-beam radiation therapy to help optimize treatment planning [56].

A relevant observation in our work was the failure to identify dosimetric parameters significantly associated with liver atrophy. The initial assumption was that a higher absorbed dose would result in a higher degree of atrophy, but the results in this study do not support this hypothesis. This suggests that the distribution of the radioactive beads or the different sensitivity of different areas of the liver acinus may play a role[140] and certainly deserves further research.

Contrary, dosimetric analysis revealed that several variables related to the dose absorbed by the NTL were significant predictors of contralateral hypertrophy or increase in FLR. In the univariate analysis, predictors of both were NTL-Dmean in PET and NTL-V30, the latter in the entire cohort and in patients with T0 FLR < 30%, not so in patients with FLR \geq 30%. To our knowledge, this is the first demonstration of a



correlation between a ^{90}Y PET dosimetric parameter and the degree of hypertrophy with resin microspheres. An inadequate FLR is one of the most common reasons for excluding otherwise suitable patients from potentially curative liver resection. A FLR of at least 30% is required for patients with preserved liver function, and at least 40% is required for cirrhotic patients [112]. Furthermore, an increase in FLR to $\geq 40\%$ was predicted by a NTL-V30 of $\geq 49\%$, with a sensitivity, specificity, and accuracy of 79.1%, 69.2% and 76.8% respectively. NTL-V30 was more accurate than NTL-Dmean in increasing FLR to 30% or to 40%, both from $^{99\text{m}}\text{Tc}$ -MAA and from ^{90}Y PET. Higher NTL-Dmean was needed to reach an FLR of 40% rather than 30% (at least 55 Gy vs. 43 Gy obtained from $^{99\text{m}}\text{Tc}$ -MAA, and similarly in ^{90}Y PET), although with lower accuracy and low sensitivity.

Palard et al.[133] evaluated dosimetric parameters associated with contralateral hypertrophy in patients treated with ^{90}Y -loaded glass microspheres. However, they studied dosimetric parameters from $^{99\text{m}}\text{Tc}$ -MAA and not from ^{90}Y PET, which demonstrates the true distribution of injected activity. In our study, we compared NTL-Dmean of $^{99\text{m}}\text{Tc}$ -MAA obtained by formula with 3D voxel-based dosimetry in ^{90}Y PET. Congruent with our study, they found that NTL-Dmean with $^{99\text{m}}\text{Tc}$ -MAA was associated with maximal hypertrophy $> 10\%$, while Dmean to the tumor and injected activity as continuous variables were not. Our study focused on the increase in FLR instead of maximal hypertrophy $>10\%$ because we believe that the former is more clinically relevant. In our study, NTL-Dmean in $^{99\text{m}}\text{Tc}$ -MAA and ^{90}Y PET were statistically significant in the univariable analysis only in patients with FLR <30 .



In our cohort, a subclinical increase in bilirubin was found, and different dosimetric parameters related to the NTL were significantly associated with increase in bilirubin after SIRT, particularly NTL-Dmean and NTL-V50. Though data in our cohort was scarce with regard to albumin, both ALBI score and ALBI grade increased after SIRT. No patients developed REILD, which supports the use of this multi-compartment method as a safe method of activity planning with our modified treatment protocol, where the size and quality of the remnant liver segments are taken into account[25]. It should be noted that all our patients were treated according to the partition model, standard at our institution for lobar and selective treatments.

When the intention is to produce ipsilateral lobar atrophy and contralateral lobe hypertrophy, the prescribed activity may need to be increased, compared to the activity prescribed when the function of the treated lobe has to be preserved. For radiation lobectomy, the proposed safety cut-off by the aforementioned expert panel was higher; a mean absorbed dose to the NTL of > 70 Gy was proposed, with strong agreement among experts[20].

In our cohort of patients, the predicted median absorbed dose to the NTL in ^{99m}Tc -MAA was 47 Gy and resulted in a slightly lower absorbed dose in ^{90}Y PET (42.7 Gy). Not all patients were treated with the primary intention to produce increase in FLR. Our center works in agreement with “Preserve as much Healthy Liver as is Possible: Any Patient Could Potentially Become a Surgical Candidate”, as described in an expert discussion and report from Mediterranean Interventional Oncology by Bilbao et al. [141]. It states, “While discussing in the Multidisciplinary Tumor Board how to design the treatment strategy for every particular patient, some of them will be



allocated to receive a palliative treatment depending on the staging, the tumor burden, and the presence of comorbidities. Some others will be guided towards a curative method (surgery and/or percutaneous ablation) and some will be initially treated by non-curative methods, but, depending on the response and if correctly downstaged/ downsized, could in theory ultimately once again become candidates to receive surgery/ablation”.

Though we consider patients as potential candidates for surgery if correctly downstaged or downsized, we wished to analyze also particularly the ones that would require hypertrophy in order for this to be possible. This is why patients were stratified according to baseline FLR $<$ or \geq 30 %.

Dosimetry is key, not only to individualize therapy for maximal tumor response but also to do this safely, respecting normal tissue tolerances [26]. Studying the relationship between the activity administered and clinical or subclinical damage aids in establishing safe thresholds. A recent subanalysis of the SORAMIC trial assessed the effect of SIRT + sorafenib on liver function compared to sorafenib alone. It found that the negative and often subclinical effect on liver function in patients with hepatocellular carcinoma may impair prognosis after treatment, and the impact of SIRT on liver function could explain the lack of survival benefit in the SIRT + sorafenib arm. An increase in survival was seen by adding SIRT to certain subgroups of patients, such as those with $<$ 65 years or with Child-Pugh 5, who had stable liver function post SIRT. Another study found that baseline ALBI was a strong predictor of toxicity, including REILD. While this parameter seems to gain importance among expert groups, with a single-arm study Lescure et al. [142] were not able to compare the decrease in liver function due to SIRT vs. due to the natural history of disease in hepatocellular carcinoma. Further studies



investigating the impact and prevention of subclinical liver damage post-SIRT, as well as the benefit of ALBI for the selection of treatment and monitoring the evolution of liver function would be welcomed, as this could impact patient outcomes. Nevertheless, when the intention is to induce the atrophy-hypertrophy complex, the subclinical liver damage post-SIRT could be accepted, though only to a point that does not compromise overall survival.

A factor that could affect toxicity is the total number of microspheres administered (related to the dose per microsphere). Currently, there are three types of microspheres (TheraSphere, SIR-Spheres and Quiremspheres) and each of them has different properties [31]. In patients treated with SIR-Spheres, the number of particles used is higher than patients treated with TheraSphere (20-40 million vs. 5 million) producing a more relative embolic effect, with lower specific activity per microsphere (20-70 vs. 4354 Bq per microsphere). Quiremspheres have an intermediate position in terms of number of particles (20 millions), specific activity (240-375 Bq/microsphere) and embolic effect [34]. As described by Pasciak et al.[38], differences in microsphere-number density may have an effect on microscopic tumor absorbed-dose inhomogeneity. In a radiobiologic model by the same author[39], the increased absorbed dose homogeneity resulted in a greater volume fraction of the liver receiving a potentially toxic absorbed dose, while in another study by the same group, D70 was decreased at a low microsphere-number density, postulating that one could compensate for decreases by an increase in the average tumor-absorbed dose, that is, by increasing the radioembolization treatment dose [38]. Our study was carried out with SIR-Spheres which present the highest number of particles injected, and the results obtained



in our study may not be extrapolated to the other two types of microspheres, with different absorbed dose distribution.

An important finding of our study is the influence of the baseline volume of the non-treated liver. It was negatively associated with contralateral hypertrophy and with an increase in FLR. In other words, and not surprisingly, larger contralateral lobes achieved a lower degree of hypertrophy than smaller ones. This may be partially attributed to larger contralateral lobes already hypertrophied due to cirrhosis, consistent with Goebel et al. [124] finding that the baseline relative left liver volume (defined as left liver volume/total liver volume) was significantly higher in patients with cirrhosis than in patients without cirrhosis. As importantly, these findings suggest that those local factors that trigger hypertrophy are not induced or are not as effective in large FLRs. A tendency was observed towards lower degree of hypertrophy in FLR after SIRT in cirrhotic patients, and in patients with higher bilirubin, though these did not reach statistical significance. With a larger sample size, cirrhosis and baseline bilirubin could prove to be significant predictors of impaired hypertrophy.

Although the volume of the FLR is important in patients that will undergo hepatectomy, it is not clear that hypertrophy always leads to an increase in function. One of the emerging nuclear medicine imaging techniques is Hepatobiliary scintigraphy (HBS), which can quantitatively assess global and regional liver function [143]. The main indication for HBS is to assess the FLR function in patients scheduled to undergo hemi-hepatectomy; to predict the risk of post-hepatectomy liver failure, particularly in patients with impaired liver function due to cirrhosis or after chemotherapy [143]. In the work-up for SIRT, patients may be further screened by HBS



given that analysis of clinical and laboratory parameters may not be sufficient. HBS may improve patient selection and treatment planning for SIRT, in order to evaluate if the liver function of the non-treated lobe is sufficient to compensate for radiation damage in the treated part of the liver[144]. Furthermore, it may be useful to assess how well the magnitude of hypertrophy correlates with changes in liver function after SIRT. Larger studies should explain the numeric relation between the absorbed dose to the functional liver parenchyma and the decline in liver function after SIRT [144].

Volume changes in our study are consistent with those reported in the literature. In a systematic review of contralateral hypertrophy after unilobar SIRT [116], contralateral liver hypertrophy ranged from 26 to 47% in a period of time between 44 days and 9 months. In our series, the mean increase in volume of the non-treated liver at T2 (2-6 months after SIRT) was 34%. Another study [21] similarly found an increase in FLR of 36% at both 3-6 and 6-9 months. In a previous report from our group the degree of hypertrophy was higher (45% at 26 weeks) [125]. This may simply reflect a different patient population or differences in the segmentation methods. In the previous study, the segmentation respected anatomical limits between right and left liver lobes[119], while in the current study the distribution of activity in ⁹⁰Y PET determined the limit between treated and non-treated segments.

In our study, neither tumor size (as a continuous variable or as smaller or larger than 100 ml) nor tumor dose (mean, maximum, or other DVH results) were significantly associated with contralateral hypertrophy. The lower degree of hypertrophy after left lobar SIRT compared to right or extended right lobar SIRT, and among cirrhotic patients have been reported elsewhere [125,145], though these factors did



not reach significance in the present study. Clinical factors associated with hypertrophy were the presence of secondary tumors and prior chemotherapy. Indeed, this may capture the absence of cirrhosis better than the positive identification of the cirrhotic status. Cirrhosis is a histological diagnosis and clinical evaluation only captures the more advanced stages of the disease. Contrary, patients with metastatic liver are rarely cirrhotics and have almost all received chemotherapy prior to SIRT.

There are several limitations in this study. Firstly, it is a retrospective study with a small sample size, which limits the predictive power of the results. On the other hand, SIRT was not always performed with the primary intention to hypertrophy the non-treated liver as a bridge to surgical resection, in patients in whom a low FLR would limit the surgery. Therefore, analyses were also performed according to the T0 FLR. Patients with lower FLR may benefit the most from a sophisticated dosimetric study prior to SIRT, in order to tailor the activity to administer for an expected dose to the tumoral volume with intention to treat, and to the NTL volume, to produce hypertrophy of the non-treated liver, along with an increase in the FLR to 30-40% [117].



VII. Conclusions

1. Lobar SIRT induced atrophy of the treated liver and hypertrophy of the non-treated liver.
2. The correlation between atrophy of the treated segments and hypertrophy of the non-treated segments was weak.
3. No relationship has been found between dosimetric parameters and the induction of atrophy of the treated lobe.
4. The mean dose to the non-tumoral liver obtained by ^{99m}Tc -MAA significantly predicted increase in the future liver remnant in patients with baseline future liver remnant $< 30\%$.
5. The mean dose to the non-tumoral liver and the percent of the non-tumoral liver volume exposed to ≥ 30 Gy obtained by ^{90}Y PET were significant predictors of contralateral hypertrophy and increase in the future liver remnant.
6. For an increase in the future liver remnant to at least 40%, a cut-off of $\geq 49.1\%$ in the non-tumoral liver volume exposed to ≥ 30 Gy obtained by PET was the most accurate dosimetric parameter, with a sensitivity, specificity and accuracy of 79.1%, 69.2% and 76.8% respectively.
7. Variables related to tumor dose or tumor size were not significant predictors of hypertrophy or increase in the future liver remnant.
8. Smaller volumes of the treated liver were associated with lower degrees of hypertrophy and increase in the future liver remnant.



9. A tendency was observed towards lower degree of hypertrophy in the future liver remnant after SIRT in cirrhotic patients, and in patients with higher bilirubin at baseline.
10. Lobar SIRT was well tolerated, and no patient developed radioembolization induced liver disease. However, subclinical liver damage can be observed after lobar SIRT.



VIII. Figures and Tables

1. FIGURES

Fig. 1. Surgical resection after SIRT with hypertrophy of the contralateral liver lobe. Illustration by Patri de Blas.

Fig. 2. Artistic rendering of microscopic microsphere deposition at days 4–12 post-calibration.

Fig. 3. Steps in ^{90}Y SIRT.

Fig. 4. Radiation pneumonitis.

Fig. 5. $^{99\text{m}}\text{Tc}$ -MAA SPECT/CT and CBCT to optimize dosimetric planning for SIRT.

Fig. 6. Process of retrospective pre- and post-treatment dosimetry.

Fig. 7. Work-up of activity calculation in our modified protocol [30].

Fig. 8. Administration of treatment with ^{90}Y - resin microspheres. Illustration by Patri de Blas.

Fig. 9. Limit for safe hepatic resection.

Fig. 10. Rapid registration with PLANET® Dose.

Fig. 11. Schematic representation of the segmentation process after right lobar SIRT.

Fig. 12. Anatomical contours on contrast-enhanced CT of right lobe, tumor and left lobe.

Fig. 13. Segmentation of non-tumoral liver (NTL) on ^{90}Y PET.

Fig. 14. Dosimetric variables extracted from dose-volume histograms.



Fig. 15. Changes in volume (%) of the treated (atrophy) and non-treated liver (hypertrophy) after radioembolization.

Fig. 16. Scatter plot between atrophy of the treated volume and hypertrophy of the non-treated volume at T2.

Fig. 17. Scatter plot of percent increase in FLR in T2 according to patients with FLR < 30% and \geq 30% at T0.

Fig. 18. ROC curve with the highest accuracy to predict an increase in FLR to \geq 40%.

2. TABLES

Table 1. Types of microspheres for SIRT.

Table 2. Safety cut-off for individual activity prescription recommendations for the use of SIRT with ^{90}Y -resin microspheres.

Table 3. General characteristics of patients in the present series.

Table 4. Dosimetric parameters.

Table 5. Atrophy, hypertrophy and changes in the future liver remnant at baseline and during follow-up.

Table 6. Univariable regression analysis. Dosimetric, clinical and volumetric variables associated with hypertrophy and increase in FLR.

Table 7. Dosimetric cut-offs to predict an increase in FLR at T2 in the total cohort of patients.

Table 8. Univariate regression analysis results. Clinical and baseline volumetric variables.



Table 9. Regression analysis of atrophy of the treated lobe in T2.

Table 10. Regression analysis of FLR change in T2: Patients with FLR > 30% at baseline.

Table 11. Laboratory data of patients at baseline and at each follow up.



IX. References

1. Braat AJAT, Smits MLJ, Braat MNGJA, van den Hoven AF, Prince JF, de Jong HWAM, et al. 90Y Hepatic Radioembolization: An Update on Current Practice and Recent Developments. *J Nucl Med.* 2015.56:1079–87.
2. Ahmadzadehfar H, Biersack HJ, Ezziddin S. Radioembolization of Liver Tumors With Yttrium-90 Microspheres. *Semin Nucl Med.* 2010.40:105–21.
3. Kennedy A. Radioembolization of hepatic tumors. *J. Gastrointest. Oncol.* 2014. p. 178–89.
4. Kennedy A, Coldwell D, Sangro B, Wasan H, Salem R. Radioembolization for the treatment of liver tumors: General principles. *Am J Clin Oncol Cancer Clin Trials.* 2012.35:91–9.
5. Gulec SA, Mesoloras G, Dezarn WA, McNeillie P, Kennedy AS. Safety and efficacy of Y-90 microsphere treatment in patients with primary and metastatic liver cancer: The tumor selectivity of the treatment as a function of tumor to liver flow ratio. *J Transl Med.* 2007.5:1–9.
6. Sato K, Lewandowski RJ, Bui JT, Omary R, Hunter RD, Kulik L, et al. Treatment of unresectable primary and metastatic liver cancer with yttrium-90 microspheres (TheraSphere®): Assessment of hepatic arterial embolization. *Cardiovasc Intervent Radiol.* 2006.29:522–9.
7. Sangro B, Iñarrairaegui M, Bilbao JI. Radioembolization for hepatocellular carcinoma. *J. Hepatol.* 2012. p. 464–73.
8. Sangro B, Gardini AC. Radioembolisation in Hepatocellular Carcinoma: Principles of Management. *Liver Cancers.* 2019.:139–52.
9. Crane CH, Koay EJ. Solutions that enable ablative radiotherapy for large liver tumors: Fractionated dose painting, simultaneous integrated protection, motion management, and



- computed tomography image guidance. *Cancer*. 2016. p. 1974–86.
10. Heckman JT, deVera MB, Marsh JW, Fontes P, Amesur NB, Holloway SE, et al. Bridging Locoregional Therapy for Hepatocellular Carcinoma Prior to Liver Transplantation. *Ann Surg Oncol* 2008 1511. 2008.15:3169–77.
11. Benson AB, D’Angelica MI, Abbott DE, Anaya DA, Anders R, Are C, et al. Hepatobiliary cancers, Version 2.2021. *JNCCN J Natl Compr Cancer Netw*. 2021.19:541–65.
12. Vogel A, Cervantes A, Chau I, Daniele B, Llovet J, Meyer T, et al. Hepatocellular carcinoma: ESMO Clinical Practice Guidelines for diagnosis, treatment and follow-up. *Ann Oncol*. 2018.29:iv238–55.
13. Vogel A, Cervantes A, Chau I, Daniele B, Llovet JM, Meyer T, et al. Corrigendum: Hepatocellular carcinoma: ESMO Clinical Practice Guidelines for diagnosis, treatment and follow-up. *Ann. Oncol*. 2019. p. 871–3.
14. Jain A, Chitturi S, Peters G, Yip D. Atezolizumab and bevacizumab as first line therapy in advanced hepatocellular carcinoma: Practical considerations in routine clinical practice. *World J Hepatol*. 2021.13:1132–42.
15. Vogel A, Martinelli E, Cervantes A, Chau I, Daniele B, Llovet JM, et al. Updated treatment recommendations for hepatocellular carcinoma (HCC) from the ESMO Clinical Practice Guidelines. *Ann Oncol*. 2021.32:801–5.
16. Braat JAT, Huijbregts JE, Molenaar Q, Borel Rinkes IHM, van den Bosch MAAJ, Lam MGEH. Hepatic radioembolization as a bridge to liver surgery. *Front. Oncol*. 2014. p. 1–23.
17. Titano J, Voutsinas N, Kim E. The Role of



Radioembolization in Bridging and Downstaging Hepatocellular Carcinoma to Curative Therapy. *Semin Nucl Med.* 2019.49:189–96.

18. Malhotra A, Liu DM, Talenfeld AD. Radiation Segmentectomy and Radiation Lobectomy: A Practical Review of Techniques. *Tech Vasc Interv Radiol.* 2019.22:49–57.

19. Riaz A, Gates VL, Atassi B, Lewandowski RJ, Mulcahy MF, Ryu RK, et al. Radiation segmentectomy: A novel approach to increase safety and efficacy of radioembolization. *Int J Radiat Oncol Biol Phys.* 2011.79:163–71.

20. Levillain H, Duran Derijkere I, Ameye L, Guiot T, Braat A, Meyer C, et al. Personalised radioembolization improves outcomes in refractory intra-hepatic cholangiocarcinoma: a multicenter study. *Eur J Nucl Med Mol Imaging.* 2019.

21. Vouche M, Lewandowski RJ, Atassi R, Memon K, Gates VL, Ryu RK, et al. Radiation lobectomy: Time-dependent analysis of future liver remnant volume in unresectable liver cancer as a bridge to resection. *J Hepatol.* 2013.59:1029–36.

22. Sirtex Medical. SIR-Spheres® Microspheres [package insert]. 2019.

23. TheraSphere® Yttrium-90 Glass Microspheres [package insert].

24. Garin E, Palard X, Rolland Y. Personalised dosimetry in radioembolisation for HCC: Impact on clinical outcome and on trial design. *Cancers (Basel).* 2020.12:1–17.

25. Gil-Alzugaray B, Chopitea A, Iñarrairaegui M, Bilbao JI, Rodriguez-Fraile M, Rodriguez J, et al. Prognostic factors and prevention of radioembolization-induced liver disease. *Hepatology.* 2013.57:1078–87.



26. Levillain H, Bagni O, Deroose CM, Dieudonné A, Gnesin S, Grosser OS, et al. International recommendations for personalised selective internal radiation therapy of primary and metastatic liver diseases with yttrium-90 resin microspheres. *Eur J Nucl Med Mol Imaging*. 2021.48:1570–84.
27. Chow PKH, Gandhi M, Tan SB, Khin MW, Khasbazar A, Ong J, et al. SIRveNIB: Selective internal radiation therapy versus sorafenib in Asia-Pacific patients with hepatocellular carcinoma. *J Clin Oncol*. 2018.36:1913–21.
28. Vilgrain V, Pereira H, Assenat E, Guiu B, Ilonca AD, Pageaux GP, et al. Efficacy and safety of selective internal radiotherapy with yttrium-90 resin microspheres compared with sorafenib in locally advanced and inoperable hepatocellular carcinoma (SARAH): an open-label randomised controlled phase 3 trial. *Lancet Oncol*. 2017.18:1624–36.
29. Ricke J, Klümper HJ, Amthauer H, Bargellini I, Bartenstein P, de Toni EN, et al. Impact of combined selective internal radiation therapy and sorafenib on survival in advanced hepatocellular carcinoma. *J Hepatol*. 2019.71:1164–74.
30. Garin E, Rolland Y, Campillo-Gimenez B, Edeline J. Negative phase 3 study of 90Y microspheres versus sorafenib in HCC. *Lancet Oncol*. 2018. p. e70.
31. Hermann AL, Dieudonné A, Ronot M, Sanchez M, Pereira H, Chatellier G, et al. Relationship of tumor radiation-absorbed dose to survival and response in hepatocellular carcinoma treated with transarterial radioembolization with 90Y in the SARAH study. *Radiology*. 2020.296:673–84.
32. Garin E, Tselikas L, Guiu B, Chalaye J, Edeline J, De Baere T, et al. Personalised versus standard dosimetry approach of selective internal radiation therapy in patients with locally advanced hepatocellular carcinoma (DOSISPHERE-01): a



randomised, multicentre, open-label phase 2 trial. *Lancet Gastroenterol Hepatol.* 2021.6:17–29.

33. Forner A, Ayuso C, Varela M, Rimola J, Hessheimer AJ, De Lope CR, et al. Evaluation of tumor response after locoregional therapies in hepatocellular carcinoma: Are response evaluation criteria in solid tumors reliable? *Cancer.* 2009.115:616–23.

34. Alsultan AA, Braat AJAT, Smits MLJ, Barentsz MW, Bastiaannet R, Bruijnen RCG, et al. Current Status and Future Direction of Hepatic Radioembolisation. *Clin Oncol.* 2020.33:106–16.

35. Kennedy AS, Kleinstreuer C, Basciano CA, Dezarn WA. Computer Modeling of Yttrium-90-Microsphere Transport in the Hepatic Arterial Tree to Improve Clinical Outcomes. *Int J Radiat Oncol Biol Phys.* 2010.76:631–7.

36. Campbell AM, Bailey IH, Burton MA. Analysis of the distribution of intra-arterial microspheres in human liver following hepatic yttrium-90 microsphere therapy. *Phys Med Biol.* 2000.45:1023–33.

37. Kennedy AS, Nutting C, Coldwell D, Gaiser J, Drachenberg C. Pathologic response and microdosimetry of ⁹⁰Y microspheres in man: Review of four explanted whole livers. *Int J Radiat Oncol Biol Phys.* 2004.60:1552–63.

38. Pasciak AS, Bourgeois AC, Bradley YC. A microdosimetric analysis of absorbed dose to tumor as a function of number of microspheres per unit volume in ⁹⁰Y Radioembolization. *J Nucl Med.* 2016.57:1020–6.

39. Pasciak AS, Abiola G, Liddell RP, Crookston N, Besharati S, Donahue D, et al. The number of microspheres in ⁹⁰Y radioembolization directly affects normal tissue radiation exposure. *Eur J Nucl Med Mol Imaging.* 2020.47:816–27.



40. Kennedy A, Nag S, Salem R, Murthy R, McEwan AJ, Nutting C, et al. Recommendations for Radioembolization of Hepatic Malignancies Using Yttrium-90 Microsphere Brachytherapy: A Consensus Panel Report from the Radioembolization Brachytherapy Oncology Consortium. *Int J Radiat Oncol Biol Phys*. 2007;68:13–23.
41. Sangro B, Martínez-Urbistondo D, Bester L, Bilbao JJ, Coldwell DM, Flamen P, et al. Prevention and treatment of complications of selective internal radiation therapy: Expert guidance and systematic review. *Hepatology*. 2017. p. 969–82.
42. Murthy R, Nunez R, Szklaruk J, Erwin W, Madoff DC, Gupta S, et al. Yttrium-90 Microsphere Therapy for Hepatic Malignancy: Devices, Indications, Technical Considerations, and Potential Complications. *RadioGraphics*. 2005;25:S41–55.
43. Lemieux S, Buies A, Turgeon AF, Hallet J, Daigle G, Côté F, et al. Effect of Yttrium-90 transarterial radioembolization in patients with non-surgical hepatocellular carcinoma: A systematic review and meta-analysis. *PLoS One*. 2021;16:e0247958.
44. Chiesa C, Maccauro M, Romito R, Spreafico C, Pellizzari S, Negri A, et al. Need, feasibility and convenience of dosimetric treatment planning in liver selective internal radiation therapy with ⁹⁰Y microspheres: The experience of the National Cancer Institute of Milan. *Q. J. Nucl. Med. Mol. Imaging*. 2011. p. 168–97.
45. Strigari L, Sciuto R, Rea S, Carpanese L, Pizzi G, Soriani A, et al. Efficacy and Toxicity Related to Treatment of Hepatocellular Carcinoma with ⁹⁰Y-SIR Spheres: Radiobiologic Considerations. *J Nucl Med*. 2010;51:1377–85.
46. Lenoir L, Edeline J, Rolland Y, Pracht M, Raoul JL, Ardisson V, et al. Usefulness and pitfalls of MAA SPECT/CT in identifying digestive extrahepatic uptake when planning



liver radioembolization. *Eur J Nucl Med Mol Imaging*. 2012.39:872–80.

47. Salem R, Thurston KG. Radioembolization with ⁹⁰yttrium microspheres: A state-of-the-art brachytherapy treatment for primary and secondary liver malignancies - Part 1: Technical and methodologic considerations. *J Vasc Interv Radiol*. 2006.17:1251–78.

48. Salem R, Hunter RD. Yttrium-90 microspheres for the treatment of hepatocellular carcinoma: A review. *Int J Radiat Oncol Biol Phys*. 2006.66:83–8.

49. Kim SP, Cohalan C, Kopek N, Enger SA. A guide to ⁹⁰Y radioembolization and its dosimetry. *Phys. Medica*. 2019. p. 132–45.

50. Chan WSW, Poon WL, Cho DHY, Chiu SSH, Luk SH. Transcatheter embolisation of intrahepatic arteriovenous shunts in patients with hepatocellular carcinoma. *Hong Kong Med J*. 2010.16:48–55.

51. Dittmann H, Kopp D, Kupferschlaeger J, Feil D, Groezinger G, Syha R, et al. A Prospective Study of Quantitative SPECT/CT for Evaluation of Lung Shunt Fraction Before SIRT of Liver Tumors. *J Nucl Med*. 2018.59:1366–72.

52. Dezarn WA, Cessna JT, Dewerd LA, Feng W, Gates VL, Halama J, et al. Recommendations of the American Association of Physicists in Medicine on dosimetry, imaging, and quality assurance procedures for ⁹⁰Y microsphere brachytherapy in the treatment of hepatic malignancies. *Med Phys*. 2011.38:4824–45.

53. Kappadath SC, Mikell J, Balagopal A, Baladandayuthapani V, Kaseb A, Mahvash A. Hepatocellular Carcinoma Tumor Dose Response After ⁹⁰Y-radioembolization With Glass Voxel Dosimetry. *Radiat Oncol Biol*. 2018.102:451–61.



54. Jiang M, Fischman A, Nowakowski FS. Segmental Perfusion Differences on Paired Tc-99m Macroaggregated Albumin (MAA) Hepatic Perfusion Imaging and Yttrium-90 (Y-90) Bremsstrahlung Imaging Studies in SIR-Sphere Radioembolization: Associations with Angiography. *J Nucl Med Radiat Ther.* 2012.03:1–5.
55. Wondergem M, Smits MLJ, Elschot M, de Jong HWAM, Verkooijen HM, van den Bosch MAAJ, et al. 99mTc-Macroaggregated Albumin Poorly Predicts the Intrahepatic Distribution of 90Y Resin Microspheres in Hepatic Radioembolization. *J Nucl Med.* 2013.54:1294–301.
56. Kafrouni M, Allimant C, Fourcade M, Vauclin S, Delicque J, Ilonca A-D, et al. Retrospective Voxel-Based Dosimetry for Assessing the Ability of the Body-Surface-Area Model to Predict Delivered Dose and Radioembolization Outcome. *J Nucl Med.* 2018.59:1289–95.
57. Chang TT, Bourgeois AC, Balias AM, Pasciak AS. Treatment modification of yttrium-90 radioembolization based on quantitative positron emission tomography/CT imaging. *J Vasc Interv Radiol.* 2013.24:333–7.
58. Morán V, Prieto E, Sancho L, Rodríguez-Fraile M, Soria L, Zubiria A, et al. Impact of the dosimetry approach on the resulting 90Y radioembolization planned absorbed doses based on 99mTc-MAA SPECT-CT: is there agreement between dosimetry methods? *EJNMMI Phys.* 2020.7.
59. Cremonesi M, Chiesa C, Strigari L, Ferrari M, Botta F, Guerriero F, et al. Radioembolization of Hepatic Lesions from a Radiobiology and Dosimetric Perspective. *Front Oncol.* 2014.4:1–20.
60. Giammarile F, Bodei L, Chiesa C, Flux G, Forrer F, Kraeber-Bodere F, et al. EANM procedure guideline for the treatment of liver cancer and liver metastases with intra-arterial



radioactive compounds. *Eur J Nucl Med Mol Imaging*. 2011.38:1393–406.

61. Rodríguez-Fraile M, Iñarrairaegui M. Radioembolization with ^{90}Y -microspheres for liver tumors. *Rev Esp Med Nucl Imagen Mol*. 2015.34:244–57.

62. Sancho L, Rodríguez-Fraile M, Bilbao JI, Beorlegui Arteta C, Iñarrairaegui M, Moran V, et al. Is a Technetium-99m Macroaggregated Albumin Scan Essential in the Workup for Selective Internal Radiation Therapy with Yttrium-90? An Analysis of 532 Patients. *J Vasc Interv Radiol*. 2017.28:1536–42.

63. Vente MAD, Wondergem M, van der Tweel I, van den Bosch MAAJ, Zonnenberg BA, Lam MGEH, et al. Yttrium-90 microsphere radioembolization for the treatment of liver malignancies: a structured meta-analysis. *Eur Radiol*. 2009.19:951–9.

64. Garin E, Lenoir L, Rolland Y, Edeline J, Mesbah H, Laffont S, et al. Dosimetry Based on $^{99\text{m}}\text{Tc}$ -Macroaggregated Albumin SPECT/CT Accurately Predicts Tumor Response and Survival in Hepatocellular Carcinoma Patients Treated with ^{90}Y -Loaded Glass Microspheres: Preliminary Results. *J Nucl Med*. 2012.53:255–63.

65. Lam MGEH, Smits MLJ. Value of $^{99\text{m}}\text{Tc}$ -macroaggregated albumin SPECT for radioembolization treatment planning. *J. Nucl. Med*. 2013. p. 1681–2.

66. Braat AJAT, Prince JF, van Rooij R, Bruijnen RCG, van den Bosch MAAJ, Lam MGEH. Safety analysis of holmium-166 microsphere scout dose imaging during radioembolisation work-up: A cohort study. *Eur Radiol*. 2018.28:920–8.

67. M E, JF N, MG L, ML S, JF P, MA V, et al. ($^{99\text{m}}\text{Tc}$)-MAA overestimates the absorbed dose to the lungs in



- radioembolization: a quantitative evaluation in patients treated with ^{166}Ho -microspheres. *Eur J Nucl Med Mol Imaging*. 2014.41:1965–75.
68. Nijssen JFW, Seppenwoolde JH, Havenith T, Bos C, Bakker CJG, Van Het Schip AD. Liver Tumors: MR Imaging of Radioactive Holmium Microspheres - Phantom and Rabbit Study. *Radiology*. 2004.231:491–9.
69. Chiesa C, Maccauro M. ^{166}Ho microsphere scout dose for more accurate radioembolization treatment planning. *Eur J Nucl Med Mol Imaging*. 2020.47:744–7.
70. Smits MLJ, Dassen MG, Prince JF, Braat AJAT, Beijst C, Buijnen RCG, et al. The superior predictive value of ^{166}Ho -scout compared with $^{99\text{m}}\text{Tc}$ -macroaggregated albumin prior to ^{166}Ho -microspheres radioembolization in patients with liver metastases. *Eur J Nucl Med Mol Imaging*. 2020.47:798–806.
71. Jadoul A, Hustinx R. Comparative dosimetry between $^{99\text{m}}\text{Tc}$ -MAA SPECT / CT and $^{90\text{Y}}$ PET / CT in primary and metastatic liver tumors. 2019.
72. Cherry S, R, James A. Sorenson and MEP. *Physics in Nuclear Medicine*. Elsevier/Saunders. 2012.
73. Smits MLJ, Elschot M, Sze DY, Kao YH, Nijssen JFW, Iagaru AH, et al. Radioembolization Dosimetry: The Road Ahead. *Cardiovasc Intervent Radiol*. 2015.38:261–9.
74. Tafti BA, Padia SA. Dosimetry of $^{90\text{Y}}$ Microspheres Utilizing $^{99\text{m}}\text{Tc}$ -SPECT and $^{90\text{Y}}$ PET. *Semin Nucl Med*. 2019.49:211–7.
75. Flamen P, Vanderlinden B, Delatte P, Ghanem G, Ameye L, Eynde M Van Den, et al. Multimodality imaging can predict the metabolic response of unresectable colorectal liver



metastases to radioembolization therapy with Yttrium-90 labeled resin microspheres. *Phys Med Biol.* 2008.53:6591–603.

76. Eaton BR, Kim HS, Schreibmann E, Schuster DM, Galt JR, Barron B, et al. Quantitative dosimetry for yttrium-90 radionuclide therapy: Tumor dose predicts fluorodeoxyglucose positron emission tomography response in hepatic metastatic melanoma. *J Vasc Interv Radiol.* 2014.25:288–95.

77. Smits MLJ, Nijssen JFW, Van Den Bosch MAAJ, Lam MGEH, Vente MAD, Huijbregts JE, et al. Holmium-166 radioembolization for the treatment of patients with liver metastases: Design of the phase I HEPAR trial. *J Exp Clin Cancer Res.* 2010.29.

78. Vauthey JN, Abdalla EK, Doherty DA, Gertsch P, Fenstermacher MJ, Loyer EM, et al. Body surface area and body weight predict total liver volume in western adults. *Liver Transplant.* 2002.8:233–40.

79. Bastiaannet R, Kappadath SC, Kunnen B, Braat AJAT, Lam MGEH, de Jong HWAM. The physics of radioembolization. *EJNMMI Phys.* 2018.5.

80. Gibbs P, GebSKI V, Van Buskirk M, Thurston K, Cade DN, Van Hazel GA, et al. Selective Internal Radiation Therapy (SIRT) with yttrium-90 resin microspheres plus standard systemic chemotherapy regimen of FOLFOX versus FOLFOX alone as first-line treatment of non-resectable liver metastases from colorectal cancer: The SIRFLOX study. *BMC Cancer.* 2014.14:1–10.

81. Van Hazel GA, Heinemann V, Sharma NK, Findlay MPN, Ricke J, Peeters M, et al. SIRFLOX: Randomized phase III trial comparing first-line mFOLFOX6 (Plus or Minus Bevacizumab) versus mFOLFOX6 (Plus or Minus Bevacizumab) plus selective internal radiation therapy in



patients with metastatic colorectal cancer. *J Clin Oncol.* 2016.34:1723–31.

82. GA van H, V H, NK S, MP F, J R, M P, et al. SIRFLOX: Randomized Phase III Trial Comparing First-Line mFOLFOX6 (Plus or Minus Bevacizumab) Versus mFOLFOX6 (Plus or Minus Bevacizumab) Plus Selective Internal Radiation Therapy in Patients With Metastatic Colorectal Cancer. *J Clin Oncol.* 2016.34:1723–31.

83. Smits MLJ, Nijsen JFW, van den Bosch MAAJ, Lam MGEH, Vente MAD, Mali WPTM, et al. Holmium-166 radioembolisation in patients with unresectable, chemorefractory liver metastases (HEPAR trial): A phase 1, dose-escalation study. *Lancet Oncol.* 2012.13:1025–34.

84. Garin E, Rolland Y, Lenoir L, Pracht M, Mesbah H, Porée P, et al. Utility of Quantitative 99m Tc-MAA SPECT/CT for 90 yttrium-Labelled Microsphere Treatment Planning: Calculating Vascularized Hepatic Volume and Dosimetric Approach . *Int J Mol Imaging.* 2011.2011:1–8.

85. Rodríguez-Fraile M, Ezponda A, Grisanti F, Morán V, Calvo M, Berrián P, et al. The joint use of 99mTc-MAA-SPECT/CT and cone-beam CT optimizes radioembolization planning. *EJNMMI Res.* 2021.11.

86. Sze DY, Lam MGEH. Reply to “the limitations of theoretical dose modeling for yttrium-90 radioembolization.” *J. Vasc. Interv. Radiol.* 2014. p. 1147–8.

87. Flux G, Bardies M, Chiesa C, Monsieurs M, Savolainen S, Strand SE, et al. Clinical radionuclide therapy dosimetry: The quest for the “holy Gray” [2]. *Eur. J. Nucl. Med. Mol. Imaging.* 2007. p. 1699–700.

88. Kao YH, Tan EH, Ng CE, Goh SW. Clinical implications of the body surface area method versus partition model



- dosimetry for yttrium-90 radioembolization using resin microspheres: A technical review. *Ann Nucl Med.* 2011.25:455–61.
89. Lam MGEH, Louie JD, Abdelmaksoud MHK, Fisher GA, Cho-Phan CD, Sze DY. Limitations of body surface area-based activity calculation for radioembolization of hepatic metastases in colorectal cancer. *J Vasc Interv Radiol.* 2014.25:1085–93.
90. Traino AC, Boni G, Mariani G. Radiodosimetric estimates for radioembolic therapy of liver tumors: Challenges and opportunities. *J. Nucl. Med.* 2012. p. 509–11.
91. Fowler KJ, Maughan NM, Laforest R, Saad NE, Sharma A, Olsen J, et al. PET/MRI of Hepatic 90Y Microsphere Deposition Determines Individual Tumor Response. *Cardiovasc Intervent Radiol.* 2016.39:855–64.
92. Fox RA, Klemp PFB, Egan G, Mina LL, Burton MA, Gray BN. Dose distribution following selective internal radiation therapy. *Int J Radiat Oncol Biol Phys.* 1991.21:463–7.
93. Campbell AM, Bailey IH, Burton MA. Analysis of the distribution of intra-arterial microspheres in human liver following hepatic yttrium-90 microsphere therapy. *Phys Med Biol.* 2000.45:1023–33.
94. Kao YH, Steinberg JD, Tay Y-S, Lim GK, Yan J, Townsend DW, et al. Post-radioembolization yttrium-90 PET/CT - part 1: diagnostic reporting. *EJNMMI Res.* 2013.3:1.
95. Walrand S, Hesse M, Demonceau G, Pauwels S, Jamar F. Yttrium-90-labeled microsphere tracking during liver selective internal radiotherapy by bremsstrahlung pinhole SPECT: feasibility study and evaluation in an abdominal phantom. 2011.:1–14.
96. Selwyn RG, Nickles RJ, Thomadsen BR, DeWerd LA,



- Micka JA. A new internal pair production branching ratio of ^{90}Y : The development of a non-destructive assay for ^{90}Y and ^{90}Sr . *Appl Radiat Isot.* 2007.65:318–27.
97. Kao YH, Tan EH, Ng CE, Goh SW. Yttrium-90 time-of-flight PET/CT is superior to bremsstrahlung SPECT/CT for postradioembolization imaging of microsphere biodistribution. *Clin Nucl Med.* 2011.36:e186-7.
98. D'Arienzo M, Chiaramida P, Chiacchiararelli L, Coniglio A, Cianni R, Salvatori R, et al. ^{90}Y PET-based dosimetry after selective internal radiotherapy treatments. *Nucl Med Commun.* 2012.33:633–40.
99. Bagni O, D'Arienzo M, Chiaramida P, Chiacchiararelli L, Cannas P, D'Agostini A, et al. ^{90}Y -PET for the assessment of microsphere biodistribution after selective internal radiotherapy. *Nucl Med Commun.* 2012.33:198–204.
100. Gates VL, Esmail AAH, Marshall K, Spies S, Salem R. Internal Pair Production of ^{90}Y Permits Hepatic Localization of Microspheres Using Routine PET: Proof of Concept. *J Nucl Med.* 2011.52:72–6.
101. Gupta A, Gill A, Shrikanthan S, Srinivas S. Nontargeted ^{90}Y Microsphere Radioembolization to Duodenum Visualized on ^{90}Y PET/CT and Bremsstrahlung SPECT/CT. *Clin Nucl Med.* 2012.37:98–9.
102. Kao YH, Tan EH, Lim KY, Goh SW. Yttrium-90 internal pair production imaging using first generation PET/CT provides high-resolution images for qualitative diagnostic purposes. *Br J Radiol.* 2012.85:1018–9.
103. Carlier T, Eugène T, Bodet-Milin C, Garin E, Ansquer C, Rousseau C, et al. Assessment of acquisition protocols for routine imaging of ^{90}Y using PET/CT. *EJNMMI Res.* 2013.3:11.



104. Padia SA, Alessio A, Kwan SW, Lewis DH, Vaidya S, Minoshima S. Comparison of positron emission tomography and bremsstrahlung imaging to detect particle distribution in patients undergoing yttrium-90 radioembolization for large hepatocellular carcinomas or associated portal vein thrombosis. *J Vasc Interv Radiol*. 2013;24:1147–53.
105. Pasciak AS, Bourgeois AC, Bradley YC. A Comparison of Techniques for 90Y PET/CT Image-Based Dosimetry Following Radioembolization with Resin Microspheres. *Front Oncol*. 2014;4:121.
106. Kao Y-HH, Steinberg JD, Tay Y-SS, Lim GK KY, Yan J, Townsend DW, et al. Post-radioembolization yttrium-90 PET/CT-part 2: Dose-response and tumor predictive dosimetry for resin microspheres. *EJNMMI Res*. 2013;3:1–27.
107. Scopinaro F, Salvatori R, Filippi L, Bagni O, Chiacchiararelli L, D'Arienzo M, et al. Absorbed dose to lesion and clinical outcome after liver radioembolization with 90Y microspheres: a case report of PET-based dosimetry. *Ann Nucl Med*. 2013;27:676–80.
108. Bourgeois AC, Chang TT, Bradley YC, Acuff SN, Pasciak AS. Intraprocedural yttrium-90 positron emission tomography/CT for treatment optimization of yttrium-90 radioembolization. *J Vasc Interv Radiol*. 2014;25:271–5.
109. Allimant C, Kafrouni M, Delicque J, Ilonca D, Cassinotto C, Assenat E, et al. Tumor Targeting and Three-Dimensional Voxel-Based Dosimetry to Predict Tumor Response, Toxicity, and Survival after Yttrium-90 Resin Microsphere Radioembolization in Hepatocellular Carcinoma. *J Vasc Interv Radiol*. 2018;29:1662-1670.e4.
110. Willowson KP, Hayes AR, Chan DLH, Tapner M, Bernard EJ, Maher R, et al. Clinical and imaging-based prognostic factors in radioembolisation of liver metastases



from colorectal cancer: a retrospective exploratory analysis. *EJNMMI Res.* 2017.7:1–13.

111. D'Arienzo M, Filippi L, Chiamida P, Chiacchiararelli L, Cianni R, Salvatori R, et al. Absorbed dose to lesion and clinical outcome after liver radioembolization with ⁹⁰Y microspheres: a case report of PET-based dosimetry. *Ann Nucl Med.* 2013.27:676–80.

112. Guglielmi A, Ruzzenente A, Conci S, Valdegamberi A, Iacono C. How much remnant is enough in liver resection? *Dig Surg.* 2012.29:6–17.

113. Goh BKP. Measured Versus Estimated Total Liver Volume to Preoperatively Assess the Adequacy of Future Liver Remnant. *Ann Surg.* 2015.262:e72.

114. Hemming AW, Reed AI, Howard RJ, Fujita S, Hochwald SN, Caridi JG, et al. Preoperative portal vein embolization for extended hepatectomy. *Ann Surg.* 2003.237:686–91; discussion 691-3.

115. Tanaka K, Shimada H, Matsuo K, Ueda M, Endo I, Togo S. Remnant liver regeneration after two-stage hepatectomy for multiple bilobar colorectal metastases. *Eur J Surg Oncol.* 2007.33:329–35.

116. Teo JY, Allen JC, Ng DC, Choo SP, Tai DWM, Chang JPE, et al. A systematic review of contralateral liver lobe hypertrophy after unilobar selective internal radiation therapy with ⁹⁰Y. *Hpb.* 2016.18:7–12.

117. Liu H, Zhu S. Present status and future perspectives of preoperative portal vein embolization. *Am J Surg.* 2009.197:686–90.

118. Bekki Y, Marti J, Toshima T, Lewis S, Kamath A, Argiriadi P, et al. A comparative study of portal vein



embolization versus radiation lobectomy with Yttrium-90 microspheres in preparation for liver resection for initially unresectable hepatocellular carcinoma. *Surg (United States)*. 2021.169:1044–51.

119. Aoki T, Imamura H, Hasegawa K, Matsukura A, Sano K, Sugawara Y, et al. Sequential preoperative arterial and portal venous embolizations in patients with hepatocellular carcinoma. *Arch Surg*. 2004.139:766–74.

120. Lewandowski RJ, Donahue L, Chokechanachaisakul A, Kulik L, Mouli S, Caicedo J, et al. ⁹⁰Y radiation lobectomy: Outcomes following surgical resection in patients with hepatic tumors and small future liver remnant volumes. *J Surg Oncol*. 2016.114:99–105.

121. Gabr A, Abouchaleh N, Ali R, Baker T, Caicedo J, Katariya N, et al. Outcomes of Surgical Resection after Radioembolization for Hepatocellular Carcinoma. *J Vasc Interv Radiol*. 2018.29:1502-1510.e1.

122. Jakobs TF, Saleem S, Atassi B, Reda E, Lewandowski RJ, Yaghami V, et al. Fibrosis, portal hypertension, and hepatic volume changes induced by intra-arterial radiotherapy with ⁹⁰Yttrium microspheres. *Dig Dis Sci*. 2008.53:2556–63.

123. Gaba RC, Lewandowski RJ, Kulik LM, Riaz A, Ibrahim SM, Mulcahy MF, et al. Radiation Lobectomy: Preliminary Findings of Hepatic Volumetric Response to Lobar Yttrium-90 Radioembolization. *Ann Surg Oncol*. 2009.16:1587–96.

124. Goebel J, Sulke M, Lazik-Palm A, Goebel T, Dechêne A, Bellendorf A, et al. Factors associated with contralateral liver hypertrophy after unilateral radioembolization for hepatocellular carcinoma. *PLoS One*. 2017.12:e0181488.

125. Fernández-Ros N, Silva N, Bilbao JI, Iñárraegui M, Benito A, D'Avola D, et al. Partial liver volume



radioembolization induces hypertrophy in the spared hemiliver and no major signs of portal hypertension. *HPB*. 2014.16:243–9.

126. Seidensticker R, Seidensticker M, Damm R, Mohnike K, Schutte K, Malfertheiner P, et al. Hepatic toxicity after radioembolization of the liver using (90)Y-microspheres: sequential lobar versus whole liver approach. *Cardiovasc Interv Radiol*. 2012.35:1109–18.

127. Noshier JL, Ohman-Strickland PA, Jabbour S, Narra V, Noshier B. Changes in liver and spleen volumes and liver function after radioembolization with yttrium-90 resin microspheres. *J Vasc Interv Radiol*. 2011.22:1706–13.

128. Kennedy AS, McNeillie P, Dezarn WA, Nutting C, Sangro B, Wertman D, et al. Treatment Parameters and Outcome in 680 Treatments of Internal Radiation With Resin 90Y-Microspheres for Unresectable Hepatic Tumors. *Int J Radiat Oncol Biol Phys*. 2009.74:1494–500.

129. Riaz A, Kulik L, Lewandowski RJ, Ryu RK, Spear GG, Mulcahy MF, et al. Radiologic-pathologic correlation of hepatocellular carcinoma treated with internal radiation using Yttrium-90 microspheres. *Hepatology*. 2009.49:1185–93.

130. Nalesnik MA, Federle M, Buck D, Fontes P, Carr BI. Hepatobiliary effects of 90yttrium microsphere therapy for unresectable hepatocellular carcinoma. *Hum Pathol*. 2009.40:125–34.

131. Schweizer W, Duda P, Tanner S, Balsiger D, Hörlin F, Blumgart LH, et al. Experimental atrophy/hypertrophy complex (AHC) of the liver: portal vein, but not bile duct obstruction, is the main driving force for the development of AHC in the rat. *J Hepatol*. 1995.23:71–8.

132. Kim RD, Kim JS, Watanabe G, Mohuczy D, Behrns KE.



Liver regeneration and the atrophy-hypertrophy complex. *Semin Intervent Radiol.* 2008.25:92–103.

133. Palard X, Edeline J, Rolland Y, Le Sourd S, Pracht M, Laffont S, et al. Dosimetric parameters predicting contralateral liver hypertrophy after unilobar radioembolization of hepatocellular carcinoma. *Eur J Nucl Med Mol Imaging.* 2018.45:392–401.

134. Ricke J, Schinner R, Seidensticker M, Gasbarrini A, van Delden OM, Amthauer H, et al. Liver function after combined selective internal radiation therapy or sorafenib monotherapy in advanced hepatocellular carcinoma. *J Hepatol.* 2021.:1–10.

135. Johnson PJ, Berhane S, Kagebayashi C, Satomura S, Teng M, Reeves HL, et al. A nssessment of liver function in patients with hepatocellular carcinoma: A new evidence-based approach - The albi grade. *J Clin Oncol.* 2015.33:550–8.

136. Peterson JL, Vallow LA, Johnson DW, Heckman MG, Diehl NN, Smith AA, et al. Complications after 90Y microsphere radioembolization for unresectable hepatic tumors: An evaluation of 112 patients. *Brachytherapy.* 2013.12:573–9.

137. Jalan R, D’Amico G, Trebicka J, Moreau R, Angeli P, Arroyo V. New clinical and pathophysiological perspectives defining the trajectory of cirrhosis. *J Hepatol.* 2021.75:S14–26.

138. Therasse P, Arbuck SG, Eisenhauer EA, Wanders J, Kaplan RS, Rubinstein L, et al. New guidelines to evaluate the response to treatment in solid tumors. *J Natl Cancer Inst.* 2000.92:205–16.

139. Martí-Climent JM, Prieto E, Elosúa C, Rodríguez-Fraile M, Domínguez-Prado I, Vigil C, et al. PET optimization for improved assessment and accurate quantification of 90Y-microsphere biodistribution after radioembolization. *Med*



Phys. 2014.41:092503.

140. Bilbao JI, De Martino A, De Luis E, Díaz-Dorronsoro L, Alonso-Burgos A, Martínez De La Cuesta A, et al. Biocompatibility, inflammatory response, and recanalization characteristics of nonradioactive resin microspheres: Histological findings. *Cardiovasc Intervent Radiol*. 2009.32:727–36.

141. Bilbao JL, Iezzi R, Goldberg SN, Sami A, Akhan O, Giuliante F, et al. The ten commandments of hepatic radioembolization: expert discussion and report from Mediterranean Interventional Oncology (MIOLive) congress 2017. *Eur Rev Med Pharmacol Sci*. 2017.21:4014–21.

142. Lescure C, Estrade F, Pedrono M, Campillo-Gimenez B, Le Sourd S, Pracht M, et al. Albi score is a strong predictor of toxicity following sirt for hepatocellular carcinoma. *Cancers (Basel)*. 2021.13:1–10.

143. van Roekel C, Reinders MTM, van der Velden S, Lam MGEH, Braat MNGJA. Hepatobiliary Imaging in Liver-directed Treatments. *Semin Nucl Med*. 2019.49:227–36.

144. Braat MNGJA, de Jong HW, Seinstra BA, Scholten M V., van den Bosch MAAJ, Lam MGEH. Hepatobiliary scintigraphy may improve radioembolization treatment planning in HCC patients. *EJNMMI Res*. 2017.7.

145. Ahmadzadehfar H, Meyer C, Ezziddin S, Sabet A, Hoff-Meyer A, Muckle M, et al. Hepatic volume changes induced by radioembolization with ⁹⁰Y resin microspheres. A single-centre study. *Eur J Nucl Med Mol Imaging*. 2013.40:80–90.



X. Annex


Grisanti, F., Prieto, E., Bastidas, J.F. *et al.* 3D voxel-based dosimetry to predict contralateral hypertrophy and an adequate future liver remnant after lobar radioembolization. *Eur J Nucl Med Mol Imaging* **48**, 3048–3057 (2021).
<https://doi.org/10.1007/s00259-021-05272-9>

ORIGINAL RESEARCH

Open Access



The joint use of ^{99m}Tc -MAA-SPECT/CT and cone-beam CT optimizes radioembolization planning

Macarena Rodríguez-Fraile^{1*} , Ana Ezponda², Fabiana Grisanti¹, Verónica Morán³, Marta Calvo², Pablo Berián², Antonio Martínez de la Cuesta², Lidia Sancho⁴, Mercedes Iñarrairaegui⁵, Bruno Sangro⁵ and José Ignacio Bilbao²

Abstract

Purpose: To determine which imaging method used during radioembolization (RE) work-up: contrast-enhanced computed tomography (CECT), ^{99m}Tc -MAA-SPECT/CT or cone beam-CT (CBCT), more accurately predicts the final target volume (TgV) as well as the influence that each modality has in the dosimetric calculation.

Methods: TgVs from ^{99m}Tc -MAA-SPECT/CT, CECT and CBCT were consecutively obtained in 24 patients treated with RE and compared with ^{90}Y PET/CT TgV. Using the TgVs estimated by each imaging modality and a fictitious activity of 1 GBq, the corresponding absorbed doses by tumor and non-tumoral parenchyma were calculated for each patient. The absorbed doses for each modality were compared with the ones obtained using ^{90}Y PET/CT TgV.

Results: ^{99m}Tc -MAA-SPECT/CT predicted ^{90}Y PET/CT TgV better than CBCT or CECT, even for selective or superselective administrations. Likewise, ^{99m}Tc -MAA-SPECT/CT showed dosimetric values more similar to those obtained with ^{90}Y PET/CT. Nevertheless, CBCT provided essential information for RE planning, such as ensuring the total coverage of the tumor and, in cases with more than one feeding artery, splitting the activity according to the volume of tumor perfused by each artery.

Conclusion: The joint use of ^{99m}Tc -MAA-SPECT/CT and CBCT optimizes dosimetric planning for RE procedures, enabling a more accurate personalized approach.

Keywords: Radioembolization (RE), CBCT, MAA, PET, Dosimetry, Target volume

Background

In radioembolization (RE), the definition of the target volume (TgV)—including tumoral and non-tumoral areas—that will receive the treatment, is decisive in many dosimetric aspects: for single-compartment medical internal radiation dose (MIRD) model because it assumes a uniform activity distribution within the TgV; for modified body surface area (mBSA) or partition model methods, because TgV is incorporated in the formulas [1]; for

3D voxel-dosimetry, because the dosimetric calculations derive precisely from the predicted TgV.

Current practice of assessing TgV is based on contrast-enhanced computed tomography (CECT) or magnetic resonance (MR), which reflect the standard anatomical venous segmentation as defined by Couinaud. However, this approach may be inaccurate in different clinical settings, such as in selective arterial (segmental and sub-segmental) administrations, in *central* tumors without a pure lobar or segmental distribution, or in patients with anatomical variations—whether innate or related to tumorigenesis [2], among others.

*Correspondence: mrodriguez@unav.es

¹ Nuclear Medicine Department, Clínica Universidad de Navarra, Pamplona, Spain

Full list of author information is available at the end of the article

Other imaging methods performed in the routine RE work-up have also been used to assess volumetric analysis. These include ^{99m}Tc -macroaggregated albumin (^{99m}Tc -MAA) SPECT/CT (^{99m}Tc -MAA-SPECT/CT) or C-arm cone-beam CT (CBCT). The use of the ^{99m}Tc -MAA-SPECT/CT as a method to calculate TgV was first described by Garin et al. [3], demonstrating its accuracy in hepatocellular carcinoma (HCC) [4] and in cholangiocarcinoma (CC) [5]. Likewise, CBCT has been proposed as a useful method for defining the TgV in total or lobar administrations [6]–[8]. Rangraz et al. [7] demonstrated that using CBCT—instead of CECT—results in a difference in volumetric parameters. However, none of the abovementioned studies has been performed in segmental or subsegmental administrations (treatment via direct tumor-feeding vessel) [9], where the evaluation of the TgV in the CBCT without clear anatomical limits may be more challenging.

Once the treatment is administered, both *bremstrahlung* SPECT/CT (BS) or Yttrium-90 (^{90}Y) PET/CT are generally used to verify the final distribution of the microspheres. Nevertheless, ^{90}Y PET/CT has been shown to be superior to BS for the assessment of target activity [10], helping in the accurate quantification of the total delivered activity [11] and to perform dose estimation [12, 13]. Moreover, ^{90}Y PET/CT-based dosimetry after RE with resin microspheres has been shown to predict outcome in patients with liver metastases from colorectal cancer (CC) [14]. Hence, ^{90}Y PET/CT is a robust and reliable tool for the estimation of the ^{90}Y -microspheres deposition.

The primary aim of this study was to determine which of the imaging methods available at the time of the initial evaluation of RE (CECT, ^{99m}Tc -MAA-SPECT/CT or CBCT) predicts more accurately the TgV, having the ^{90}Y PET/CT final TgV as the reference parameter. A secondary objective was to evaluate the influence that the differences in the estimated TgV for each technique has in the dosimetric calculation.

Finally, since in order to reduce the risk of RE-induced liver disease (REILD) [15], it is highly recommended to minimize the irradiation of the non-tumoral tissue [16, 17], RE administrations are becoming increasingly selective. In this sense, the contribution of ^{99m}Tc -MAA-SPECT/CT and CBCT to the standard images (CECT) for a better dosimetric planning, especially in segmental or subsegmental approaches, was also analyzed [15].

Materials and methods

Same-day RE protocol

Patients

All patients treated with resin ^{90}Y -microspheres (SIR-spheres[®], SIRTex Medical Limited) in our center from October 2018 to April 2019 were consecutively studied.

After being considered as a candidate for RE by the hepatobiliary multidisciplinary team (MDT), a same-day planning and treatment was performed in all cases. Both the aim and the approach of the treatment (total, lobar, segmental or subsegmental) were always defined by the MDT.

Pre-treatment angiography

After the oral administration of 600 mg sodium perchlorate to block free ^{99m}Tc -pertechnetate uptake by stomach [18], a 4F catheter was advanced via common femoral artery, and a selective angiography of both the superior mesenteric artery and the celiac trunk was performed. Coil embolization was performed, if necessary, to prevent the delivery of particles to the non-target tissue. The interventional radiologist (IR) performed in all cases the angiographic simulation to cover the entire tumoral tissue while preserving as much volume of non-tumoral parenchyma as possible. When multiple extra or intrahepatic vessels feeding the TgV were detected, a selective catheterization of each one was carried out. Thus, same-day flow redistribution was performed, when deemed necessary, to treat the complete tumoral area reducing the number of injection points [19, 20].

Diagnostic angiography and endovascular intervention were performed using the robotic digital subtraction angiography system (Artis Zeego Q, VE 40 A, Siemens Healthineers, Forchheim, Germany). CBCT was routinely performed immediately after the angiography to determine the best arterial access. It consisted of an unenhanced rotation (mask run) and contrast-enhanced rotations. Rotation time was 4 s. Parameters of CT acquisition were: tube voltage, 90 kV; 248 frames; 0.8° per frame; pixel size, 616 μm ; acquisition time, 12 s. Once the selected arterial access was defined, 111–185 MBq ^{99m}Tc -MAA was injected to mimic the future distribution of ^{90}Y -microspheres.

TgV from CBCT image was delineated by a technician in radiology and supervised by the IR using a volume calculation software (Syngo DynaCT, Siemens Healthineers). The reconstruction used was as follows: voxel size 0.5 mm³ (full); slice matrix, 512 \times 512; kernel type, HU (W 1400; C 550); 0.5 mm slice thickness; image characteristics, normal; reconstruction model, Nat Fill; viewing preset, Syngo Dyna CT. A 0.5 mm slice thickness was employed. Images were windowed to emphasize liver parenchyma (W 1400; C 550). Regions of interest (ROIs) were manually drawn every two axial images and then interpolated. The obtained volume was reviewed in sagittal and coronal dimensions and corrected if needed. For target volume delineation, MIP (maximum intensity projection) datasets were also employed. Edge enhancement was included in the volume determination. Tumor

volume was more clearly visualized with MIP representation (6 mm).

The TgVs of CECT studies were obtained using Syngo.via software (Siemens Healthineers). CECT TgV was defined on cross-sectional images by a radiologists, using a fixed slice thickness (3 mm). The volumes of each slice were summed, independent of anatomical landmarks. Region of interest (ROI) were manually drawn in each slice involving the target/tumor volume. A unified window level (W, 300 HU) and window width (C, 40 HU) was determined. In all cases, tumoral volumes were also assessed by CECT images.

^{99m}Tc-MAA scintigraphy and SPECT/CT

Within 40 min after ^{99m}Tc-MAA administration, planar scintigraphy and SPECT/CT (128 × 128, 180°, 64 projections, 20 s/projection) were performed (Symbia 2, Siemens Healthcare). The images were used to define: (a) the intrahepatic distribution of ^{99m}Tc-MAA, (b) to calculate the hepatopulmonary shunt (HPS) and (c) to determine the tumor/non-tumor ratio (TNR), as described elsewhere [1]. A HPS, calculated on planar images, above 20% was considered a contraindication for the treatment.

TgV in ^{99m}Tc-MAA-SPECT/CT was defined using the multimodality reading software Syngo.via for MI (Siemens Healthineers). Using the “VOI+ isocontour” tool, a volume of interest (VOI) in the target liver (including tumor and non-tumor) was drawn by a nuclear medicine (NM) physician and by means of the isocontour

definition, the “molecular tumor volume or MTV” in milliliters (ml) obtained was used as the ^{99m}Tc-MAA-SPECT/CT TgV. The isocontour threshold was visually adjusted to include the ^{99m}Tc-MAA uptake volume into the VOI (Fig. 1).

Dosimetric calculation

The activities were calculated considering the absorbed doses (Gy) by tumor and healthy parenchyma as proposed by Gil-Alzugaray [21]. These absorbed doses were defined by formula [1] using the parameters obtained in the ^{99m}Tc-MAA-SPECT/CT and CECT studies. In general terms, in cirrhotic patients with a predicted spared volume less than 40%, the activity was estimated to produce a safe absorbed dose by the non-tumoral compartment (≤40 Gy). In contrast, when the predicted TgV was small (<60%) and the patient had a preserved liver function, a tumoricidal absorbed dose (>100 Gy) was estimated, irrespective of the dose delivered to the non-tumoral tissue [21].

TNR values used for dosimetric calculations derived in all cases from ^{99m}Tc-MAA-SPECT/CT.

Treatment administration

More than four hours after ^{99m}Tc-MAA, resin ⁹⁰Y-microspheres were administered during a new angiographic procedure. When ^{99m}Tc-MAA-SPECT/CT showed an adequate distribution in the tumoral area, the vascular introducer was left in the same place for

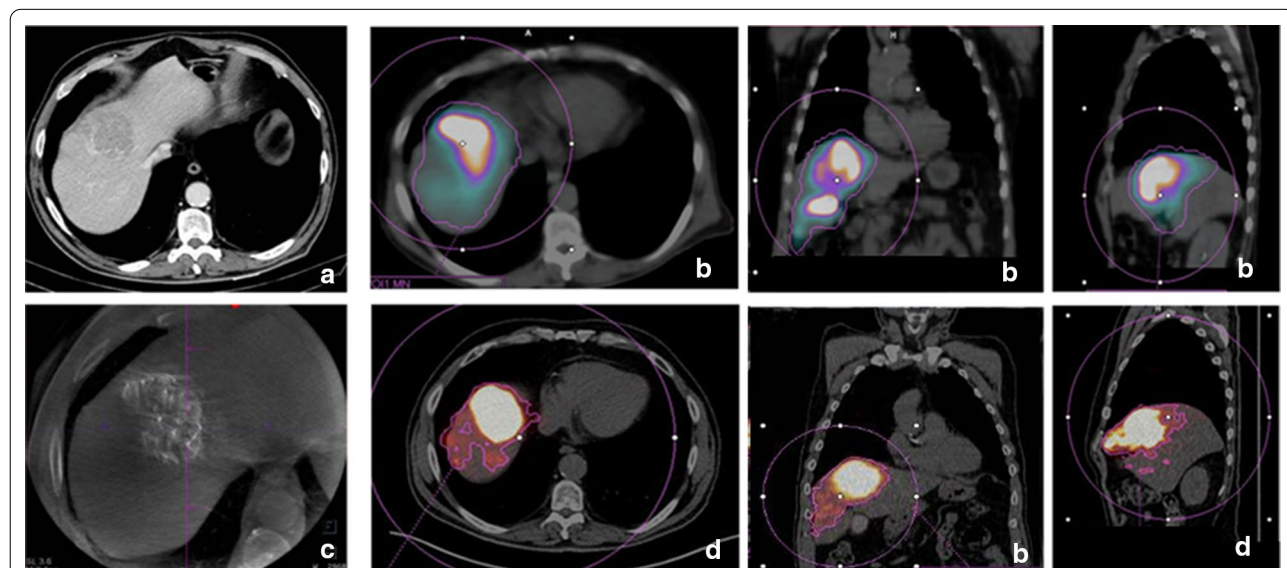


Fig. 1 a Contrast-enhanced computed tomography (CECT) image in a patient with HCC located between segments IV and VIII. b Volumetric assessment of the target volume in SPECT/CT fusion images after the injection of ^{99m}Tc-MAA through IV and VIII segments arteries. The volume was obtained using a “volume of interest and isocontour” tool, drawn in purple. c C-arm cone-beam CT (CBCT) showing contrast uptake in the tumoral lesion with no perfusion in non-tumoral parenchyma. d Volumetric assessment of the final target volume in the ⁹⁰Y PET/CT fusion images

both procedures. In cases in which the arterial access selected by the IR did not optimally reach the tumoral area in the ^{99m}Tc -MAA-SPECT/CT images, the angiography images were re-evaluated. In these cases, if a better access was identified, the site of injection between ^{99m}Tc -MAA and RE differed. Although it is advisable to repeat ^{99m}Tc -MAA evaluation when changes are made, it can be avoided if the modifications are minimal or do not have an impact on the safety of the treatment.

Post-treatment PET/CT

The morning after the RE treatment, a ^{90}Y PET/CT scan centered on the liver region (two beds, 10 min/bed) was performed using a Biograph mCT-TrueV (Siemens Medical Solutions), which combines a 64-slice CT with a 21.8 cm field of view time-of-flight PET scanner comprised by lutetium-based crystals (LSO) detector blocks [22]. The reconstruction protocol used (one iteration, 21 subsets, a 6-mm Gaussian filter and a 200×200 matrix) was previously optimized by Martí-Climent et al. [11].

Final TgV in ^{90}Y PET/CT was defined using the multimodality reading software Syngo.via for MI (Siemens Healthineers) as previously described for ^{99m}Tc -MAA-SPECT/CT.

Comparison of the TgV and the predicted dosimetry for each image method

TgVs calculated by ^{99m}Tc -MAA-SPECT/CT, CECT and CBCT were compared with the TgV obtained in the ^{90}Y PET/CT study.

In order to evaluate the influence that the differences that TgV for each technique has in the dosimetry, the absorbed doses calculated using the different TgV imaging modalities were compared using in all cases a fictitious prescribed activity of 1 GBq. The use of a fixed amount of activity makes it easier to appreciate the impact that the use of each TgV would have had on the absorbed doses. The TNR and tumor volumes were the real ones calculated for each patient. The absorbed doses for each modality were compared with the ones obtained using ^{90}Y PET/CT TgV. Considering the latter as the actual ones [3, 4], the percentage of change between absorbed doses ($[(\text{Gy for } ^{90}\text{Y PET/CT TgV} - \text{Gy for TgV modality})/\text{Gy for TgV modality}] \times 100\%$), was calculated for each patient. A positive value indicates a percentage increase. (Gy in ^{90}Y PET/CT is higher than the predicted using the TgV for each modality.) A negative value indicates a percentage decrease (Gy in ^{90}Y PET/CT is lower than predicted using the TgV for each modality).

Contribution of ^{99m}Tc -MAA-SPECT/CT and CBCT for a better dosimetric RE planning

The contribution of CBCT and ^{99m}Tc -MAA-SPECT/CT to the standard images (CECT) for a more personalized RE planning were evaluated by an IR and a NM physician (both with more than 15 years of experience in RE). The additional information provided by both techniques was especially focused on those clinical settings in which CECT may present some limitations for dosimetric calculations, such as selective or superselective approaches, several tumoral feeding arteries, flow redistribution, etc.

Statistical analysis

To assess agreement between studies, the Lin Concordance Correlation Coefficient (CCC) and its 95% Confidence Interval (95% CI) were used. To define which study best predicts the final TgV, the determination coefficient (R^2) from the regression model was utilized. For each modality, the difference changes of absorbed doses between treatment approaches were analyzed with the t students test. A p value less than 0.05 was used to determine the presence of a significant difference. The data were analyzed using Statistical Package for Social Science (SPSS) software version 22.

Results

During the study period, 24 consecutive patients (18 men, 63.54 years (± 6.6)) underwent same-day RE with resin ^{90}Y microspheres (20 HCC, three CC and one neuroendocrine tumor).

Flow redistribution was performed in 10 patients (41.7%), being the embolized vessels: phrenic arteries ($n=5$), segment IV artery ($n=2$), left gastric artery ($n=4$), renal capsular artery ($n=1$), gastroduodenal artery ($n=1$) and middle hepatic artery ($n=1$).

For cases with two or more supply arteries, ^{99m}Tc -MAA activity was divided into 25%, 50% or 75% at the IR discretion, depending on the findings obtained during mapping arteriography. CBCT was performed in 23/24 patients (in 1/24 was not possible due to lack of patient collaboration). Four CBCT studies were excluded from the TgV analysis. An insufficient CBCT technique did not allow the correct assessment of TgV.

In all cases CBCT volumetry was obtained after ^{99m}Tc -MAA injection, so the calculation was not used to split ^{99m}Tc -MAA activity.

CECT and ^{99m}Tc -MAA-SPECT/CT TgVs were calculated in all patients during RE planning, not knowing the final distribution of ^{90}Y -microspheres on ^{90}Y PET/CT (Table 1).

Mean HPS was 6.9% (± 3.4). Mean TNR was 2.6 (± 1.5). In the majority of cases TNR was an average of

the uptake in all tumors, while in 4 cases it was calculated for each tumor as described elsewhere [23]. To simplify the results, a mean of the TNR of all tumors was calculated in these 4 patients.

In 17/24 patients (71%), RE injection were performed through segmental or subsegmental arteries. Seven patients were treated with just one infusion of ^{90}Y -microspheres, four were lobar (right) and three were segmental. Fifteen patients were treated from two different arteries, three of them received a whole-liver treatment (right and left hepatic arteries), two were treated through a lobar and a segmental branch, eight through two different segmental/subsegmental branches and two through

the inferior phrenic artery in association with a lobar (1) or a segmental (1) artery. Finally, two patients required three different infusions through segmental and accessory arteries (Table 1).

In four patients (16%), as depicted in Table 1, $^{99\text{m}}\text{Tc}$ -MAA-SPECT/CT and RE administrations differed due to patient motion during RE (Patient #4), vasospasm (Patient #1) or minimal deliberate changes to improve tumor coverage (Patients #3 and #12).

Median (interquartile range or IQR) administered activity was 1.2 (0.5–3.4) GBq, obtained in 23 patients by partition model formula and in one patient by BSA (– 20%).

Table 1 $^{99\text{m}}\text{Tc}$ -MAA and ^{90}Y -microspheres injection sites, percentage of $^{99\text{m}}\text{Tc}$ -MAA activity administered through every artery (decided by IR based on liver and tumor volumes) and split of ^{90}Y -microspheres prescribed by each artery (in up to 42% of patients according to CBCT volumetric information)

Patient	$^{99\text{m}}\text{Tc}$ -MAA injection (%)	CECT TgV (ml)	CBCT TgV (ml)	MAA-SPECT/CT TgV (ml)	^{90}Y -microspheres injection (prescribed) (GBq)	^{90}Y -PET/CT TgV (ml)
1•	I (75), LHA (25)	640	626	640	I (0.75), LHA (0.25)	1445
2	VI (50), VIII(50)	392	NA	412	VI (0.5), VIII (0.2)	654
3•#	IV (50), VIII (50)	270	206	537	LHA (0.8), RHA (0.7)	1561
4•	IV (50) and VIII (50) subsegmental arteries	25	25	83	IV (0.3) and VIII (0.6) subsegmental arteries	405
5	IV	99	144	218	IV (1)	257
6	V–VIII (50), IV (50)	267	292	858	V–VIII (0.5), IV (1)	755
7	IV	135	70	133	IV (1)	181
8	VI–VII	276	228	451	VI–VII (1.5)	420
9	VIII (50), VI (50)	746	511	1127	VIII (1.1), VI (0.5)	1277
10	V–VIII (50), Inferior Phrenic artery (50)	340	480	707	V–VIII (0.65), Inferior Phrenic artery (0.65)	870
11	RHA (50), Right Inferior Phrenic artery (50)	1147	1515	1097	RHA (0.9), Right Inferior Phrenic artery (0.7)	1298
12•	IV	361	NA	350	Branches 1 (0.4) and 2 (0.4) of IV artery	399
13	VIII (33), VII (33) II (33)	960	NA	917	VIII (0.5), VII (0.5), II (0.2)	1118
14	V–VIII (75), IV (25)	537	NA	489	V–VIII (0.3), IV (0.7)	622
15	RHA (75), IV (25)	1550	1860	1276	RHA (1.2), IV (0.3)	1373
16	VIII (50), VII (50)	510	903	1260	VIII (0.7), VII (0.7)	1357
17	IV (75), II (25)	290	450	254	IV (0.65), II (0.25)	350
18	Accessory HA (42), Proper HA (35), IV (22)	1186	NA	1313	Accessory HA (1.7), Proper HA (1.3), IV (0.4)	1380
19#	RHA (25), LHA (75)	1955	1975	1468	RHA (0.4), LHA (1)	1536
20#	RHA	2260	2305	2279	RHA (3.4)	2420
21#	RHA (75), LHA (25)	1285	1387	1516	RHA (1), LHA (0.18)	1683
22#	RHA	760	974	986	RHA (0.82)	992
23#	RHA	700	971	802	RHA (0.64)	922
24#	RHA	580	966	795	RHA (1)	792

Target volumes obtained for each patient with CECT, CBCT, $^{99\text{m}}\text{Tc}$ -MAA SPECT/CT as well as final target volume ^{90}Y -PET/CT, are also reported

•Patients with intended or unintended changes between MAA and ^{90}Y -microspheres administrations

Pure lobar and total treatments

RHA Right Hepatic Artery, LHA Left Hepatic Artery, NA non available

Comparison of the TgV and the predicted dosimetry for each image method

Medians TgVs were 558.5 (25–2260) ml for CECT, 626 (25–2305) ml for CBCT, 798.5 (83–2279) ml for ^{99m}Tc-MAA-SPECT/CT, and 957 (181–2420) ml for ⁹⁰Y PET/CT (Table 1).

Isocontour mode was 3% (range=1–9%) for both ^{99m}Tc-MAA-SPECT/CT and ⁹⁰Y PET/CT. This value was used for the definition of TgV in 16/24 patients (67%) for ^{99m}Tc-MAA-SPECT/CT and in 17/24 patients (71%) for ⁹⁰Y PET/CT.

The concordance with ⁹⁰Y PET/CT final TgV was substantial for CBCT (CCC=0.71; 95% CI=0.42–0.87) and for CECT (CCC=0.72; 95% CI=0.49–0.85). Maximal

concordance was reached by ^{99m}Tc-MAA-SPECT/CT (CCC=0.85; 95% CI=0.7–0.87). This concordance was even higher when those four patients with changes between ^{99m}Tc-MAA and RE administration were excluded (CCC=0.97; 95% CI=0.94–0.99) (Fig. 2).

When only segmental or subsegmental administrations were evaluated (n=17), the concordance with ⁹⁰Y PET/CT final TgV was moderate for CECT (CCC=0.5; 95% CI=0.2–0.74) while was substantial for CBCT (CCC=0.67; 95% CI=0.26–0.87) and for ^{99m}Tc-MAA-SPECT/CT (CCC=0.71; 95% CI=0.42–0.87). Exclusion of the four patients with changes between ^{99m}Tc-MAA and RE administration supposed a substantial improvement for ^{99m}Tc-MAA-SPECT/CT (CCC=0.95;

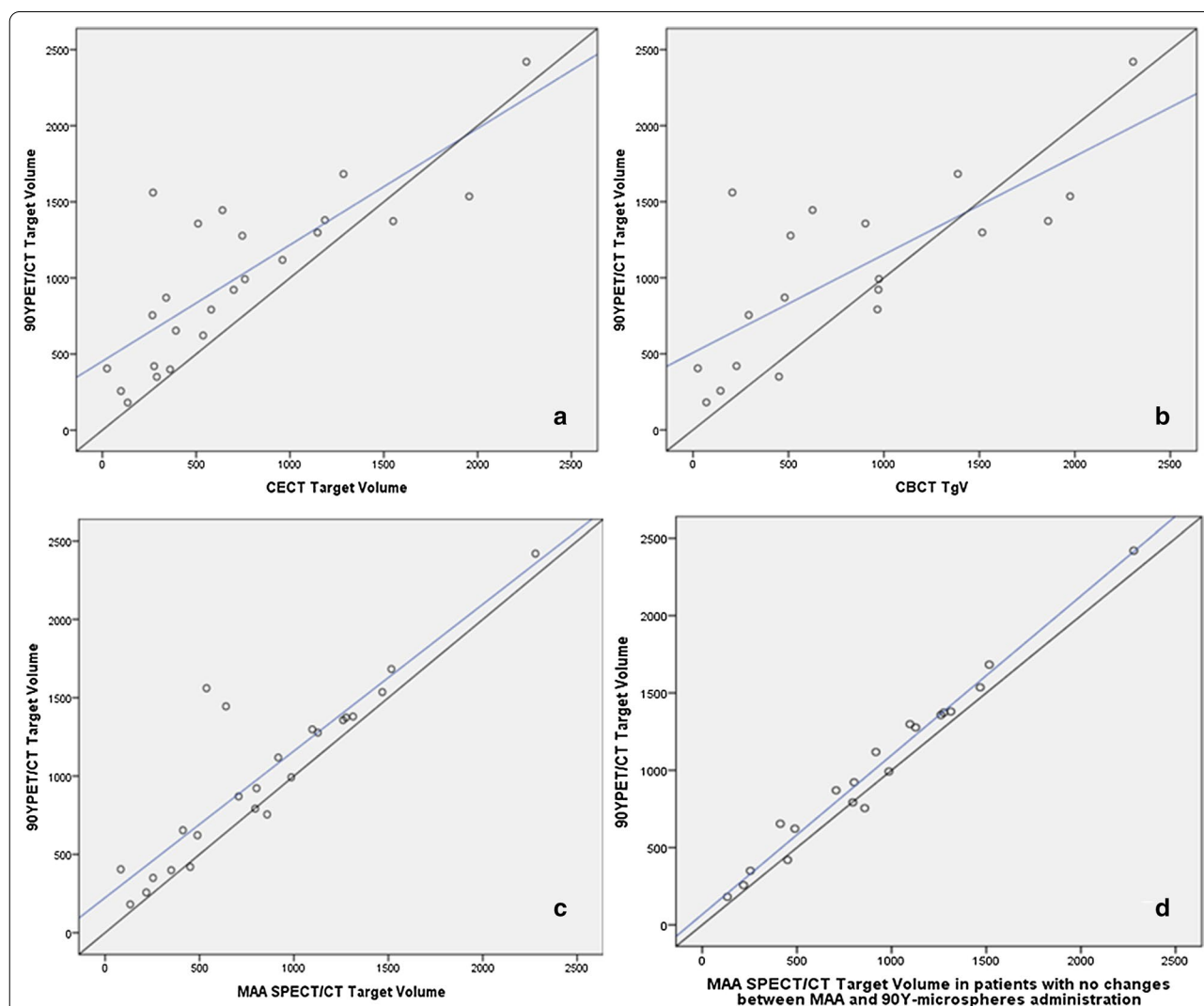


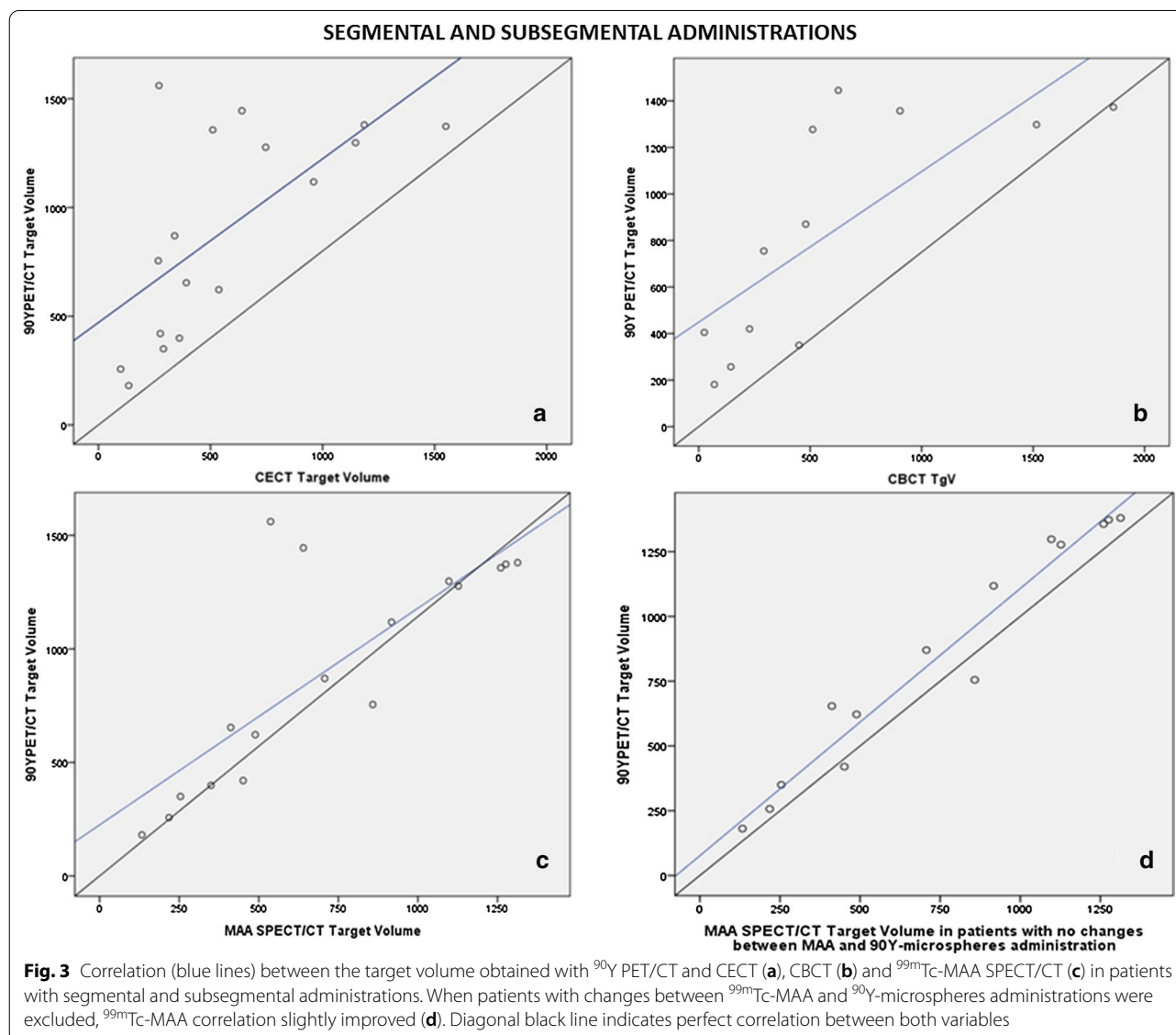
Fig. 2 Correlation (blue line) between the target volume obtained with ⁹⁰Y PET/CT and CECT (a), CBCT (b) and ^{99m}Tc-MAA SPECT/CT in all patients (c) and excluding patients with changes between MAA and ⁹⁰Y-microspheres administrations (d). Diagonal black line indicates perfect correlation between both variables

95% CI=0.87–0.98) (Fig. 3) but minimal for CBCT (CCC=0.73; 0.3–0.91).

The three studies predicted linearly the ⁹⁰Y PET/CT final TgV. However, both CBCT ($R^2=0.66, p<0.05$) and CECT ($R^2=0.68, p<0.01$) showed a moderate weak R^2 , being strong for ^{99m}Tc-MAA-SPECT/CT ($R^2=0.96, p<0.01$).

The median of the absorbed doses by tumor calculated using a fictitious activity of 1 GBq was 152 (98–250) Gy for CECT TgV, 125 (73–253) Gy for CBCT TgV, 116 (70–244) Gy for ^{99m}Tc-MAA-SPECT/CT TgV and 102 (64–162) Gy ⁹⁰Y PET/CT TgV. The median of the absorbed doses by non-tumoral liver using CECT was 74 (36–113) Gy, CBCT was 51 (31–104) Gy, ^{99m}Tc-MAA-SPECT/CT was 46 (35–95) Gy and ⁹⁰Y PET/CT

TgV was 40 (30–75) Gy. The absorbed doses by tumor calculated using ⁹⁰Y PET/CT showed a median difference with the ones predicted by CECT of – 33 (– 65 to – 13) Gy, by CBCT of – 20 (– 194 to 14) Gy and by ^{99m}Tc-MAA-SPECT/CT of – 14 (– 54 to – 1) Gy. For non-tumoral liver of – 15 (– 38 to – 4) Gy using CECT, of – 17 (– 52 to 5) Gy using CBCT and of – 5 (– 37 to – 1) Gy using ^{99m}Tc-MAA-SPECT/CT. These values represent a mean percentage of change between the absorbed doses obtained using ⁹⁰Y PET/CT TgV and the ones predicted with CECT of – 29 (±30)%, with CBCT of – 23 (±38)% and with ^{99m}Tc-MAA-SPECT/CT of – 18 (±24)%. There were no statistically significant differences between the treatment approach (lobar and lobar extended/ total vs. selective



and superselective) and the percentage of change for CECT and for ^{99m}Tc -MAA-SPECT/CT. However, CBCT showed values of absorbed doses more similar to ^{90}Y PET/CT for lobar and total approaches ($-2.5 \pm 31\%$) than for selective ($-38 \pm 37\%$) administrations ($p < 0.05$).

Contribution of ^{99m}Tc -MAA-SPECT/CT and CBCT for a better dosimetric RE planning

The information provided by ^{99m}Tc -MAA-SPECT/CT was determinant in 17 patients (71%), due to its capability: (a) to predict ^{90}Y -microspheres distribution in patients with segmental or subsegmental treatments ($n=8$); (b) to confirm the TgV after flow redistribution ($n=7$) and (c) to detect tumoral areas not covered with the selected arterial access ($n=2$).

CBCT helped to define the percentage of tumor volume perfused by each artery in 10 patients (42%) in whom the tumor was fed by more than one artery. This volumetric information was used to split the activity of ^{90}Y -microspheres accordingly (Fig. 4). Moreover, CBCT allowed to ensure the tumor coverage in six patients (25%) and to rule out the presence of microsatellite lesions in one patient (4%). Globally, CBCT information was used for a personalized and more accurate planning in 17/24 patients (71%).

Discussion

The results of this study show that ^{99m}Tc -MAA-SPECT/CT predicts more accurately the final TgV—as defined in the ^{90}Y PET/CT—than CBCT or even than the conventional method (CECT). This superiority is even more notable in segmental and subsegmental administrations. The differences obtained in the TgV for each method would have had a significant impact on the dosimetric calculation. Additionally, ^{99m}Tc -MAA-SPECT/CT and CBCT information were determinant for RE planning in a significant proportion of patients. Our study therefore suggests that the joint use of both techniques optimizes dosimetry planning for RE procedures.

In this study, TgV obtained with different imaging modalities using the ^{90}Y PET/CT as the method of validation, which has proven to be the most accurate technique for determining the final distribution of the microspheres [11, 12].

Since all consecutive patients treated with RE in our center in a period of time were studied, not only the optimal situations (identical ^{99m}Tc -MAA and RE administrations) were included. As it occurs in daily practice, patients with intended or unintended modifications between both procedures were considered. Furthermore, flow redistribution was performed in 41.7% of the patients. Despite all these complex circumstances, the ^{99m}Tc -MAA-SPECT/CT TgV reached maximal concordance with ^{90}Y PET/CT final TgV (CCC=0.85). As expected, when the four patients with changes between

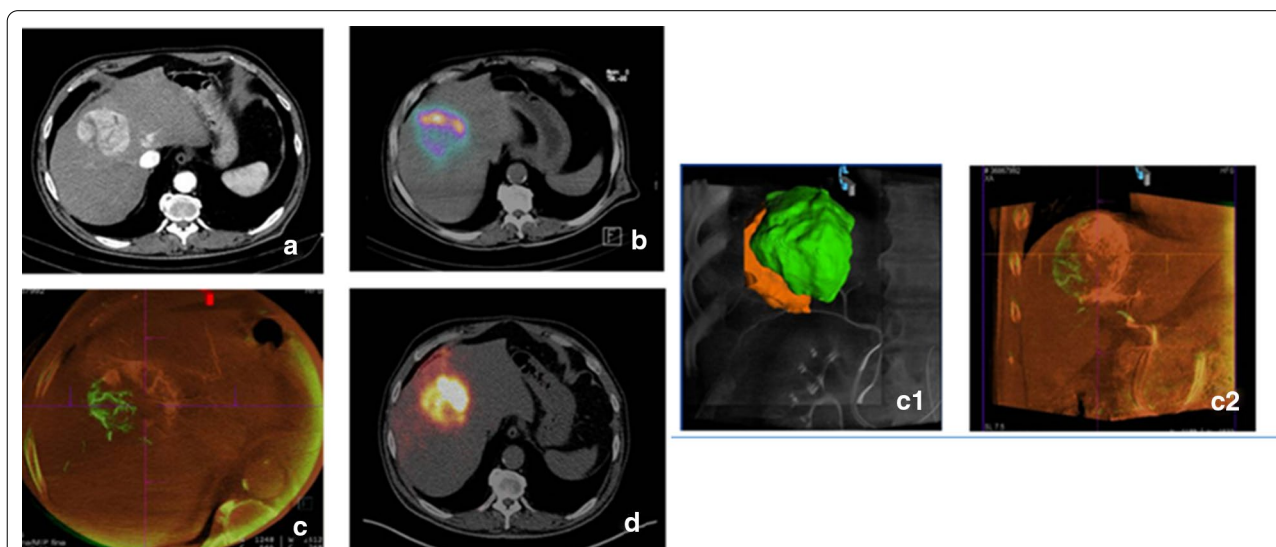


Fig. 4 Same patient as Fig. 1. **a** Contrast-enhanced computed tomography (CECT) image: HCC located between segments IV and VIII. **b** ^{99m}Tc -MAA SPECT/CT fusion image shows low uptake in the lateral part of the tumoral nodule. ^{99m}Tc -MAA activity was split in two doses of 50% each by IR decision, based on liver and tumoral volumes. **c**, **c1** and **c2** C-arm cone-Beam CT (CBCT) volumetric assessment of the tumoral territory perfused by each artery. VIII segments artery (in green) fed only 32% of the tumoral volume while IV segment artery fed most of it (in orange). **d** ^{90}Y PET/CT fusion image after splitting the activity according to CBCT volumes shows the adequate distribution of the microspheres throughout the lesion

^{99m}Tc -MAA and RE administrations were excluded, ^{99m}Tc -MAA-SPECT/CT increased its concordance value ($\text{CCC}=0.97$). The high concordance found between ^{99m}Tc -MAA-SPECT/CT and ^{90}Y PET/CT volumetry supports the use of ^{99m}Tc -MAA-SPECT/CT as the most reliable available tool for predicting final TgV. Although 3D voxel-dosimetry is currently recommended, the methodology followed here sustains its reliability even using a simple tool available by most groups performing RE.

In 71% of patients, RE administrations were performed through segmental or subsegmental arteries. When only these selective administrations were analyzed, ^{99m}Tc -MAA-SPECT/CT showed to be superior to CECT ($\text{CCC}=0.5$) and to CBCT ($\text{CCC}=0.67$) for predicting TgV, with a substantial concordance ($\text{CCC}=0.71$) with ^{90}Y PET/CT TgV. These findings demonstrate that ^{99m}Tc -MAA-SPECT/CT is also an effective tool for defining the TgV in segmental or subsegmental administrations, where CECT has some limitations [2, 8]. Because of the benefit to patient outcome of the parenchyma-sparing RE administrations [16, 17], selective administrations are recommended when possible. Hitherto, CECT volumes have been traditionally used for these selective administrations. However, and according to the results obtained in this study, CECT volumes poorly predict the final TgV obtained with ^{90}Y PET/CT.

As for the reproducibility of ^{99m}Tc -MAA-SPECT/CT and ^{90}Y PET/CT isocontour definition, our results are comparable to previous studies: the isocontour mode was 3% (range 1–9%) for them both. This is in accordance with Richetta et al. [24] that using a mean threshold of 3% (range of 2–4%) found a good dose agreement between ^{99m}Tc -MAA-SPECT/CT and ^{90}Y PET/CT. Martí-Clement et al. [11] in a series of 10 patients found that 5% was the isocontour level that provided the lowest relative difference between reconstructed activity and activity delivered to the whole-liver ($(10.2 \pm 14.7)\%$). Moreover, Garin et al. [3], in a phantom study using an adaptive thresholding method based on SPECT/CT images, as used in our study, encountered a mean error of $<2.5\%$ for volumes larger than 16 ml. Therefore, it seems that the visual adjustment of the isocontour level for the definition of the total treated liver is feasible and there are not significant variations on the value used between groups. It should be noted that all TgV ^{99m}Tc -MAA-SPECT/CT were prospectively defined, not knowing the final microsphere distribution.

CBCT showed only a moderate concordance with ^{90}Y PET/CT final TgV, lower than for ^{99m}Tc -MAA-SPECT/CT. Although both are functional modalities, CBCT depends on the lapse of time between injection of the contrast agent and the image acquisition and also on the speed and volume of the injection. In some of our cases,

this contrast volume could be insufficient to precisely demarcate the limits of the TgV. This was sometimes done deliberately to avoid contrast reflux to non-target areas or because CBCT was performed to detect other tumoral nodules—and not with volumetric purposes. Therefore, more studies are needed to discern whether CBCT moderate accuracy encountered was due to a limited capacity to define TgV in segmental/subsegmental administrations without clear anatomical limits or due to technical issues. Nevertheless, CBCT has other advantages not explored in this study such as its capability to detect extrahepatic arterial supply [25], feeding arteries not identified by CECT [26] or the exclusion of necrotic areas with no contrast uptake for a more precise volumetric assessment of the tumor.

Using the TgVs estimated by each imaging modality and a fictional administered activity of 1 GBq, the corresponding absorbed doses by tumor and non-tumor were calculated for each patient. Consistent with the results obtained for volumetry, ^{99m}Tc -MAA-SPECT/CT showed lower differences with the values obtained with ^{90}Y PET/CT TgV, than the rest of modalities. Therefore, and as described before [3, 7, 8], the use of ^{99m}Tc -MAA-SPECT/CT volumes reduces the risk of underdosing. Even so, using ^{90}Y PET/CT as the method to define the actual TgV, the calculated Gy in the tumor were 18% lower than those predicted using ^{99m}Tc -MAA-SPECT/CT TgV (median of -14 Gy). This difference was almost half for absorbed doses by non-tumor liver (median of -5 Gy). These results are in accordance with other studies founding that ^{99m}Tc -MAA-SPECT/CT tends to overestimate posttherapy dosimetry in tumor, being more accurate for the non-tumor liver dosimetric assessment [27, 28]. Regarding the influence that the treatment approach could have in the differences in dosimetry, CBCT showed lower differences for lobar or total treatments than for selective or superselective approaches. As mentioned above, probably the delimitation of TgV in more selective administrations, without clear anatomical boundaries, can be a limitation of this technique. Therefore, more studies are needed to elucidate this.

Another important aspect of the study lies on the added utility that each modality has in RE planning:

- the information obtained from ^{99m}Tc -MAA-SPECT/CT was determinant in 71% of the patients due to its capability to define and confirm the TgV in segmental and subsegmental treatments or after flow redistribution; it also helped to detect tumoral areas not receiving ^{99m}Tc -MAA with the selected arterial access.

- CBCT was especially useful in 29% of the patients, ensuring the total coverage of the tumor and ruling out the presence of microsatellite lesions that would have changed the selected arterial access. Moreover, thanks

to CBCT information it was possible to split the activity according to the volume of tumor perfused by each feeding artery in up to 42% of patients. This approach, which as far as we know has not been published before, enables a better coverage of the microspheres in the target area.

The strengths of this study are worth highlighting. First, all ^{99m}Tc -MAA-SPECT/CT TgV were obtained blindly during RE work-up, not knowing the final ^{90}Y -microsphere distribution. Second, the same IR performed RE evaluation and treatment in one day in all patients. This reduces the risk of undesired changes in catheter position and therefore the agreement between the distribution of ^{99m}Tc -MAA and the ^{90}Y -microspheres is less subject to non-measurable errors.

This study has also some limitations. It is a single-center study involving a relatively small number of patients. Shallow breathing was allowed during SPECT/CT and PET/CT acquisition and breathing motion was not corrected. However, as Bastiaannet et al. [29] described, healthy liver parenchyma suffered only marginally from breathing and collimator effects due to the larger volume, being individual tumors the most affected. Despite these limitations, the results herein presented are promising and can help to plan a more precise and personalized treatment with those imaging methods routinely used during RE work-up.

Conclusion

^{99m}Tc -MAA-SPECT/CT has shown to be a reliable tool to predict the liver volume that will be treated during RE. Its concordance with the TgV obtained with ^{90}Y PET/CT has demonstrated to be superior to that obtained with CBCT or CECT, used in current practice. This superior prediction persisted also for segmental and subsegmental infusions performed for a more effective and safer RE. Moreover, the use of ^{99m}Tc -MAA-SPECT/CT TgV could have reduced the risk of underdosing with respect to the use of CECT or CBCT TgV. Nonetheless, CBCT provided essential information for a personalized RE planning, ensuring the total coverage of the tumor and, in cases with more than one feeding artery, splitting the activity according to the volume of tumor perfused by each artery. Therefore, the joint use of ^{99m}Tc -MAA-SPECT/CT and CBCT optimizes dosimetric planning for RE procedures, enabling a more accurate personalized approach.

Abbreviations

RE: Radioembolization; SIRT: Selective internal radiation therapy; BSA: Body surface area; mBSA: Modified BSA; TgV: Target volume; TgVs: Target volumes; BS: Bremsstrahlung; REILD: Radioembolization-induced liver disease; IR: Interventional radiologist; NM: Nuclear medicine; CECT: Contrast-enhanced computed tomography; MR: Magnetic resonance; ^{99m}Tc -MAA: ^{99m}Tc -macroaggregated albumin; CBCT: C-arm cone-beam CT; HCC: Hepatocellular

carcinoma; CC: Cholangiocarcinoma; MDT: Multidisciplinary team; ROIs: Regions of interest; HPS: Hepatopulmonary shunt; TNR: Tumor/non-tumor ratio; VOI: Volume of interest; VOIs: Volumes of interest; CCC: Lin Concordance Correlation Coefficient; 95% CI: 95% Confidence Interval.

Acknowledgements

Not applicable.

Authors' contributions

MRF and JIB designed the study and were involved in the evaluation of the contribution of the different imaging modalities to an improvement of the dosimetric planning. MRF interpreted the results and drafted the manuscript. MRF and FG contributed to ^{99m}Tc -SPECT/CT and ^{90}Y -PET/CT data acquisition. AE and MC contributed to CECT data acquisition. PB, JIB and AMC contributed to CBCT data acquisition. BS, VM, MI, LS and JIB contributed by enhancing its intellectual content. All the authors contributed in drafting parts of the manuscript and approved the final content of the manuscript.

Funding

Not applicable.

Availability of data and material

All data collected is anonymized and saved by the first author (Macarena Rodríguez-Fraile). It is available on reasonable request. This study was partially presented in the Annual Congress of the European Association of Nuclear Medicine October 12–16, 2019, Barcelona, Spain. *Eur J Nucl Med Mol Imaging* 46, 1–952 (2019). <https://doi.org/10.1007/s00259-019-04486-2> [30].

Code availability

Not applicable.

Ethics approval and consent to participate

The Institutional Ethics Committee of Clínica Universidad de Navarra approved the protocol (2020/181) for this retrospective study and waived the need for patient informed consent. The study was performed in accordance with the ethical standards laid down in the 1964 Declaration of Helsinki and all subsequent revisions.

Consent for publication

Not applicable.

Competing interests

Macarena Rodríguez-Fraile, Antonio Martínez de la Cuesta and José Ignacio Bilbao have received consultation fees and speaker honoraria from Sirtex Medical Europe. Lidia Sancho has received speaker honoraria from Sirtex Medical Europe. Bruno Sangro received scientific grants consultation fees and speaker honoraria from Sirtex Medical Europe.

Author details

¹ Nuclear Medicine Department, Clínica Universidad de Navarra, Pamplona, Spain. ² Radiology Department, Clínica Universidad de Navarra, Pamplona, Spain. ³ Medical Physics Department, Clínica Universidad de Navarra, Madrid, Spain. ⁴ Nuclear Medicine Department, Clínica Universidad de Navarra, Madrid, Spain. ⁵ Department of Internal Medicine-Hepatology, Clínica Universidad de Navarra, Pamplona, Spain.

Received: 15 October 2020 Accepted: 18 February 2021

Published online: 04 March 2021

References

- Rodríguez-Fraile M, Iñarrairaegui M. Radioembolization with ^{90}Y -microspheres for liver tumors. *Rev Esp Med Nucl Imagen Mol.* 2015;34:244–57.
- Toskich BB, Liu DM. ^{90}Y Radioembolization dosimetry: concepts for the interventional radiologist. *Tech Vasc Interv Radiol.* 2019;22(2):100–11.
- Garin E, Rolland Y, Lenoir L, Pracht M, Mesbah H, Porée P, et al. Utility of quantitative ^{99m}Tc -MAA SPECT/CT for ^{90}Y yttrium-labelled microsphere treatment planning: calculating vascularized hepatic volume and dosimetric approach. *Int J Mol Imaging.* 2011;2011:398051.

4. Garin E, Rolland Y, Laffont S, Edeline J. Clinical impact of ^{99m}Tc-MAA SPECT/CT-based dosimetry in the radioembolization of liver malignancies with ⁹⁰Y-loaded microspheres. *Eur J Nucl Med Mol Imaging*. 2016;43(3):559–75.
5. Manceau V, Palard X, Rolland Y, Pracht M, le Sourd S, Laffont S, *et al.* A MAA-based dosimetric study in patients with intrahepatic cholangiocarcinoma treated with a combination of chemotherapy and ⁹⁰Y-loaded glass microsphere selective internal radiation therapy. *Eur J Nucl Med Mol Imaging*. 2018;45(10):1731–41.
6. O'Connor PJ, Pasik SD, van der Bom IM, Bishav V, Radaelli A, Kim E. Feasibility of yttrium-90 radioembolization dose calculation utilizing intra-procedural open trajectory cone beam CT. *Cardiovasc Interv Radiol*. 2020;43(2):295–301.
7. Jafarholi Rangraz E, Coudyzer W, Maleux G, Baete K, Deroose CM, Nuyts J. Multi-modal image analysis for semi-automatic segmentation of the total liver and liver arterial perfusion territories for radioembolization. *EJNMMI Res*. 2019;9(1):19.
8. Ertreo M, Choi H, Field D, Lischalk JW, Cohen E, Lynskey GE, *et al.* Comparison of cone-beam tomography and cross-sectional imaging for volumetric and dosimetric calculations in resin yttrium-90 radioembolization. *Cardiovasc Interv Radiol*. 2018;41(12):1857–66.
9. Gaba RC, Lewandowski RJ, Hickey R, Baerlocher MO, Cohen EI, Dariushnia SR, *et al.* Transcatheter therapy for hepatic malignancy: standardization of terminology and reporting criteria. *JVIR*. 2016;27:457–73.
10. Kao YH, Steinberg JD, Tay YS, Lim GK, Yan J, Townsend DW, *et al.* Post-radioembolization yttrium-90 PET/CT-part 1: diagnostic reporting. *EJNMMI Res*. 2013;3(1):56.
11. Martí-Climent JM, Prieto E, Elosúa C, Rodríguez-Fraile M, Domínguez-Prado I, Vigil C, *et al.* PET optimization for improved assessment and accurate quantification of ⁹⁰Y-microsphere biodistribution after radioembolization. *Med Phys*. 2014;41(9):092503.
12. Willowson KP, Tapner M, The QUEST Investigator Team, Bailey DL, Willowson KP, Tapner MJ, *et al.* A multicentre comparison of quantitative ⁹⁰Y PET/CT for dosimetric purposes after radioembolization with resin microspheres: the QUEST phantom study. *Eur J Nucl Med Mol Imaging*. 2015;42(8):1202–22.
13. Lhommel R, van Elmbt L, Goffette P, van den Eynde M, Jamar F, Pauwels S, *et al.* Feasibility of ⁹⁰Y TOF PET-based dosimetry in liver metastasis therapy using SIR-Spheres. *Eur J Nucl Med Mol Imaging*. 2010;37(9):1654–62.
14. Levillain H, Duran Derijckere I, Marin G, Guiot T, Vouche M, Reynaert N, *et al.* ⁹⁰Y-PET/CT-based dosimetry after selective internal radiation therapy predicts outcome in patients with liver metastases from colorectal cancer. *EJNMMI Res*. 2018;8(1):60.
15. Sangro B, Gil-Alzugaray B, Rodriguez J, Sola I, Martinez-Cuesta A, Viudez A, *et al.* Liver disease induced by radioembolization of liver tumors: description and possible risk factors. *Cancer*. 2008;112(7):1538–46.
16. Sangro B. Liver function considerations for post-selective internal radiation therapy resection (hepatocellular carcinoma and metastatic colorectal cancer). *Future Oncol*. 2014;10:57–9.
17. Allimant C, Kafrouni M, Delicque J, Ilonca D, Cassinotto C, Assenat E, *et al.* Tumor targeting and three-dimensional voxel-based dosimetry to predict tumor response, toxicity, and survival after yttrium-90 resin microsphere radioembolization in hepatocellular carcinoma. *J Vasc Interv Radiol*. 2018;29(12):1662–70.
18. Sabet A, Ahmadzadehfahar H, Muckle M, Haslerud T, Wilhelm K, Biersack H-J, *et al.* Significance of oral administration of sodium perchlorate in planning liver-directed radioembolization. *J Nucl Med*. 2011;52(7):1063–7.
19. Ezponda A, Rodríguez-Fraile M, Morales M, Vivas I, de La Torre M, Sangro B, *et al.* Hepatic flow redistribution is feasible in patients with hepatic malignancies undergoing same-day work-up angiography and yttrium-90 microsphere radioembolization. *Cardiovasc Interv Radiol*. 2020;43:987–95.
20. Bilbao JI, Garrastachu P, Herráiz MJ, Rodríguez M, Iñarrairaegui M, Rodríguez J, *et al.* Safety and efficacy assessment of flow redistribution by occlusion of intrahepatic vessels prior to radioembolization in the treatment of liver tumors. *Cardiovasc Interv Radiol*. 2010;33(3):523–31.
21. Gil-Alzugaray B, Chopitea A, Iñarrairaegui M, Bilbao JI, Rodríguez-Fraile M, Rodríguez J, *et al.* Prognostic factors and prevention of radioembolization-induced liver disease. *Hepatology*. 2013;57:1078–87.
22. Martí-Climent JM, Prieto E, Domínguez-Prado I, García-Velloso MJ, Rodríguez-Fraile M, Arbizu J, *et al.* Contribution of time of flight and point spread function modeling to the performance characteristics of the PET/CT biograph mCT scanner. *Rev Esp Med Nucl Imagen Mol*. 2013;32(1):13–21.
23. Morán V, Prieto E, Sancho L, Rodríguez-Fraile M, Soria L, Zubiria A, *et al.* Impact of the dosimetry approach on the resulting ⁹⁰Y radioembolization planned absorbed doses based on ^{99m}Tc-MAA SPECT-CT: is there agreement between dosimetry methods? *EJNMMI Physics*. 2020;7:72.
24. Richetta E, Pasquino M, Poli M, Cutaia C, Valero C, Tabone M, *et al.* PET-CT post therapy dosimetry in radioembolization with resin ⁹⁰Y microspheres: comparison with pre-treatment SPECT-CT ^{99m}Tc-MAA results. *Phys Med*. 2019;64:16–23.
25. van den Hoven AF, Prince JF, de Keizer B, Vonken E-JPA, Bruijnen RCG, Verkooijen HM, *et al.* Use of C-arm cone beam CT during hepatic radioembolization: protocol optimization for extrahepatic shunting and parenchymal enhancement. *Cardiovasc Interv Radiol*. 2016;39(1):64–73.
26. Miyayama S, Yamashiro M, Hashimoto M, Hashimoto N, Ikuno M, Okumura K, *et al.* Identification of small hepatocellular carcinoma and tumor-feeding branches with cone-beam CT guidance technology during transcatheter arterial chemoembolization. *J Vasc Interv Radiol*. 2013;24(4):501–8.
27. Gnesin S, Canetti L, Adib S, Cherbuin N, Silva Monteiro M, Bize P, *et al.* Partition model-based ^{99m}Tc-MAA SPECT/CT predictive dosimetry compared with ⁹⁰Y TOF PET/CT posttreatment dosimetry in radioembolization of hepatocellular carcinoma: a quantitative agreement comparison. *J Nucl Med*. 2016;57(11):1672–8.
28. Jadoul A, Bernard C, Lovinfosse P, Gérard L, Lilet H, Cornet O, *et al.* Comparative dosimetry between ^{99m}Tc-MAA SPECT/CT and ⁹⁰Y PET/CT in primary and metastatic liver tumors. *Eur J Nucl Med Mol Imaging*. 2020;47:828–37.
29. Bastiaannet R, Viergever MA, de Jong HWAM. Impact of respiratory motion and acquisition settings on SPECT liver dosimetry for radioembolization. *Med Phys*. 2017;44(10):5270–9.
30. Rodríguez-Fraile M, Morales MI, Ezponda A, Calvo M, Grisanti F, Berán P, *et al.* The joint use of MAA SPECT/CT and CBCT enables better dosimetry planning for SIRT procedures. Annual congress of the European Association of Nuclear Medicine October 12–16, 2019 Barcelona, Spain. *Eur J Nucl Med Mol Imaging*. 2019;46:1–952.

Publisher's Note

Springer Nature remains neutral with regard to jurisdictional claims in published maps and institutional affiliations.